Developing Synthetic Methods for Redox-active and Luminescent Cyclometalated Complexes with Third-row Transition Metals

A Dissertation Presented to

The Faculty of the Department of Chemistry

University of Houston

In Partial Fulfillment

of the Requirements for the Degree of

Doctor of Philosophy

By

Evanta Kabir

August 2019

Developing Synthetic Methods for Redox-active and Luminescent Cyclometalated Complexes with Third-row Transition Metals

Evanta Kabir

Approved:

Dr. Thomas S. Teets

Dr. Olafs Daugulis

Dr. Arnold Guloy

Dr. Allan Jacobson

Dr. Megan Robertson

Dr. Dan E. Wells
Dean, College of Natural Sciences and Mathematics

Acknowledgements

First, I would like to express my deepest gratitude to my advisor, Professor Thomas S. Teets, for his support, encouragement, and patience throughout my graduate career. He gave me lots of freedom of research direction and working with him in the lab was always enjoyable. I feel rewarded for my last wonderful five years in Teets group, and I believe it was one of the best decisions in my life.

I would also like to thank the members of my dissertation committee, Professors Olafs Daugulis, Arnold Guloy, Allan Jacobson and Megan Robertson for their support and guidance throughout my graduate career.

I am grateful to both the former and present members of the Teets group, for their friendship and support throughout this journey. A special thanks to Dr. Ayan Maity for his mentorship and I really appreciate all his efforts to make our graduate life exciting by arranging lots of activities. I also like to thank Hanah, who was my best friend in the lab, and I will never forget all our fun talks about lots of things. My gratitude to Burny and Jong-Hwa for teaching me various technical stuff.

I want to thank my Family, and especially my parents and siblings, for their love and support throughout my entire academic career and for always encouraging me to chase my dreams. Lastly, I truly appreciate my husband, Nasir for his love and support throughout my every step of the way. Having him is a true blessing in my life, and I look forward to living a life with him by fulfilling our dreams together.

Developing Synthetic Methods for Redox-active and Luminescent Cyclometalated Complexes with Third-row Transition Metals

An Abstract of a Dissertation Presented to

The Faculty of the Department of Chemistry

University of Houston

In Partial Fulfillment

of the Requirements for the Degree of

Doctor of Philosophy

By

Evanta Kabir

August 2019

Abstract

Formazans are a class of conjugated organic N-chelating ligands with an established coordination chemistry with many transition and main group metals. The formazans and the complexes derived from them generally have notable visible absorption coupled with accessible reduction potentials, making them a good candidate for accessing new coordination complexes with intriguing electronic properties. Transition metal complexes of formazan ligands with numerous p-block metals and several first-row transition metals have been reported, but their potential as redox-active chelating ligands with heavier transition metal remain underexplored. In Chapters 2 and 3, a series of di/triarylformazanate cyclometalated complexes with platinum (II) and iridium (III) is described, where unique redox and photophysical properties are observed by combining third-row transition metals with formazanate ligands. X-ray crystallography reveals the molecular structure of several Pt/Ir formazanate complexes. An intense visible $\pi \rightarrow \pi^*$ absorption is observed in both types of metal formazanate complexes; and solvent-dependent electronic absorption spectra reveal some charge-transfer character in the HOMO → LUMO transition in Pt complexes. The formazanate-based reduction potential shifts anodically in presence of electron withdrawing group and the opposite effect is observed for electron donors, establishing that the redox potentials of both the Pt/Ir formazanate complexes could be controlled by altering the substituents in the formazan backbone. The easy synthetic routes to prepare these metal complexes provides opportunities to expand the coordination chemistry of this ligand class to other third row metals, to discover new binding modes and structural motifs involving formazanate ligands and heavy transition metals; and to demonstrate the effect of metal d-orbital

mixing on the formazanate-derived redox and optical properties. In Chapter 3, a suite of red-emitting iridium complexes featuring two different cyclometalated ligands and a variety of ancillary ligands are described, featuring the effect of strongly π-donating ancillary ligand on electrochemical and photophysical properties. Electron-donating substituents can augment the radiative rate constant (k_r) and photoluminescent quantum yield, and/or shift the luminescence to the near-IR region. The work described here motivate further pursuit of the more ancillary ligand modification along with computational studies to control and optimize the structural properties to design better red phosphors.

To my Family and friends

Contents

List of Tables

List of Figures

List of Schemes

Abbreviations

Me = methyl

Et = ethyl

SMe = methionine sulfoxide

CN = nitrile

NO_2 = nitro

HOMO = highest occupied molecular orbital

LUMO = lowest unoccupied molecular orbital

C^N = cyclometalating ligand

fac = facial

mer = meridional

LL' = ancillary ligand(s)

L^X = ancillary ligand(s)

ppy = 2-phenylpyridine

F_2ppy = 2,4-difluorophenylpyridine

btp = 2-(2-pyridyl)benzothiophene

piq = 1-phenylisoquinoline

thpy = 2-(2'-thienyl)pyridine

ppz = 1-phenylpyrazole

bpy = bipyridine

pic = picolinate

acac = acetylacetonate

acNac = β-ketoiminate

NacNac = β-diketiminate

MLCT = metal-to-ligand charge transfer

LLCT = ligand-to-ligand charge transfer

LC = ligand-centered

o = ortho

p = para

Fz = formazan

bt = 2-phenylbenzothiazole

pq = 2-phenylquinoline

ε = molar extinction coefficient

λ = wavelength

DFT = density-functional theory

Fc = ferrocene

TLC = thin layer chromatography

$E_{p,c}$ = cathodic peak potential

$E_{p,a}$ = anodic peak potential

E^{red} = reduction potential

E^{ox} =oxidation potential

Φ_{PL} = photoluminescence quantum yield

k_r = radiative rate constant

k_{nr} = non-radiative rate constant

Cy = cyclohexyl

τ = lifetime

Chapter 1

Introduction

1.1 Formazan ligands

Formazans are a class of conjugated organic molecules with a 1,2,4,5-tetraazapentadienyl core, whose syntheses and structures were first described over 100 years ago.[1,2] Much of the early work on formazans focused on synthetic procedures and structural studies, from which successful applications in biomedical assays, textile dyes, and colorimetric indicators of cell activity have emerged over the years.[3–6] Three types of crystallographically characterized conformations[7] of formazans have been noted for these compounds – closed, open, and linear, with their structures depicted in Figure 1.1. The "open" form is generally favored by the formazans with aryl or bulky alkyl substituents. Ligands with smaller R^3 groups (e.g., H, Me, Et, and SMe) can favor either "open" or "linear" form. Other than that, most of the crystallized structures show the adaptation of the "closed" structure, where delocalization in formazan backbone is observed.

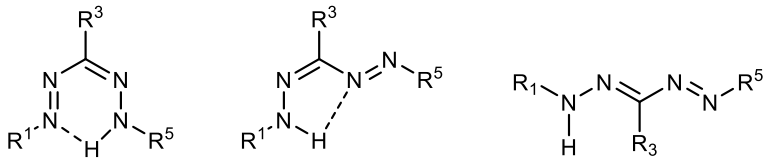

Figure 1.1. Structural conformations of formazans.

Numerous combinations of R^1, R^3, and R^5 substituents are known for formazans, although the most common involve aryl groups at the flanking R^1 and R^5 positions, with either a third aryl substituent or an electron-withdrawing group (cyano, nitro) at the R^3 position. Many routes for preparing formazans have emerged, though the most frequently

employed synthetic strategies, especially in recent studies, involve diazonium chemistry. Scheme 1.1 summarizes the two general synthetic procedure of formazan ligands. Triarylformazans are prepared via reaction of a diazonium salt with a diaryl-substitued hydrazone,[8] whereas for the preparation of diarylformazans with R^3= CN or NO_2 the diazonium reacts with an in-situ deprotonated methylene acid (cyanoacetic acid or nitromethane).[3,7]

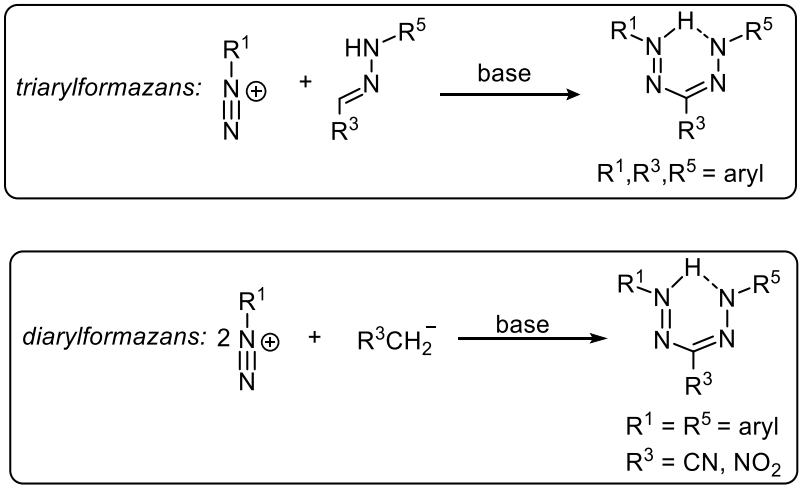

Scheme 1.1. General synthesis of formazan ligands.

1.2 Redox active nature of formazanate ligands

The redox chemistry of formazans, summarized in Scheme 1.2, has been studied extensively over the past several decades and remains one of their most noteworthy features, an aspect of their properties that has long been recognized even before the advent of their coordination chemistry. Oxidation of a free formazan by two electrons with concomitant removal of a proton generates a tetrazolium cation. The colorless to lightly colored tetrazolium can be reduced under physiological conditions to the highly

colored formazan, and this property has led to the development of numerous physiological assays using tetrazolium reagents.[9] Formazans can also be converted into verdazyls, a class of organic six-membered radicals whose stability rivals that of the nitroxide family.[10] The fundamental redox and optical properties of these verdazyl radicals have been the subject of continuing scrutiny,[8] and their coordination chemistry with transition metals has also been explored, primarily with the goal of designing molecules with interesting magnetic properties.[11,12]

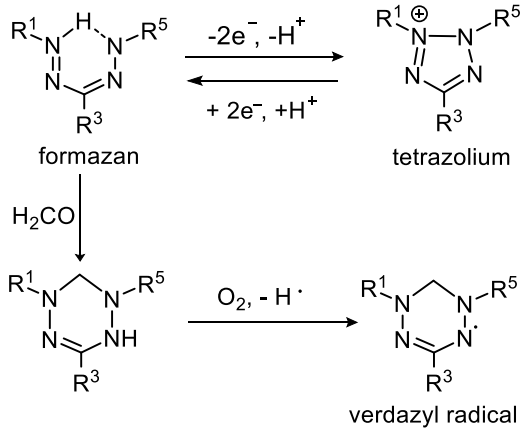

Scheme 1.2. Redox chemistry of formazans.

Ligand-based redox processes are one of the main features that have spurred the significant recent interest in formazanate complexes, allowing the formazanate to serve as an electron reservoir when designing platforms for small-molecule activation.[13–16] Unlike structurally analogous β-diketiminates,[17–20] which have become a popular ancillary ligand in past decades for main group and transition metal chemistry,[21] electrochemical reductions of formazanates by one or two electrons are comparatively accessible at mild potentials and produce relatively stable products, owing to the stabilized LUMOs these

ligands present. Utilizing the redox-active properties of the β-diketiminate for catalytic reaction is quite difficult, due to the low-stability of their oxidized forms and requirement of higher reduction potential to access reduced forms. On the contrary, the four nitrogen atoms in the formazan ligand backbone make the reduction process much more accessible and stabilize the reduced product.

1.3 Coordination complexes of formazanate ligand

The coordination chemistry of formazanates (deprotonated formazans) has long been recognized, with systematic studies of their coordination chemistry starting to appear in the 1940's.[22] Sporadic accounts of transition metal formazanate complexes appeared over the next several decades, with most of the reports focusing on bis-chelate complexes of divalent first-row transition metals[23–26] and their spectroscopic[27–30] and electrochemical[31,32] properties. With the recognition that formazanates (in their "closed" form) are isostructural and isoelectronic with β-diketiminates, a well-known class of supporting ligands in numerous contexts,[21] the coordination chemistry of formazanates garnered much attention in recent years. The desirable optical properties of formazans, namely, intense visible absorption, coupled with their accessible reduction potentials, make them attractive ligands for a number of applications. The latest accounts have expanded the chemistry of formazans with first-row transition metals[7,33] and palladium,[34] demonstrated their utility as supporting ligands for copper-mediated oxygen activation,[35,36] and paired formazans with other redox-active ligands in heteroleptic cobalt complexes.[37,38] Furthermore, zinc complexes of formazanates have been used to showcase their redox noninnocence,[13,14] and luminescent boron chelates have emerged,[39–

[44] which further expound the redox and optical properties of these compounds. In spite of the long history of formazanate coordination complexes and the continuing interest in them, third-row transition metal complexes of formazanates have not been extensively explored and offer an avenue for important discoveries. In this scope of work, we will introduce the novel examples of heteroleptic cyclometalated formazanate complexes of third-row transition metal.

1.4 Cyclometalated iridium(III) complexes

Cyclometalated iridium(III) complexes have garnered much attention due to their chemical inertness, good thermal and photostability, and desirable photophysical properties. Two types of structure class are known for cyclometalated iridium complexes – homoleptic and heteroleptic complexes as depicted in Figure 1.2.

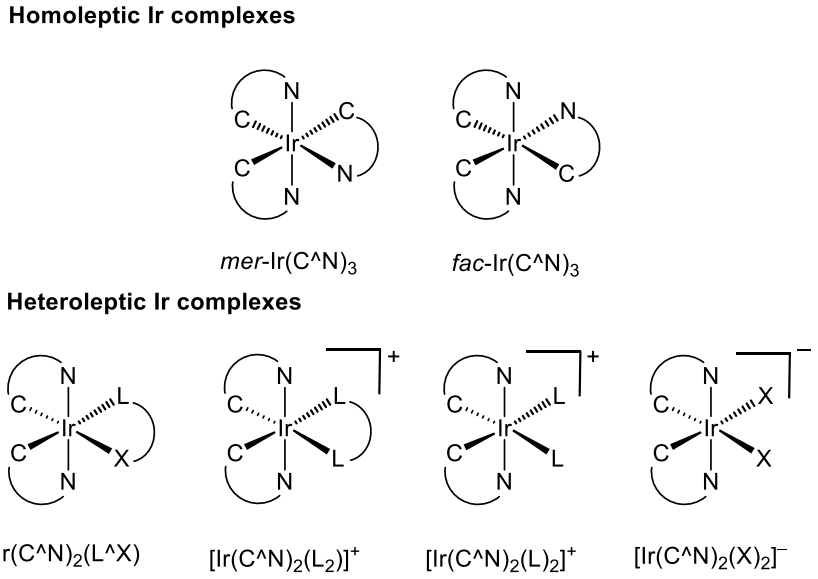

Figure 1.2. General structure types of cyclometalated iridium(III) complexes.

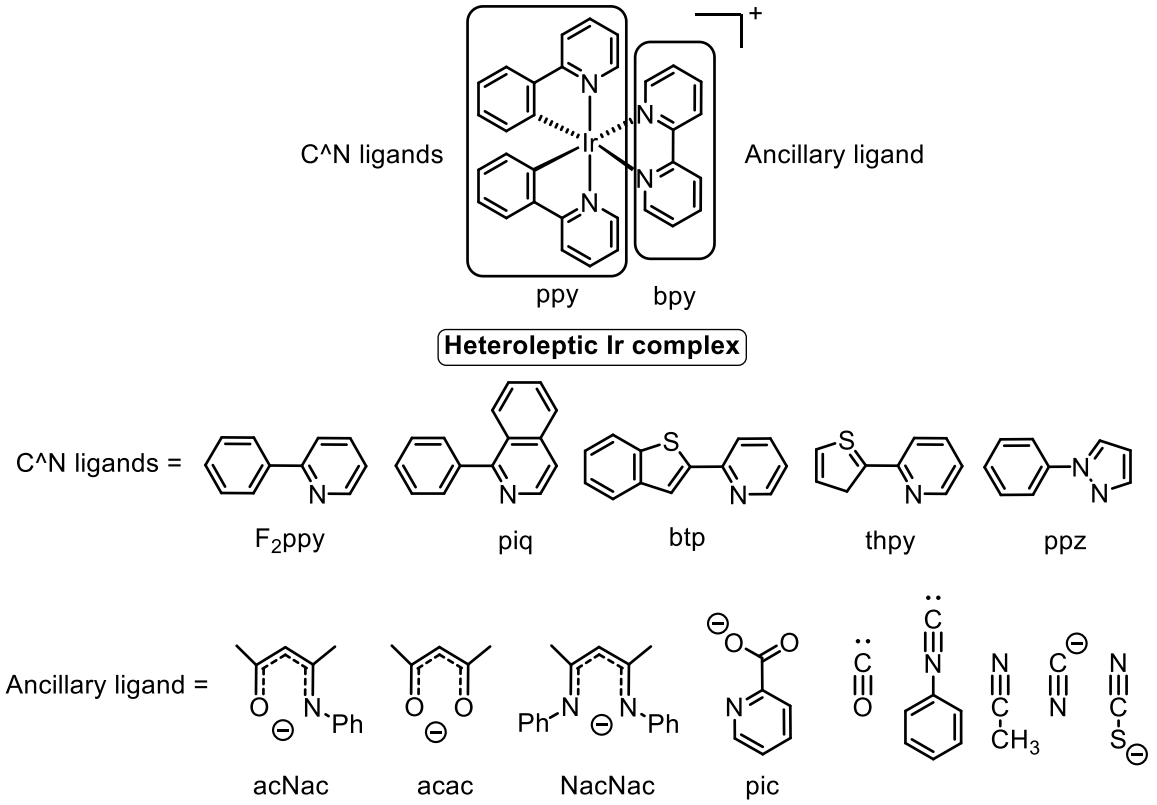

Figure 1.3. Structure of archetypal heteroleptic Ir(III) complexes and commonly used cyclometalating and ancillary ligands.

The general formula for the homoleptic iridium complexes is $Ir(C^N)_3$, where C^N = cyclometalating ligand ("C" represents anionic carbon donor, and "N" is charge-neutral nitrogen donor). Two geometric isomers are observed for homoleptic complexes, the facial (*fac*) and the meridional (*mer*) form. Heteroleptic complexes is described with the general formula $[Ir(C^N)_2(LL')]^n$ (LL' = ancillary ligand(s), n = −1, 0, +1). In order to exhibit the typical types of cyclometalating and ancillary ligands that are generally used to design cyclometalated iridium(III) complexes, Figure 1.2 display a representative archetypal heteroleptic iridium(III) complex and structural examples of cyclometalating C^N and ancillary ligands. Most commonly used choices of cyclometalating (C^N)

ligands include 2-phenylpyridine (ppy),[45–47] 2,4-difluorophenylpyridine (F_2ppy),[46,48] 2-(2-pyridyl)benzothiophene (btp),[49,50] 1-phenylisoquinoline (piq),[49,51] 2-(2'-thienyl)pyridine (thpy),[52,53] and 1-phenylpyrazole (ppz).[46,54] As for ancillary ligand, both bidentate and monodentate types of ligands can be utilized in designing iridium complexes. Choices of bidentate ligands include bipyridine (bpy),[54] picolinate (pic),[55] acetylacetonate (acac),[48,56] β-ketoiminate (acNac), and β-diketiminate (NacNac).[47,49,50] Structural diversity can be obtained in iridium(III) complexes by incorporating monodentate ligands such as cyanide,[57,58] isocyanide,[45,48,59,60] and CO[61] or combination of these ligands. Varying the cyclometalated ligands can tune the emission color over the spectrum,[55,62] while the ancillary ligands has generally minimal influence on emission color but have profound impacts on the redox properties and excited-state dynamics.[47–49]

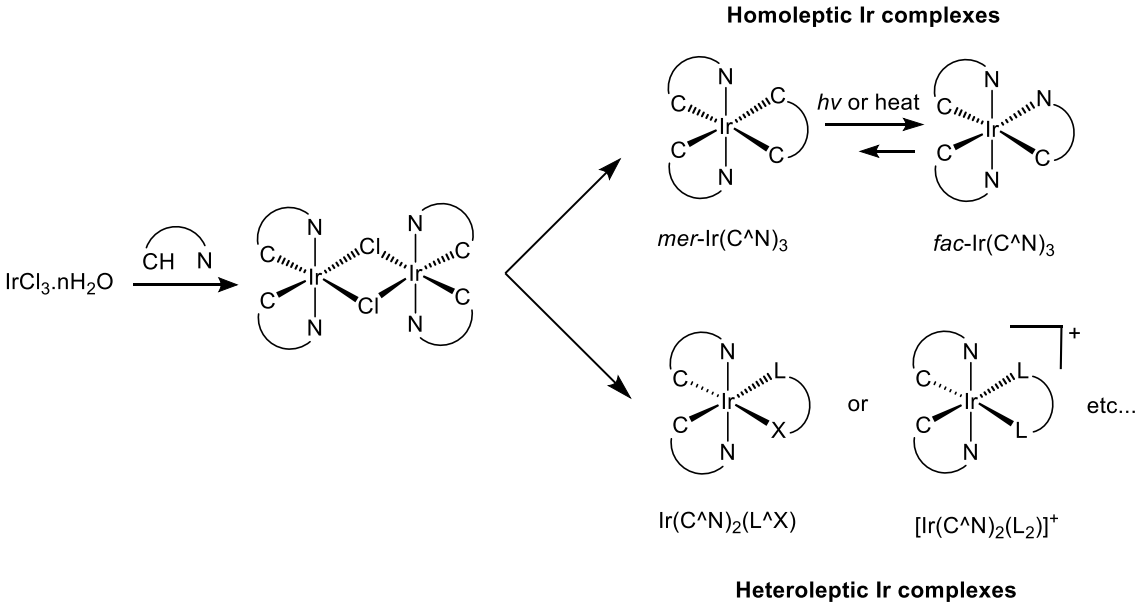

Scheme 1.3. General synthesis of cyclometalated iridium(III) complexes.

General synthesis of cyclometalated iridium(III) complexes involves a standard two-step synthesis procedure, as shown in Scheme 1.3. In the first step which is called Nonoyama reaction,[63] the cyclometalated (C^N) ligand precursor and $IrCl_3.nH_2O$ are refluxed in an aqueous alcoholic solution to generate μ-chloro bridged Ir(III) dimer. Different types of third ligands are replaced with the chloride ligands in the dimers to prepare heteroleptic ligands. If same type of third ligand is used to that in the μ-chloro bridged Ir(III) dimer, homoleptic Ir(III) complexes can be obtained, where coexistence of two isomers is typically observed. But applying heating or photoexcitation can convert the kinetic product *mer*-$Ir(C^N)_3$ into the thermodynamic product *fac*-$Ir(C^N)_3$.

Cyclometalated iridium(III) compounds have been well-known for their photophysical properties. Multiple optical excitation paths such as metal-to-ligand charge transfer (MLCT), ligand-to-ligand charge transfer (LLCT), and ligand-centered charge transfer (LC) are observed in the Ir(III) complexes. Studies on Ir(III) complexes has shown, the nature of the emissive state T_1, often involves mixed ligand-centered (^{3}LC or $^3\pi\pi^*$) and singlet and triplet metal-to-ligand charge transfer (^{1,3}MLCT or $^3d\pi^*$) states through the configuration interaction. The spin-orbit interaction between the triplet states and the higher lying singlet states allows the spin-forbidden radiative transition by relaxing spin-selection rules, and give rise to high phosphorescence efficiency at room temperature. Ligand-centered phosphorescence generally exhibits well-resolved vibronic structure while MLCT phosphorescence spectra typically have structureless emission profile. Moreover, strong rigidochromism[64] and solvatochromism[49,65] are observed in MLCT phosphorescence due to a large dipole moment change in the excited state.[66]

1.5 Overview of thesis

The goal of the research presented is to establish the chemistry of formazanate complexes of third-row metals and optimize the design of ancillary ligands for red-emitting cyclometalated iridium(III) complexes for enhanced phosphorescent properties.

In *Chapter 2*, the complexes of platinum(II) with tri/diarylformazans ligands and insight into their electronic structure is described. Effects of structural and electronical modification of cyclometalating ligands and formazanate ligands on the properties of heteroleptic platinum complexes give us some control to tune the redox and absorption properties of these complexes to a wide range.

In *Chapter 3*, the first examples of cyclometalated iridium formazanate complexes are prepared by a general synthetic strategy and a thorough study of the electronic modification of the formazanate ligand on the electrochemical and photophysical properties is presented.

In *Chapter 4*, In this project, a suite of red-emitting iridium complexes featuring two different cyclometalated ligands and a variety of ancillary ligands are described. Electron-rich, strongly π-donating ancillary ligands were used based on the fact that they can lead to larger radiative rates and higher phosphorescence quantum yields in the red and near-IR region which has proven to be effective for some of the complexes.

1.6 References

(1) Pechmann, H. v. "Ueber Die Einwirkung von Diazobenzol Auf Malonsäure." *Berichte Dtsch. Chem. Ges.* **1892**, *25*, 3175–3190.

(2) Bamberger, Eug.; Wheelwright, E. "Ueber die Einwirkung von Diazobenzol auf Acetessigäther." *Berichte Dtsch. Chem. Ges.* **1892**, *25*, 3201–3213.

(3) Nineham, A. W. "The Chemistry of Formazans and Tetrazolium Salts." *Chem. Rev.* **1955**, *55*, 355–483.

(4) Szymczyk, M.; El-Shafei, A.; Freeman, H. S. "Design, Synthesis, and Characterization of New Iron-Complexed Azo Dyes." *Dyes Pigments* **2007**, *72*, 8–15.

(5) Gruden, C. L.; Fevig, S.; Abu-Dalo, M.; Hernandez, M. "5-Cyano-2,3-Ditolyl Tetrazolium Chloride (CTC) Reduction in a Mesophilic Anaerobic Digester: Measuring Redox Behavior, Differentiating Abiotic Reduction, and Comparing FISH Response as an Activity Indicator." *J. Microbiol. Methods* **2003**, *52*, 59–68.

(6) Frederiks, W. M.; Marle, J. van; Oven, C. van; Comin-Anduix, B.; Cascante, M. "Improved Localization of Glucose-6-Phosphate Dehydrogenase Activity in Cells with 5-Cyano-2, 3-Ditolyl-Tetrazolium Chloride as Fluorescent Redox Dye Reveals Its Cell Cycle-Dependent Regulation." *J. Histochem. Cytochem.* **2006**, *54*, 47–52.

(7) Gilroy, J. B.; Patrick, B. O.; McDonald, R.; Hicks, R. G. "Transition Metal Complexes of 3-Cyano- and 3-Nitroformazans." *Inorg. Chem.* **2008**, *47*, 1287–1294.

(8) Gilroy, J. B.; McKinnon, S. D. J.; Koivisto, B. D.; Hicks, R. G. "Electrochemical Studies of Verdazyl Radicals." *Org. Lett.* **2007**, *9*, 4837–4840.

(9) Berridge, M. V.; Herst, P. M.; Tan, A. S. "Tetrazolium Dyes as Tools in Cell Biology: New Insights into Their Cellular Reduction." In *Biotechnology Annual Review*; Elsevier, 2005; Vol. 11, pp 127–152.

(10) Kuhn, R.; Trischmann, H. "Surprisingly Stable Nitrogenous Free Radicals." *Angew. Chem. Int. Ed. Engl.* **1963**, *2*, 155–155.

(11) Brook, D. J. R.; Lynch, V.; Conklin, B.; Fox, M. A. "Spin Delocalization in the Copper(I) Complexes of Bis(Verdazyl) Diradicals." *J. Am. Chem. Soc.* **1997**, *119*, 5155–5162.

(12) Hicks, R. G.; Lemaire, M. T.; Thompson, L. K.; Barclay, T. M. "Strong Ferromagnetic and Antiferromagnetic Exchange Coupling between Transition Metals and Coordinated Verdazyl Radicals." *J. Am. Chem. Soc.* **2000**, *122*, 8077–8078.

(13) Chang, M.-C.; Dann, T.; Day, D. P.; Lutz, M.; Wildgoose, G. G.; Otten, E. "The Formazanate Ligand as an Electron Reservoir: Bis(Formazanate) Zinc Complexes Isolated in Three Redox States." *Angew. Chem. Int. Ed.* **2014**, *53*, 4118–4122.

(14) Chang, M.-C.; Roewen, P.; Travieso-Puente, R.; Lutz, M.; Otten, E. "Formazanate Ligands as Structurally Versatile, Redox-Active Analogues of β-Diketiminates in Zinc Chemistry." *Inorg. Chem.* **2015**, *54*, 379–388.

(15) Mandal, A.; Schwederski, B.; Fiedler, J.; Kaim, W.; Lahiri, G. K. "Evidence for Bidirectional Noninnocent Behavior of a Formazanate Ligand in Ruthenium Complexes." *Inorg. Chem.* **2015**, *54*, 8126–8135.

(16) Singha Hazari, A.; Mandal, A.; Beyer, K.; Paretzki, A.; Kaim, W.; Lahiri, G. K. "Metal–Metal Bridging Using the DPPP Dye System: Electronic Configurations within Multiple Redox Series." *Inorg. Chem.* **2017**, *56*, 2992–3004.

(17) Eisenstein, O.; Hitchcock, P. B.; Khvostov, A. V.; Lappert, M. F.; Maron, L.; Perrin, L.; Protchenko, A. V. "Mono-, Di-, and Trianionic β-Diketiminato Ligands: A Computational Study and the Synthesis and Structure of [(YbL)3(THF)], L = [{N(SiMe3)C(Ph)}2CH]." *J. Am. Chem. Soc.* **2003**, *125*, 10790–10791.

(18) Khusniyarov, M. M.; Bill, E.; Weyhermüller, T.; Bothe, E.; Wieghardt, K. "Hidden Noninnocence: Theoretical and Experimental Evidence for Redox Activity of a β-Diketiminate(1−) Ligand." *Angew. Chem. Int. Ed.* **2011**, *50*, 1652–1655.

(19) Bai, G.; Wei, P.; Stephan, D. W. "Reductions of β-Diketiminato−Titanium(III) Complexes." *Organometallics* **2006**, *25*, 2649–2655.

(20) Tomson, N. C.; Arnold, J.; Bergman, R. G. "Synthesis, Characterization, and Reactions of Isolable (β-Diketiminato)Niobium(III) Imido Complexes." *Organometallics* **2010**, *29*, 5010–5025.

(21) Bourget-Merle, L.; Lappert, M. F.; Severn, J. R. "The Chemistry of β-Diketiminatometal Complexes." *Chem. Rev.* **2002**, *102*, 3031–3066.

(22) Hunter, L.; Roberts, C. B. "145. The Associating Effect of the Hydrogen Atom. Part IX. The N–H–N Bond. Virtual Tautomerism of the Formazyl Compounds." *J. Chem. Soc. Resumed* **1941**, *0*, 820–823.

(23) Irving, H.; Gill, J. B.; Cross, W. R. "423. The Structure of Some Di-(3-Methyl-1,5-Diarylformazyl)-Nickel(II) Complexes." *J. Chem. Soc. Resumed* **1960**, *0*, 2087–2095.

(24) Dale, D. “The X-Ray Crystallographic Determination of the Structure of Di-[3-Methyl-1(or 5)-Phenyl-5(or 1)-p-Tolylformazyl]Nickel(II).” *J. Chem. Soc. Inorg. Phys. Theor.* **1967**, *0*, 278–287.

(25) Budesinsky, B.; Svecova, J. “Hydrogen and Metal Complexes of Some 3-Cyanoformazans.” *Inorg. Chem.* **1971**, *10*, 313–317.

(26) Siedle, A. R.; Pignolet, L. H. “Formazanylpalladium Compounds. Synthesis and Structure of Bis(1,3,5-Tri-p-Tolylformazanyl)Palladium.” *Inorg. Chem.* **1980**, *19*, 2052–2056.

(27) Petersen, R. L.; McFarland, J. T.; Watters, K. L. “Resonance Raman Study of Metal-Formazans: A Model for Complexes of Metalloenzymes with Chelate Inhibitors.” *Bioinorg. Chem.* **1978**, *9*, 355–367.

(28) Kawamura, Y.; Yamauchi, J.; Ohya-Nishiguchi, H. “Spectroscopic and Structural Characterization of Formazanyl Copper Complexes.” *Bull. Chem. Soc. Jpn.* **1993**, *66*, 3593–3599.

(29) Kawamura, Y.; Deguchi, Y.; Yamauchi, J.; Ohya-Nishiguchi, H. “An ESR Study of 5-Formazanyl Copper(II) Complexes as an Analogy to Three Types of Copper-Containing Proteins.” *Bull. Chem. Soc. Jpn.* **1988**, *61*, 181–186.

(30) Tezcan, H.; Uzluk, E. “The Synthesis and Spectral Properties of 1,3-Substituted Phenyl-5-Phenylformazans and Their Ni(II) Complexes.” *Dyes Pigments* **2008**, *76*, 733–740.

(31) Tezcan, H.; Uzluk, E.; Aksu, M. L. “Electrochemical and Spectroscopic Properties of 1:2 Ni Complexes of 1,3-Substitued (CH3, OCH3) Phenyl-5-Phenylformazans.” *Electrochimica Acta* **2008**, *53*, 5597–5607.

(32) Tezcan, H.; Uzluk, E. “Electrochemical Studies of Bis [1-Substituted (–NO2, –COOH, –Cl, –Br) Phenyl-3,5-Diphenylformazanato]Nickel(II) Complexes.” *Dyes Pigments* **2008**, *77*, 635–645.

(33) Pavlova, I. S.; Pervova, I. G.; Belov, G. P.; Khasbiullin, I. I.; Slepukhin, P. A. “Ethylene Oligomerization Mediated by Iron Formazanates and Organoaluminum Compounds.” *Pet. Chem.* **2013**, *53*, 127–133.

(34) Gilroy, J. B.; Ferguson, M. J.; McDonald, R.; Hicks, R. G. “Synthesis and Characterization of Palladium Complexes of 3-Nitroformazans.” *Inorganica Chim. Acta* **2008**, *361*, 3388–3393.

(35) Hong, S.; Gupta, A. K.; Tolman, W. B. “Intermediates in Reactions of Copper(I) Complexes with N-Oxides: From the Formation of Stable Adducts to Oxo Transfer.” *Inorg. Chem.* **2009**, *48*, 6323–6325.

(36) Hong, S.; Hill, L. M. R.; Gupta, A. K.; Naab, B. D.; Gilroy, J. B.; Hicks, R. G.; Cramer, C. J.; Tolman, W. B. “Effects of Electron-Deficient β-Diketiminate and Formazan Supporting Ligands on Copper(I)-Mediated Dioxygen Activation.” *Inorg. Chem.* **2009**, *48*, 4514–4523.

(37) Protasenko, N. A.; Poddel’sky, A. I.; Bogomyakov, A. S.; Fukin, G. K.; Cherkasov, V. K. “Heteroligand O-Semiquinonato-Formazanato Cobalt Complexes.” *Inorg. Chem.* **2015**, *54*, 6078–6080.

(38) Protasenko, N. A.; Poddel’sky, A. I.; Bogomyakov, A. S.; Starikov, A. G.; Smolyaninov, I. V.; Berberova, N. T.; Fukin, G. K.; Cherkasov, V. K. “The Chemical and Electrochemical Reduction of Heteroligand O-Semiquinonato-Formazanato Cobalt Complexes.” *Inorganica Chim. Acta* **2019**, *489*, 1–7.

(39) Barbon, S. M.; Gilroy, J. B. “Boron Difluoride Formazanate Copolymers with 9,9-Di-n-Hexylfluorene Prepared by Copper-Catalyzed Alkyne–Azide Cycloaddition Chemistry.” *Polym. Chem.* **2016**, *7*, 3589–3598.

(40) Barbon, S. M.; Price, J. T.; Reinkeluers, P. A.; Gilroy, J. B. “Substituent-Dependent Optical and Electrochemical Properties of Triarylformazanate Boron Difluoride Complexes.” *Inorg. Chem.* **2014**, *53*, 10585–10593.

(41) Barbon, S. M.; Staroverov, V. N.; Gilroy, J. B. “Structurally Diverse Boron–Nitrogen Heterocycles from an N2O23− Formazanate Ligand.” *Angew. Chem. Int. Ed.* **2017**, *56*, 8173–8177.

(42) Barbon, S. M.; Staroverov, V. N.; Gilroy, J. B. “Effect of Extended π Conjugation on the Spectroscopic and Electrochemical Properties of Boron Difluoride Formazanate Complexes.” *J. Org. Chem.* **2015**, *80*, 5226–5235.

(43) Hesari, M.; Barbon, S. M.; Staroverov, V. N.; Ding, Z.; Gilroy, J. B. “Efficient Electrochemiluminescence of a Readily Accessible Boron Difluoride Formazanate Dye.” *Chem. Commun.* **2015**, *51*, 3766–3769.

(44) Hesari, M.; Barbon, S. M.; Mendes, R. B.; Staroverov, V. N.; Ding, Z.; Gilroy, J. B. “Structural Tuning of Boron Difluoride Formazanate Electrochemiluminescence Mediated by Tri- *n* -Propylamine.” *J. Phys. Chem. C* **2018**, *122*, 1258–1266.

(45) Nazeeruddin, Md. K.; Humphry-Baker, R.; Berner, D.; Rivier, S.; Zuppiroli, L.; Graetzel, M. "Highly Phosphorescence Iridium Complexes and Their Application in Organic Light-Emitting Devices." *J. Am. Chem. Soc.* **2003**, *125*, 8790–8797.

(46) Tamayo, A. B.; Alleyne, B. D.; Djurovich, P. I.; Lamansky, S.; Tsyba, I.; Ho, N. N.; Bau, R.; Thompson, M. E. "Synthesis and Characterization of Facial and Meridional Tris-Cyclometalated Iridium(III) Complexes." *J. Am. Chem. Soc.* **2003**, *125*, 7377–7387.

(47) Radwan, Y. K.; Maity, A.; Teets, T. S. "Manipulating the Excited States of Cyclometalated Iridium Complexes with β-Ketoiminate and β-Diketiminate Ligands." *Inorg. Chem.* **2015**, *54*, 7122–7131.

(48) Li, J.; Djurovich, P. I.; Alleyne, B. D.; Yousufuddin, M.; Ho, N. N.; Thomas, J. C.; Peters, J. C.; Bau, R.; Thompson, M. E. "Synthetic Control of Excited-State Properties in Cyclometalated Ir(III) Complexes Using Ancillary Ligands." *Inorg. Chem.* **2005**, *44*, 1713–1727.

(49) Lai, P.-N.; Brysacz, C. H.; Alam, M. K.; Ayoub, N. A.; Gray, T. G.; Bao, J.; Teets, T. S. "Highly Efficient Red-Emitting Bis-Cyclometalated Iridium Complexes." *J. Am. Chem. Soc.* **2018**, *140*, 10198–10207.

(50) Lai, P.-N.; Teets, T. S. "Ancillary Ligand Effects on Red-Emitting Cyclometalated Iridium Complexes." *Chem. – Eur. J.* **2019**, *25*, 6026–6037.

(51) Deaton, J. C.; Young, R. H.; Lenhard, J. R.; Rajeswaran, M.; Huo, S. "Photophysical Properties of the Series *Fac*- and *Mer*- (1-Phenylisoquinolinato-N ^ C $^{2'}$) $_x$ (2-Phenylpyridinato-N ^ C $^{2'}$) $_{3-x}$ Iridium(III) (x = 1−3) ^{61†}." *Inorg. Chem.* **2010**, *49*, 9151–9161.

(52) Na, H.; Lai, P.; Cañada, L. M.; Teets, T. S. "Photoluminescence of Cyclometalated Iridium Complexes in Poly(Methyl Methacrylate) Films." *Organometallics* **2018**, *37*, 3269–3277.

(53) Colombo, M. G.; Brunold, T. C.; Riedener, T.; Guedel, H. U.; Fortsch, M.; Buergi, H.-B. "Facial Tris Cyclometalated Rhodium(3+) and Iridium(3+) Complexes: Their Synthesis, Structure, and Optical Spectroscopic Properties." *Inorg. Chem.* **1994**, *33*, 545–550.

(54) Tamayo, A. B.; Garon, S.; Sajoto, T.; Djurovich, P. I.; Tsyba, I. M.; Bau, R.; Thompson, M. E. "Cationic Bis-Cyclometalated Iridium(III) Diimine Complexes and Their Use in Efficient Blue, Green, and Red Electroluminescent Devices." *Inorg. Chem.* **2005**, *44*, 8723–8732.

(55) You, Y.; Park, S. Y. “Inter-Ligand Energy Transfer and Related Emission Change in the Cyclometalated Heteroleptic Iridium Complex: Facile and Efficient Color Tuning over the Whole Visible Range by the Ancillary Ligand Structure.” *J. Am. Chem. Soc.* **2005**, *127*, 12438–12439.

(56) Lamansky, S.; Djurovich, P.; Murphy, D.; Abdel-Razzaq, F.; Lee, H.-E.; Adachi, C.; Burrows, P. E.; Forrest, S. R.; Thompson, M. E. “Highly Phosphorescent Bis-Cyclometalated Iridium Complexes: Synthesis, Photophysical Characterization, and Use in Organic Light Emitting Diodes.” *J. Am. Chem. Soc.* **2001**, *123*, 4304–4312.

(57) Dedeian, K.; Djurovich, P. I.; Garces, F. O.; Carlson, G.; Watts, R. J. “A New Synthetic Route to the Preparation of a Series of Strong Photoreducing Agents: Fac-Tris-Ortho-Metalated Complexes of Iridium(III) with Substituted 2-Phenylpyridines.” *Inorg. Chem.* **1991**, *30*, 1685–1687.

(58) Di Censo, D.; Fantacci, S.; De Angelis, F.; Klein, C.; Evans, N.; Kalyanasundaram, K.; Bolink, H. J.; Grätzel, M.; Nazeeruddin, M. K. “Synthesis, Characterization, and DFT/TD-DFT Calculations of Highly Phosphorescent Blue Light-Emitting Anionic Iridium Complexes.” *Inorg. Chem.* **2008**, *47*, 980–989.

(59) Na, H.; Maity, A.; Teets, T. S. “Bis-Cyclometalated Iridium Complexes with Electronically Modified Aryl Isocyanide Ancillary Ligands.” *Dalton Trans.* **2017**, *46*, 5008–5016.

(60) Maity, A.; Le, L. Q.; Zhu, Z.; Bao, J.; Teets, T. S. “Steric and Electronic Influence of Aryl Isocyanides on the Properties of Iridium(III) Cyclometalates.” *Inorg. Chem.* **2016**, *55*, 2299–2308.

(61) Chin, C. S.; Eum, M.-S.; Kim, S. yi; Kim, C.; Kang, S. K. “Blue-Light-Emitting Complexes: Cationic (2-Phenylpyridinato)Iridium(III) Complexes with Strong-Field Ancillary Ligands.” *Eur. J. Inorg. Chem.* **2007**, *2007*, 372–375.

(62) Lowry, M. S.; Bernhard, S. “Synthetically Tailored Excited States: Phosphorescent, Cyclometalated Iridium(III) Complexes and Their Applications.” *Chem. – Eur. J.* **2006**, *12*, 7970–7977.

(63) Nonoyama, M. “Benzo[h]Quinolin-10-Yl-N Iridium(III) Complexes.” *Bull. Chem. Soc. Jpn.* **1974**, *47*, 767–768.

(64) Ueno, T.; Urano, Y.; Kojima, H.; Nagano, T. “Mechanism-Based Molecular Design of Highly Selective Fluorescence Probes for Nitrative Stress.” *J. Am. Chem. Soc.* **2006**, *128*, 10640–10641.

(65) Cummings, S. D.; Eisenberg, R. “Tuning the Excited-State Properties of Platinum(II) Diimine Dithiolate Complexes.” *J. Am. Chem. Soc.* **1996**, *118*, 1949–1960.

(66) Hanah Na, “New Synthetic Strategies for Luminescent Platinum(II) and Iridium(III) Complexes” PhD Dissertation, University of Houston, Houston, May 2019.

Chapter 2

Spectroscopic and Electrochemical properties of Electronically Modified Cycloplatinated Formazanate Complexes

Portions of this work have been previously published:

Reprinted in part with permission from Kabir, E.; Wu, C.-H.; Wu, J. I.-C.; Teets, T. S. *Inorg. Chem.* **2016**, *55*, 956–963. Copyright 2016 American Chemical Society.

Reprinted in part with permission from Kabir, E.; Patel, D.; Clark, K.; Teets, T. S. *Inorg. Chem.* **2018**, 57, 10906–10917. Copyright 2018 American Chemical Society.

2.1 Introduction

Formazans are a class of conjugated organic molecule with a 1,2,4,5-tetraazapentadienyl core, and their monoanionic form (referred to as "formazanate") is a well-known *N*-chelating ligand class with a rich coordination chemistry with transition metals and main-group metals. Much of the early work on formazans focused on synthetic procedures and structural studies, from which successful applications in biomedical assays, textile dyes, and colorimetric indicators of cell activity have emerged over the years.[1–4] The coordination chemistry of formazanates has long been investigated with sporadic accounts of their transition-metal coordination chemistry appearing over the past several decades.[5–9] In recent years, the chemistry of formazans with transition metals has been reinvigorated due to the desirable optical properties and accessible redox states of the formazanate scaffold. Complexes of formazans and related ligands with first-row transition metals[10,11] and palladium have been reported,[12] and applications of formazanates as supporting ligands for copper complexes which mediate oxygen activation[13,14] and low-coordinated iron complexes with ligand-based redox chemistry were recently established.[15,16] In addition, bis(formazanate) iron and heteroleptic cobalt complexes have demonstrated unique magnetic properties.[17–19] Beyond transition metals, boron chelates have been used to expound the optical properties of formazanates, which include intense absorption bands and electrochemiluminescence,[20–23] with zinc and boron complexes being especially valuable in revealing the ligand-based redox activity of formazanates.[20,24–27]

Despite the diverse accounts of formazanate coordination complexes and the growing interest in them, third-row transition metal complexes have not been extensively explored and offer an avenue for important discoveries. Third-row complexes of dithizonates are known, which contain a formazan-like core, (Figure 2.1 (**a**)) but coordination of sulfur was observed in these compounds, leaving one nitrogen atom uncoordinated.[28]

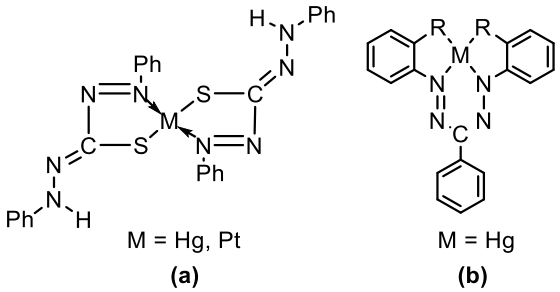

Figure 2.1. Example of third-row metal complexes with formazan-like core.

There are a few third-row transition metal complexes of dianionic aryl formazanates which involve auxiliary *o*-phenoxy or *o*-benzoate donors and coordinate in a tridentate fashion, (Figure 2.1 (**b**)) these previous studies described a number of spectroscopic and reactivity properties of the complexes but none of these are extensively characterized or pursued on in subsequent studies.[29–32] A partnership between third-row transition metals and formazanates offers the possibility of designing new complexes with unique bond activation chemistry and/or triplet excited-state processes engendered by the metal center, along with the formazanates desired intense visible absorption and redox activity. The strong orbital overlap between radially extended 5d orbitals of third-row metals and the formazanate π system could perturb the inherent redox properties of

the formazanate, motivating further study on such compounds. In this chapter, a diverse set of heteroleptic cyclometalated complexes of platinum (II) with tri/diarylformazanate is described and insight into their electronic structures is provided by characterizing the molecular structure, photophysical, and electrochemical properties of such complexes along with computational analysis. Reasoning that C^N cyclometalated ligands would provide a robust and tunable platform to support platinum formazanate complexes, heteroleptic bis-chelated complexes were prepared with both a formazanate and a C^N cyclometalated ligand. The 18 neutral complexes described here include four different cyclometalated ligands and five structurally and electronically varied triaryl- and diarylformazanates. The new compounds presented here are synthesized by following two general procedure and 10 of them are structurally characterized by X-ray diffraction. This approach permits electronic tuning of both the C^N ligand and the formazanate as a means of gauging the extent of electronic communication between the platinum center and the formazanate π system. This structural diversity affords substantial control over the ligand-based redox properties and results in redox-potential that are exquisitely sensitive to the incorporation of electron-donating or electron-withdrawing groups on the formazan ligand's NNCNN backbone. The formazanate based redox potentials are moderately responsive to the identity of the C^N ligand, revealing some mixing between the platinum d-orbital and formazanate π orbitals and giving an additional layer of control over these redox features. The absorption spectra show intense bands featuring contributions from both the formazanate and the Pt−C^N fragments. The latter band can be tuned over a wide range by varying the C^N ligand, such that it is possible to design complexes with nearly panchromatic absorption over the visible range. Solvatochromic

studies reveal additional insights into the nature of the intense absorption bands observed in these complexes. Solvent-dependent electronic absorption spectra reveal some charge-transfer character in the HOMO → LUMO transition, which is confirmed by TD-DFT analysis. This work introduces a new class of robust coordination complexes and demonstrates how binding the formazanate to cyclometalated platinum perturbs the formazanate's electronic structure and demonstrates the ability to control the key redox and optical properties by independently altering the C^N and formazanate ligands.

2.2 Results and Discussion

2.2.1 Synthesis of heteroleptic Cycloplatinated formazanate complexes

The general synthetic procedure for preparing neutral heteroleptic platinum formazanate complexes is outlined in Scheme 2. Pairing the five formazanate ligands with any of the four cyclometalating ligands 2-phenylpyridine (ppy), 2-(2,4-difluorophenyl) pyridine (F_2ppy), 2-phenylbenzothiazole (bt), or 2-phenylquinoline (pq) furnishes a set of 18 complexes. The chloro-bridged dimers $[Pt(C^N)(\mu\text{-}Cl)]_2$ were treated with stoichiometric amounts of the free formazan in the presence of a base; a distinct color change from dark red (free formazan) to green or blue (platinum complex) signified the completion of reaction. Reactions was carried out in refluxing methanol solution with excess sodium carbonate (Na_2CO_3) as base, but improved reaction condition in dichloromethane (CH_2Cl_2) solvent with excess triethylamine (Et_3N) acting as a base could lower the reaction times and increase reaction yields is regarded as the preferred route for the synthesis of the heteroleptic platinum formazanate complexes. Formazanate ligands with electron-withdrawing cyano groups at the R_2 (i.e.

diarylformazans, $Fz^{Me,CN}$ and $Fz^{CN,CN}$) seemed to require shorter reaction times when compared to the triarylformazan analogues. The isolated yields of the 18 complexes was observed to be dependent on the identity of the C^N ligands. For C^N = ppy, F_2ppy, and pq, yields are more than 60% for

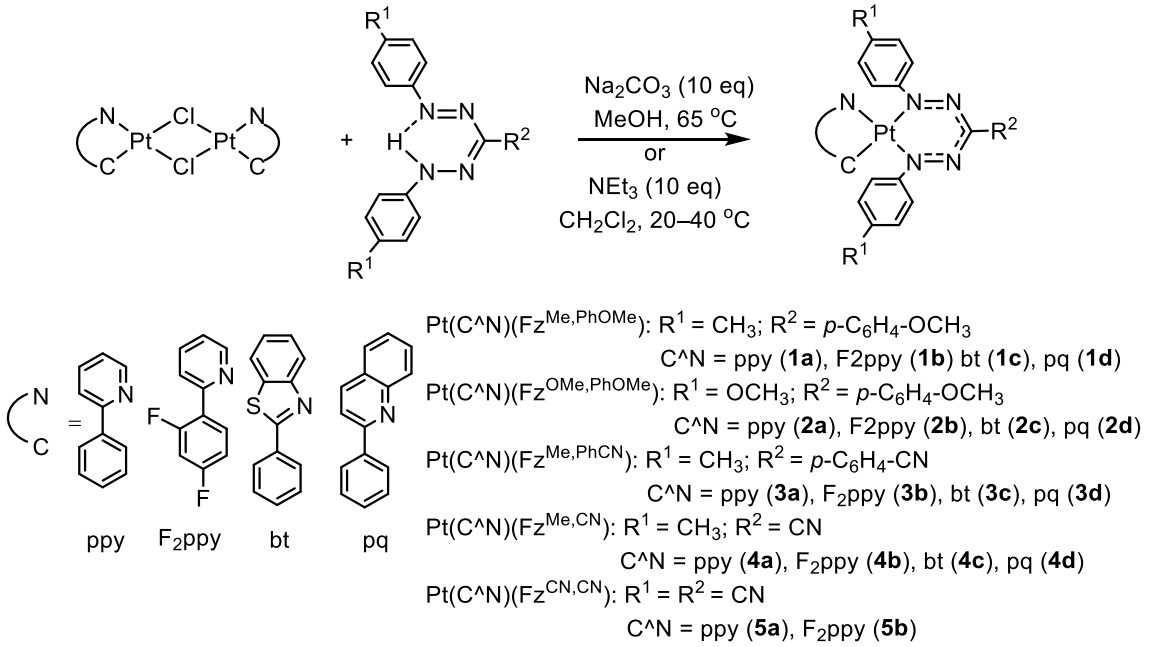

Scheme 2.1. General synthesis of complexes **1** – **5**.

all formazanate ligands. In contrast, bt complexes give lower isolated yields (45−55%), mainly due to the difficulty of purifying the starting material $[Pt(bt)(\mu\text{-}Cl)]_2$. Complexes **1a**–**1b** and **2a**–**2b** were synthesized by refluxing the reagents with Na_2CO_3 as base in methanol solution as part of the primary investigation to prepare the platinum formazanate complexes. Later, it was observed that using triethylamine as base and dichloromethane as reaction solvent was more of an efficient choice for the synthetic procedure as it could shorten the reaction time and improve yields, and rest of the 14

complexes were synthesized by following this method. All of the complexes were air and moisture stable and fully characterized by ^{1}H, $^{13}C\{^{1}H\}$, and ^{19}F (for **1b**, **2b**, **3b**, **4b,** and **5b**) NMR spectroscopy, IR spectroscopy, and elemental analysis, which establish the identity and bulk purity of all complexes.

2.2.2 Crystal Structures

Complexes **1a**–**1b**, **2a**, **2c**, **3a**, **3d**, **4a** – **4c**, and **5b** were characterized by single crystal X-ray diffraction, with the structures depicted in Figure 2.2–2.3. Diffraction data and refinement index of all ten complexes are summarized in Table 2.7–2.10. Relevant bond lengths and angles for all complexes are provided in Table 2.1–2.2. Single crystals for complexes were grown via either vapor diffusion of pentane into dichloromethane or tetrahydrofuran or chloroform solution or by layering pentane onto a dichloromethane solution of the appropriate compound at room temperature. In all cases, the crystal structures indicated the expected planar coordination environment for Pt(II), distorted from perfectly square planar by virtue of the imposed chelate angles of ca. 80°. Small deviations of the platinum atom from the mean plane of the N_3C coordination environment were observed, and the bond angles around the Pt center summed to very nearly 360° within experimental error. Each complex has two N−N and two C−N bond lengths in the formazanate backbone, which in all cases were nearly equivalent to each other, evincing full electronic delocalization within the ligand's backbone. These observed bond lengths were very similar to some other observed formazanate compounds.[8,10,18,33] The Pt–N bond distances to the chelated formazanate show slight asymmetry as the distances trans to the phenyl–C are longer compared to the distances

trans to the pyridyl–N, indicating a stronger trans influence of phenyl compare to pyridine.

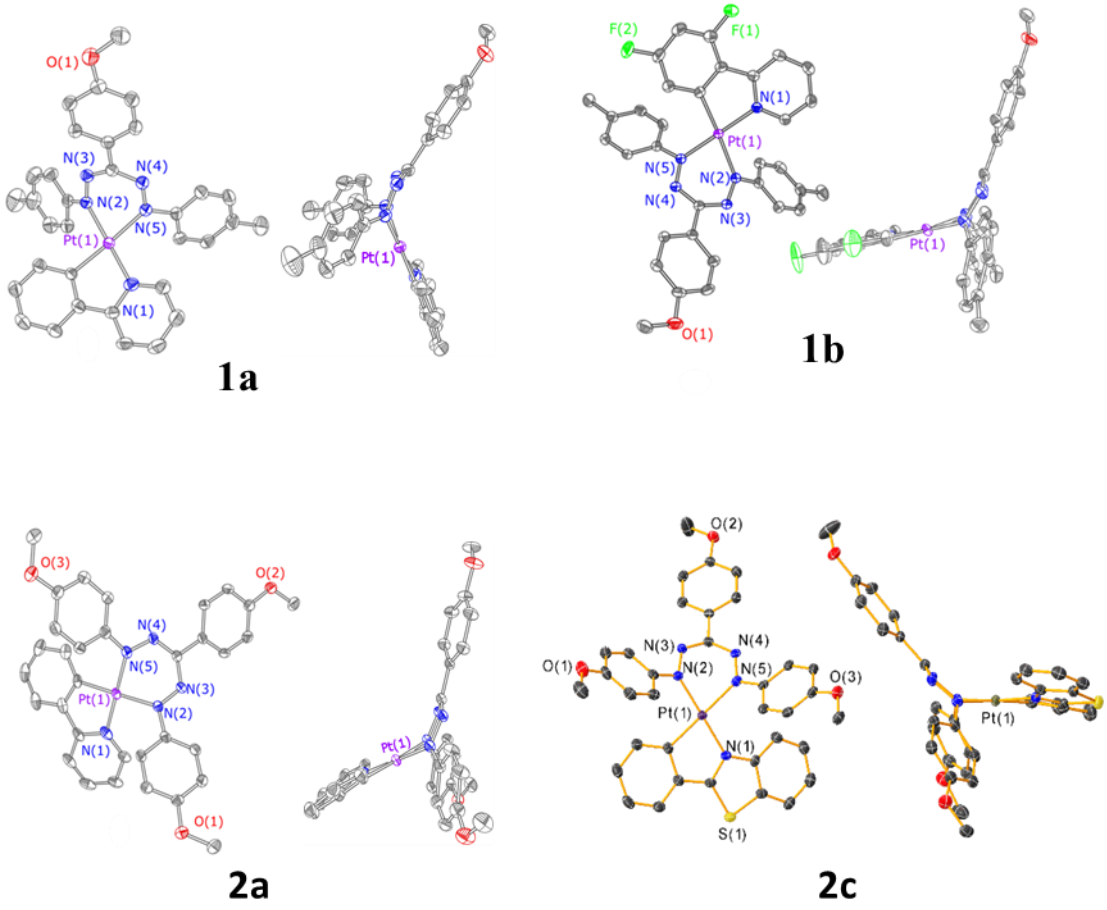

Figure 2.2. X-ray crystal structure of complexes **1a**, **1b**, **2a**, and **2c**. Sideview of all crystal structures showing the "dragonfly" conformation of the complexes. Hydrogen atoms and solvated molecules are omitted for clarity. Ellipsoids are shown at the 50% probability level.

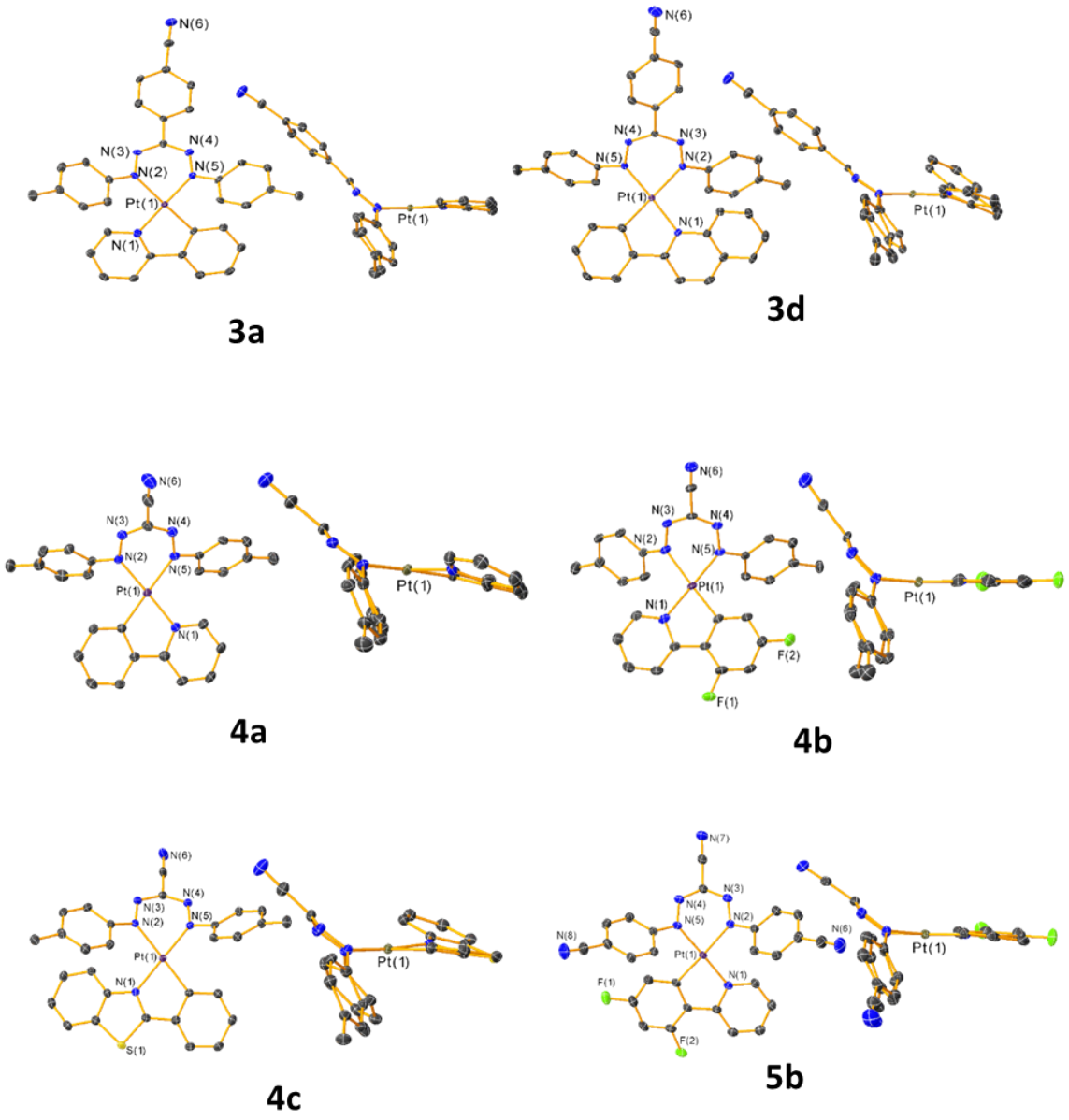

Figure 2.3. X-ray crystal structure of complexes **3a**, **3d**, **4a**, **4b**, **4c**, and **5b**. Sideview of all crystal structures showing the "dragonfly" conformation of the complexes. Hydrogen atoms and solvated molecules are omitted for clarity. Ellipsoids are shown at the 50% probability level.

Table 2.1. Summary of crystallographic bond lengths (Å) and Angles (deg) for Complexes **1a**, **1b**, **2a**, **2c**, and **3a**

	1a*	**1b**	**2a**	**2c**	**3a**
d(Pt–N) (Å)[a]	2.041(4) 2.055(4)	2.003(2)	2.021(4)	1.993(5)	2.032(5)
d(Pt–N) (Å)[b]	2.065(4) 2.059(4)	2.084(2)	2.058(3)	2.085(5)	2.090(4)
d(Pt–N)(Å) (C^N)	2.022(4) 2.055(4)	2.036(2)	2.020(4)	2.049(5)	2.026(5)
d(Pt–C) (Å) (C^N)	2.006(4) 2.011(4)	1.998(3)	2.015(4)	2.022(6)	2.024(5)
∠N–Pt–N (°)[c]	78.67(16) 78.30(15)	78.92(9)	80.84(14)	79.6(2)	80.43(18)
∠N–Pt–C (°) (C^N)	80.14(19) 80.30(19)	80.31(10)	80.60(17)	80.0(2)	79.6(2)
Σ bond angles (°)	359.9(7) 359.8(7)	359.7(4)	360.0(6)	360.18(2)	359.96(1 9)

*Two crystallographicallly independent molecules. [a]=formazanate, trans to N, [b]= formazanate, trans to C, [c]=formazanate

The azo N(2)−N(3) and N(4)−N(5) distances are nearly equal across the series and relatively short (ca. 1.30 Å), indicating minimal backbonding into the formazanate which would partially populate N═N π* orbitals and elongate these bonds. There does not appear to be any systematic dependence of the key structural metrics on the presence of electron-withdrawing or electron-donating groups on the formazanate periphery. The Pt−N bond distances to the formazanate lie in the same range as the distance between the

platinum and the nitrogen atom of the C^N ligand. No apparent Pt−Pt interaction was observed for these complexes.

Table 2.2. Summary of crystallographic bond lengths (Å) and Angles (deg) for Complexes **3d**, **4a**, **4b**, **4c**, and **5b**

	3d	**4a**	**4b**	**4c**	**5b**
d(Pt–N) (Å)[a]	1.992(2)	2.023(5)	2.011(5)	1.998(2)	2.007(2)
d(Pt–N) (Å)[b]	2.092(2)	2.087(8)	2.098(5)	2.091(2)	2.106(2)
d(Pt–N)(Å) (C^N)	2.057(2)	2.037(5)	2.027(6)	2.033(2)	2.041(2)
d(Pt–C) (Å) (C^N)	2.006(2)	2.026(5)	2.008(1)	2.022(2)	2.012(2)
N(2)−N(3), N(5)−N(4)	1.299(3), 1.309(3)	1.293(1), 1.302(6)	1.296(7), 1.302(6)	1.290(3), 1.304(3)	1.297(3), 1.293(3)
∠N–Pt–N (°)[c]	82.53(8)	83.48(17)	79.4(11)	81.20(7)	80.98(8)
∠N–Pt–C (°) (C^N)	79.97(9)	80.12(11)	80.7(2)	79.78(8)	80.37(10)
Σ bond angles (°)	360.01(9)	360.14(14)	359.57(7)	360.19(8)	359.82(19)

[a]=formazanate, trans to N, [b]= formazanate, trans to C, [c]=formazanate

Distortion of the formazanate's tetraazapentadienyl core from planarity was observed for all structurally characterized molecules, in which the N-aryl substituents and three non-coordinated atoms of the formazanate core were inclined in opposite directions out of the coordination plane. This feature has been referred as a "dragonfly" conformation that has been observed in several other formazanate complexes,[8,10,18,20,25,34] and this conformation persists across all members of the series with either

triarylformazanate (**1a**–**b**, **2a**, **2c**, **3a**, and **3d**) or diarylformazanates (**4a**–**c**, and **5b**) ligands (Figure 2.2 and 2.3).

2.2.3 Optical properties of cyclometalated platinum formazanate complexes

Electronic absorption spectra of platinum formazanate complexes **1**–**5** were measured by UV-vis absorption spectroscopy in dichloromethane solution at room temperature and the data is summarized in Table 2.3. Figure 2.4 represent the overlaid absorption spectra of complexes **1**–**4** with respect to their free formazan ligand and Figure 2.5 displays overlaid absorption spectra of ppy- and F_2ppy-ligated platinum formazanate complexes. All the complexes described here were highly colored, appeared green to blue in solution and displayed highly intense absorption bands in the visible range of spectrum. The broad, intense visible absorption bands in $Fz^{Me,OMe}$ and $Fz^{OMe,OMe}$ occurred at 524 nm (ε = 15000 $M^{-1}cm^{-1}$) and 545 nm (ε = 14000 $M^{-1}cm^{-1}$), respectively. The free ligand $Fz^{Me,PhCN}$ showed a characteristic broad absorption band at 486 nm (ε = 14200 $M^{-1}cm^{-1}$), which blue-shifted by 33 nm in $Fz^{Me,CN}$ (λ = 453 nm, ε = 16800 $M^{-1}cm^{-1}$) when the R^2 position of the formazan ligand was changed from 4-cyanophenyl to cyano. A notable bathochromic shift of >100 nm (> 3000 cm^{-1}) was observed for the low-energy absorption maxima of the formazans upon coordination of the formazan to platinum in complexes **1**–**5**. This absorption band was assigned as a formazanate-centered $\pi \rightarrow \pi^*$ with a small amount of Pt(d)$\rightarrow\pi^*$ metal-to-ligand charge transfer (MLCT) character.

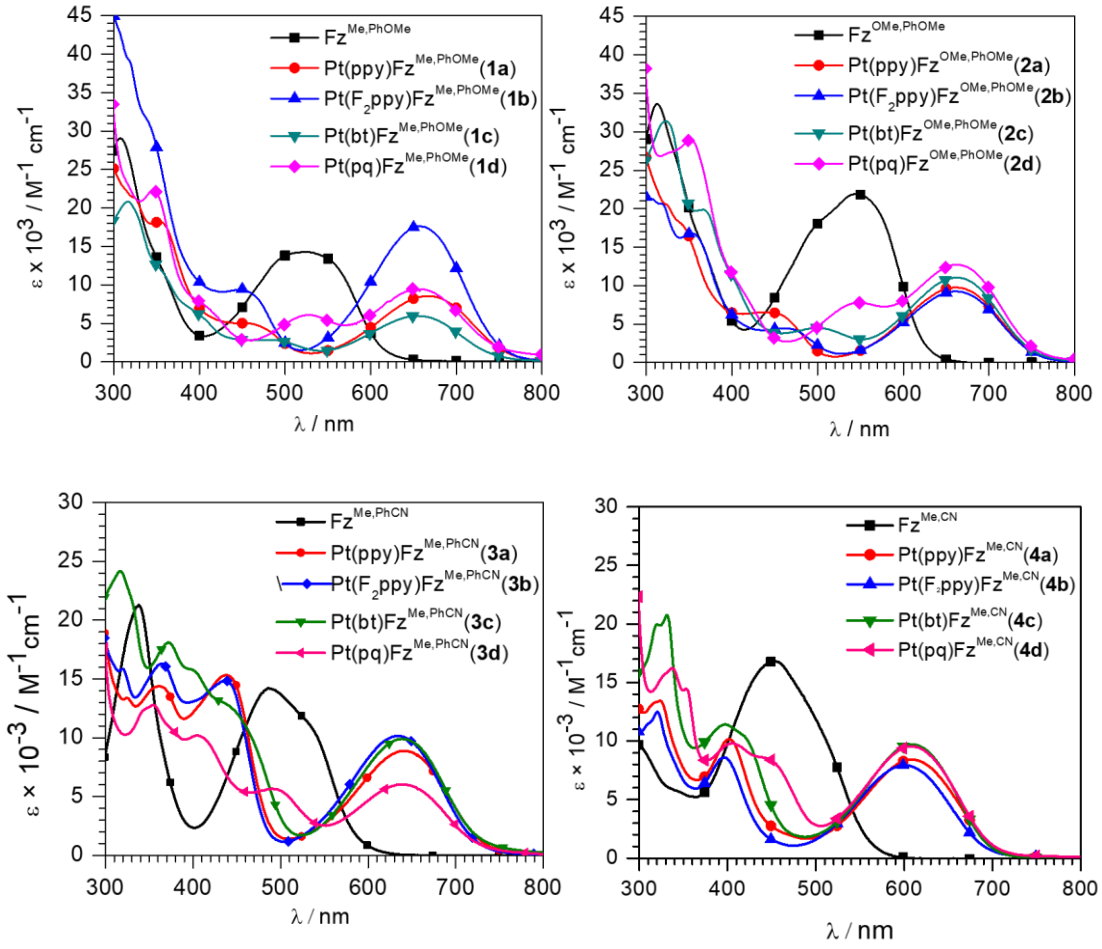

Figure 2.4. Electronic absorption spectra of **1a**–**1d**, **2a**–**2d**, **3a**–**3d**, and **4a**–**4d**, overlaid with their respective free formazan ligand.

As shown in Figure 2.4 and Table 2.3, the low-energy absorption maxima for complexes with the same formazans are largely similar, with little dependence on the C^N ligands. In general, complexes with the more electron-rich $Fz^{OMe,PhOMe}$ ligand (**2a**–**2d**) have low-energy maxima that are slightly red-shifted (~10 nm, 200 cm^{-1}) when compared to complexes with $Fz^{Me,PhOMe}$ (**1a**–**1d**). Introducing an electron-withdrawing group at the center (R^2) position of the triarylformazanate complexes, i.e. $Fz^{Me,PhCN}$ complexes **3a**–**3d**, induces a slight hypsochromic shift of the low-energy band, observed at 634 – 640 nm (**3a**–**3d**). Placing a cyano group directly at the R^2 position in $Fz^{Me,CN}$

complexes **4a**–**4d** results in a larger blue-shift, with maxima for these complexes ranging between 600 and 608 nm, about 800 cm^{-1} blue-shifted when compared to the $Fz^{Me,PhCN}$ complexes where there is a phenyl spacer between the formazanate backbone and the electron-withdrawing group.

Table 2.3. Summary of UV-vis absorption maxima for spectra recorded in CH_2Cl_2

	Absorbance λ, nm, ($\varepsilon \times 10^3$ / $M^{-1}cm^{-1}$)
1a	252 (39) 280 (41), 339[a] (22), 444 (7.9), 664 (12)
1b	251 (35), 269 (32), 294 (25), 338[a] (17), 449 (5.5), 653 (9.6)
1c	265 (22), 316 (20), 355[a] (11), 481 (2.8), 655 (5.9)
1d	291 (40), 338 (21), 527 (6), 650 (9)
2a	256 (36), 277 (33), 353 (18), 449[a] (4.9), 665 (8.3)
2b	254 (43), 292[a] (27), 353 (21), 462 (5.5), 662 (11)
2c	262 (36), 323 (31), 368 (19), 498 (4.0), 663 (11)
2d	289 (48), 352 (29), 548 (7), 663(12)
3a	275 (41), 363 (18), 437 (20), 640 (11)
3b	251 (36), 364 (16), 437 (14), 634 (10)
3c	264(35), 318 (24), 372 (18), 403 (16), 447[a] (12), 639 (10)
3d	289 (25), 355 (12), 405 (10), 490 (5.7), 640 (6.0)
4a	274 (30), 323 (13), 402 (10), 608 (8.4)
4b	267 (25), 320 (12), 396 (8.6), 600 (7.9)
4c	256 (26), 331 (20), 398 (11), 422[a] (10), 608 (9.7)
4d	286 (42), 337 (16), 404 (9.8), 608 (9.5)
5a	273 (40), 307 (28), 382 (12), 642 (10)
5b	266 (23), 305 (18), 380 (8.1), 629 (7.4)

[a] Shoulder.

Placing electron-withdrawing groups at the peripheral R^1 positions had the opposite effect, and the absorption maxima of complexes **5a** and **5b**, with $Fz^{CN,CN}$, were *red*-shifted by > 750 cm^{-1} when compared to their analogous $Fz^{Me,CN}$ complexes **4a** and **4b** (Figure 2.5). Taken together, this data showed that the low-energy UV-vis absorption

maxima were somewhat responsive to substituent changes on the periphery of the formazanate, and that the direction of this effect (red-shift or blue-shift) can depend on the location of the substituent.

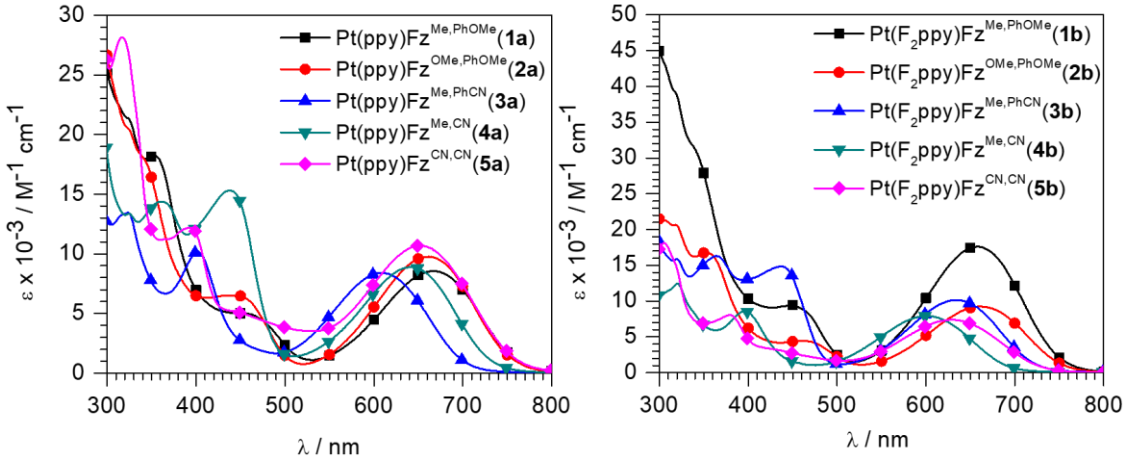

Figure 2.5. Overlaid electronic absorption spectra of **1a**–**5a** and **1b**–**5b**.

In addition to the formazanate-centered band which dominates low-energy region of the spectra, all complexes display additional absorption bands in the near-UV and visible regions that depend on the identity of the cyclometalating ligand. In general, this band occurs at λ ~ 400 nm in F_2ppy and ppy complexes, ~ 450 nm in bt complexes, and ~ 500 nm in pq complexes, though in some cases this additional band overlapped with or was obscured by other intraligand bands, particularly in cyano-substituted formazanates. This additional absorption feature was particularly evident in pq complexes **1d**, **2d**, **3d**, and **4d**, where it overlaps with the formazanate-centered band and gives rise to nearly panchromatic absorption over the entire visible range, (Figure 2.4) resulting in a very dark blue color for these complexes.

Table 2.4. Summary of UV-vis absorption maxima for spectra recorded in CH_2Cl_2, toluene, and MeOH

	λ (nm)		
	CH_2Cl_2	Toluene	MeOH
1a	252, 280, 339[a], 444, 664	341[a], 460, 668	250, 278, 340[a], 413[a], 657
1b	251, 269, 294, 338[a], 449, 653	347[a], 461, 658	248, 266a, 291, 338[a], 433, 658
1c	265, 316, 355[a], 481, 655	317, 356[a], 496, 661	263, 313, 353[a], 478[a], 651
1d	291, 338, 52, 650	297, 348, 542, 662	281. 340, 511, 662
2a	256, 277, 353, 449[a], 665	355, 458[a], 671	255, 276, 351, 444[a], 662
2b	254, 292[a], 353, 462, 662	354, 477, 665	246, 290[a], 346, 445, 655
2c	262 , 323 , 368, 498 , 663	326, 369, 514, 667	261, 319, 364, 491, 661
2d	289, 352, 548, 663	296, 354, 568, 669	287, 352, 539, 664
3a	275, 363, 437, 640	283, 361, 439, 648	270, 354, 432, 640
3b	251, 364, 437, 634	283, 363, 433, 640	261, 361, 431, 631
3c	264, 318, 372, 403, 447[a], 639	318, 371, 399, 460, 647	261, 315, 369, 396[a], 437[a], 639
3d	289, 355, 405, 490, 640	295, 356, 406, 507, 646	287, 354, 401, 473[a], 640
4a	274, 323, 402, 608	284, 319, 410, 616	271, 322, 396, 607
4b	267, 320, 396, 600	283, 322, 403, 605	264, 319, 391, 597
4c	256, 331, 398, 422[a], 608	323, 401, 429[a], 613	264, 330, 396, 607
4d	286, 337, 404, 608	292, 339, 409, 614	281,336, 406, 608
5a	273, 307, 382, 642	284, 304 393, 647	270, 303, 372, 637
5b	266, 305, 380 , 629	283, 307, 388, 631	263, 303, 373, 621

[a] Shoulder.

On the basis of comparisons with other cyclometalated platinum complexes,[35] this band was assigned as a Pt(d)→C^N(π*) MLCT transition, hence the large dependence on the C^N ligand. To further investigate the nature of the UV-vis absorption bands, spectra were recorded in three different solvents of varying polarity: toluene (ε = 2.38), CH_2Cl_2 (ε = 8.93), and methanol (ε = 32.7). The results of these experiments for complex **5a** are shown in Figure 2.6 as a representative example. Absorption maxima in these three solvents are tabulated in Table 2.5.

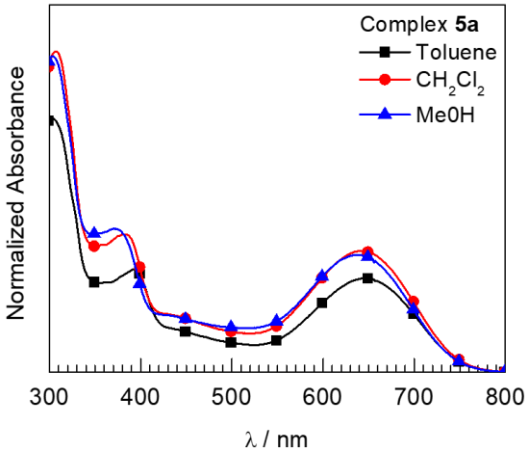

Figure 2.6. Electronic absorption spectra of Pt(ppy)(FzCN,CN) (5a) recorded in CH2Cl2, toluene, and MeOH at room temperature. The spectra are normalized to the low-energy absorption maximum.

The low-energy band was minimally sensitive to solvent polarity, and there was a systematic blue shift as the solvent polarity increased, though the difference in absorption maxima was rather small (<10 nm) when comparing toluene solutions to MeOH solutions, and this minimal dependency on solvent polarity was consistent with the assignment of this low-energy band as a π→π* transition with very little charge-transfer character. The nature of this transition was analyzed from TD-DFT calculations, which revealed this low-energy transition as primarily HOMO→LUMO consisting mostly of

formazanate π→π* character. In contrast, the higher-energy visible absorption features were strongly solvatochromic, with a pronounced blue shift as the solvent polarity increased. The absorption maximum shifted by 15 nm or more when the solvent was changed from MeOH to toluene, confirming the assignment of this band as a Pt(d)→C^N(π*) MLCT transition, which is frequently observed in similar regions of the spectrum for other cyclometalated platinum complexes.[36] For example, this band in complex **5a** (Figure 2.6) occurred at 393 nm in toluene and shifted to 382 nm in CH_2Cl_2 and 372 nm in methanol, a range that spanned ~1400 cm^{-1}. Similar trends were observed in all other complexes. The formazanate low-energy HOMO→LUMO transition in the absorption spectra of **1**–**5** did not show any significant dependence on the C^N ligand, but the higher energy visible band attributed to a Pt(d)→C^N(π*) MLCT was sensitive to these substitutions. In complexes with C^N = pq, the red-shifted MLCT band overlapped significantly with the formazanate π→π* band, and strong panchromatic absorption was observed, giving the complexes a very dark blue color in solution in contrast to the rest of the series, which appeared green or bluish green in solution.

The formazanate π→π* band can be perturbed somewhat by introducing substituents onto the periphery. In the cyano-substituted (R^2 position) $Fz^{Me,CN}$ complexes, the low-energy band was blue-shifted by ca. 50 nm relative to the triarylformazanate series. Introducing additional cyano groups to the R^1 positions, i.e. in $Fz^{CN,CN}$ complexes **5a** and **5b**, counteracted this blue shift somewhat, such that the absorption bands for these complexes were intermediate between those of triarylformazanate complexes and the $Fz^{Me,CN}$ complexes. This observation showed that the effect of a particular substituent on

the UV-vis absorption features can depend on the location of that substituent. The perturbation of the formazanate's $\pi \rightarrow \pi^*$ absorption in these platinum complexes was larger than that observed in boron[20,21] or zinc formazanate[27,33] complexes, though in group 10 Ni(II)[10] complexes, similarly large bathochromic shifts were observed. The participation of Pt atomic orbitals in the frontier orbitals was responsible for the large perturbation of the HOMO→LUMO gap when the formazanate was coordinated to platinum. All told, the results described here show that there is some predictive control over the low-energy visible absorption features, which can span a relatively narrow range of 600–665 nm depending on the choice of substituents. Complexes **1**–**5** were non-emissive in the visible region at room temperature and 77 K.

2.2.4 Effect on redox properties

The electrochemical properties of complexes **1**–**5** were investigated by cyclic voltammetry (CV) experiments, and the results are summarized in Table 2.6 with the voltammograms shown in Figure 2.7. The most noteworthy electrochemical features of formazanate complexes are ligand-centered reductions occurring at mild potentials, so most of the discussion is focused on the reduction waves observed in these experiments. The first reduction wave for all 18 complexes was assigned as a formazanate-based one-electron reduction which was in the range of –0.80 to –1.59 V (all potentials referenced to the ferrocenium/ferrocene couple). The reduction potential spanned a wide range for all complexes and was primarily affected by the substituents at the R^1 and R^2 positions of the formazan ligand. The first reduction potentials for **1a**–**1d** were largely similar, fluorination in **1b** induced a small anodic shift (**1b**, E_{red} = −1.44 V) compared to **1a** (**1a**,

E_{red} = −1.49 V). Replacing ppy with either bt (**1c**, E_{red} = −1.49 V) or piq (**1d**, E_{red} = −1.54 V) had minimal effect. Two additional reduction waves were observed, an irreversible wave ranging between −2.06 V and −2.12 V and another reversible feature between −2.34 V and −2.65 V. The third reversible waves were sensitive to the identity of the C^N ligands, hence it was assigned as a Pt-C^N centered reduction.

Table 2.5. Summary of electrochemical data for complexes **1**–**5**[a]

	E^{red} (V)		
	MeCN		CH_2Cl_2
	Fz-centered	Pt-C^N-centered	
1a	–1.49, –2.12[b]	–2.65	–1.60, –2.23[b]
1b	–1.44, –2.09[b]	–2.57	–1.66, –2.31[b]
1c	–1.49, –2.07[b]	–2.43	–1.59, –1.96[b]
1d	–1.54, –2.06[b]	–2.34	–1.62
2a	–1.55, –2.23[b]	–2.66	–1.62, –2.19[b]
2b	–1.50, –2.14[b]	– 2.59	–1.58, –2.24[b]
2c	–1.56, –1.87[b]	–2.44	–1.65, –2.18[b]
2d	–1.59, –2.09[b]	–2.33	–1.67
3a	–1.45, –2.08[b]		–1.55, –2.27[b]
3b	–1.50, –2.07[b]	–2.43	–1.54
3c	–1.42, –2.03[b]	–2.41	–1.52
3d	–1.45, –2.03[b]	– 2.29	–1.56
4a	–1.27, –2.03		–1.40, –2.12[b]
4b	–1.21, –1.98	– 2.66	–1.35, –2.08[b]
4c	–1.27, –2.03[b]	–2.44	–1.38, –2.10[b]
4d	–1.27, –1.99[b]	–2.27	–1.39, –2.16[b]
5a	–0.84, –1.40	–2.61	–0.96, –1.48
5b	–0.80, –1.35	–2.53	–0.88, –1.41[b]

[a] Experiments were performed in the indicated solvent with 0.1 M NBu_4PF_6 electrolyte with scan rate of 0.1 V/s using a glassy carbon working electrode and a silver wire pseudo-reference electrode. Potentials are referenced against the ferrocene/ferrocenium redox couple. [b]Irreversible reduction.

For the series of $Fz^{OMe,PhOme}$ complexes (**2a**–**2d**) the reduction waves displayed similar pattern to the $Fz^{Me,PhOMe}$ complexes. The potential of these waves shifted cathodically when the *p*-methyl group was replaced with the methoxy group at the R^1 position of the formazanate backbone. The second reduction waves for these four complexes were found to be irreversible, where **2c** (**2c**, E_{red} = −1.87 V) was easier to reduce compared to **2a**, **2b**, and **2d**. The third reduction wave was reversible for **2a**–**2d** and complexes **2c/d** reduced at milder potential compared to **2a/b** and similar pattern was also observed in the **1c/d** pair which were easier to reduce compared to **1a/b**. Figure 2.7 showed the first reduction potential for complex **3a** is –1.45 V. Replacing ppy in **3a** with F_2ppy in **3b** induced a small cathodic shift of 50 mV, resulting in a first reduction potential of –1.50 V. Replacing ppy with either bt (**3c**, E_{red} = –1.42 V) or pq (**3d**, E_{red} = –1.45 V) had minimal effect. These potential values were anodically shifted by a small amount from those of more electron-rich $Fz^{Me,PhOMe}$ or $Fz^{Me,PhOMe}$ complexes. The second reduction waves for complexes **3a**–**d** were irreversible with peak potentials that were nearly invariant, ranging between –2.03 and –2.08 V. Another reversible feature was observed for complex **3b**–**d** in the range of – 2.29 and – 2.43 V, while this third reduction wave was absent in **3a**. Introduction of a cyano group directly to the R^2 position in the $Fz^{Me,CN}$ complexes (**4a**–**d**) resulted in a larger anodic shift of the reduction potentials, by ca. 250–300 mV relative to **3a**–**d**. Complex **4a** (C^N = ppy) was reduced at –1.27 V (Figure 2.7) and similar values were observed for complexes **4c** and **4d** (Table 2.6). In this case fluorination of phenylpyridine induced an anodic shift in the reduction potential of complex **4b,** which was easier to reduce at −1.21 V.

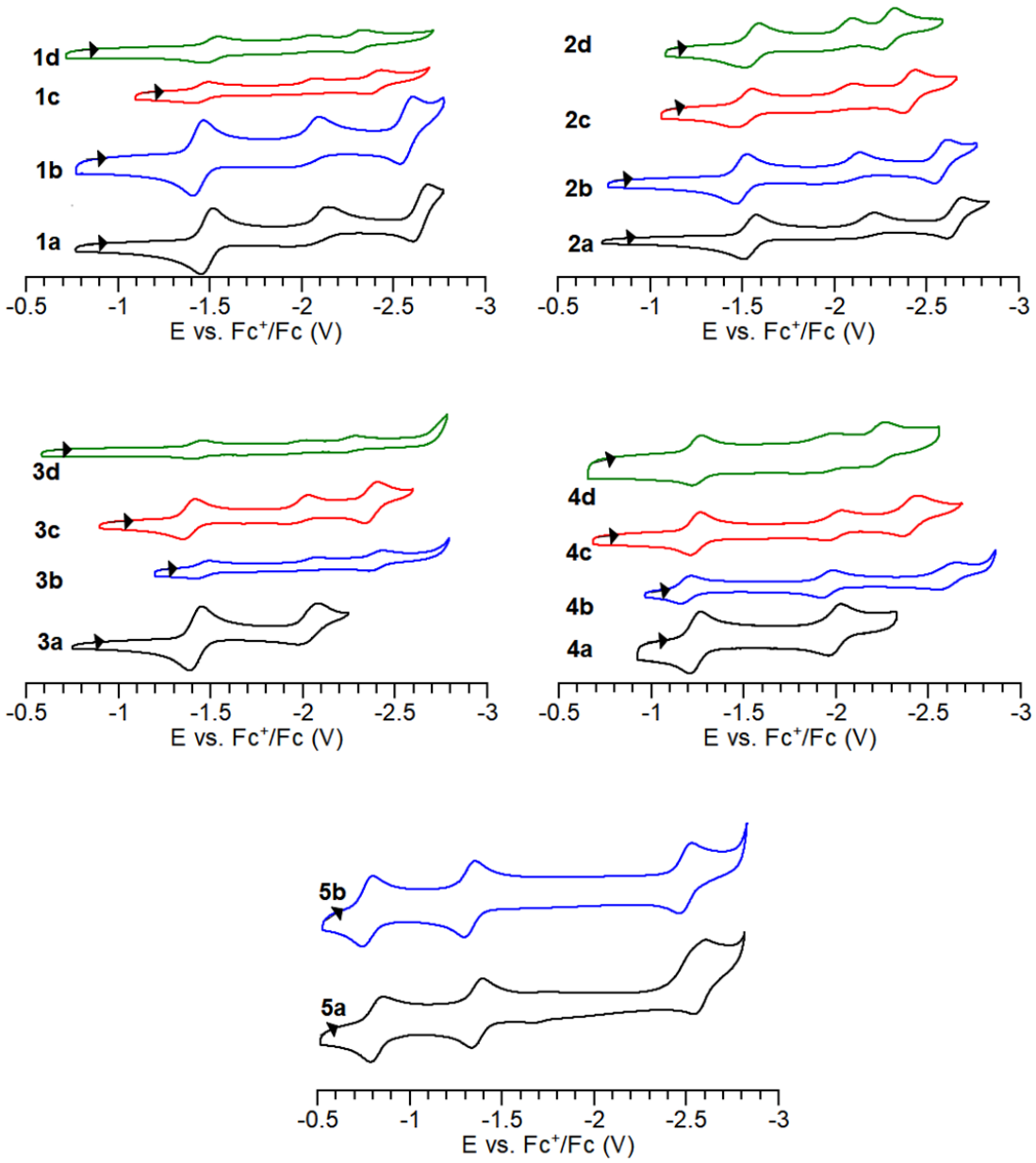

Figure 2.7. Overlaid cyclic voltammograms of complexes **1**–**5**, showing the reduction waves only. CVs were recorded in acetonitrile with 0.1 M NBu_4PF_6 supporting electrolyte, using a glassy carbon working electrode and a scan rate of 0.1 V/s. The arrows indicate the scan direction. Concentrations were not carefully controlled, and currents were low in some of plots because of the limited solubility of some of the compounds in acetonitrile.

Introduction of the electron-withdrawing *p*-benzonitrile substituents at R^1 positions of the formazan ligands along with the cyano group at the R^2 position ($Fz^{CN,CN}$) cathodically decreased the first two reduction potentials even further in complexes **5a** and **5b**. While complex **5a** reduced at −0.84 V, fluorination of C^N ligand resulted in a small anodic shift of 40 mV for the first reduction potential of complex **5b**. The presence of electron-withdrawing cyano groups at the R^1 and R^2 positions made the complexes electron deficient and easy to reduce. The second reduction became reversible for complexes **4a**, **4b**, **5a**, and **5b**, while it was irreversible for rest of the complexes in **1**–**5**. A third reduction was observed in most cases, except for ppy complexes **3a** and **4a** where no third wave was observed inside of the solvent window. In general, this third wave spans a much narrower range of potentials and depends most strongly on the C^N ligand. In F_2ppy complexes (**1b**, **2b**, **3b, 4b**, and **5b**) this third wave occurred between –2.43 and –2.66 V while in all cases the 2-phenylbenzothiazole (bt) and 2-phenylquinoline (pq) complexes were easier to reduce at parity of formazanate ligand.

The oxidation waves of complexes **1**–**5** in acetonitrile were complex and mostly irreversible, and the subsequent reduction peaks after oxidation remained unchanged regardless of the scan direction. We postulated that the source of irreversibility was solvent binding to the oxidized species. To evaluate this possibility, the electrochemical behavior of complex **1**–**5** were also recorded in dichloromethane (CH_2Cl_2) to compare with the cyclic voltammograms recorded in acetonitrile. The first reduction potentials for all 14 complexes exhibited a cathodic shift (~ 100 mV) when measured in CH_2Cl_2 (Table 2.6). A few of the complexes showed a second reduction wave which in most cases was

irreversible, and sweeping to the third reduction potentials was not possible as they were out of the solvent window in CH_2Cl_2. The oxidation waves measured in CH_2Cl_2 became reversible for a few of the complexes. Complexes **1c**, **2c,** and **2d** showed a first reversible oxidation at 0.21 V, 0.10 V, and 0.07 V, respectively, whereas a second reversible oxidation was observed in complexes **2c** and **2d** at 0.75 V and 0.72 V, respectively. Thus, the reversibility of the oxidation waves did improve in some cases, suggesting that solvent binding could play a role in the irreversibility observed in MeCN, but in many cases the electrochemical oxidation was irreversible in both MeCN and CH_2Cl_2.

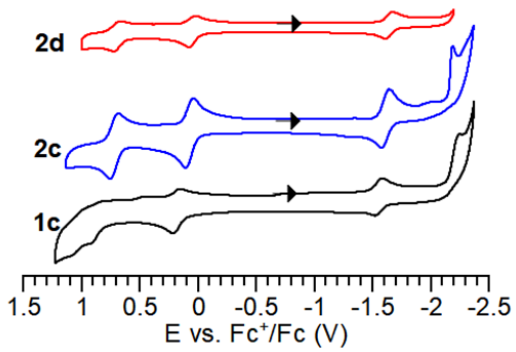

Figure 2.8. Overlaid cyclic voltammograms of complexes **1c**, **2c**, and **2d** in CH_2Cl_2.

To summarize the electrochemical data, all cyclometalated platinum formazanate complexes were investigated by cyclic voltammetry, to determine the effects of structurally and electronically varied C^N ligands and electron-withdrawing groups on the formazanate ligands. The first reversible reduction wave was assigned as a formazanate-centered reduction and its potential was primarily controlled by the structure of the formazanate. The second reduction was assigned as the second formazanate-based reduction, whereas the third wave was assigned to the Pt-C^N fragment. The reduction

potential for this second wave shifted dramatically based on the substituents at R^1 and R^2 positions of the formazanate backbone, whereas the third reversible reductions were less sensitive to these substitutions. Moreover, the separation between the first and second reduction potentials was fairly constant across the series and not too different from the subsequent reduction potentials of some previously reported boron formazanate complexes.[21,37,38] And the potential of the third reduction wave seemed to depend on the identity of the C^N ligand, appearing at more positive potentials in the bt and pq complexes, consistent with the expectation that these more highly conjugated ligands have lower LUMO energies than ppy and F_2ppy. Interestingly we could span a large potential range within this series of heteroleptic Pt formazanate complexes, with electron-withdrawing groups perturbing redox potentials to a much greater extent than they perturb the UV-vis absorption bands. Across the full series of complexes (**1**–**5**) the low-energy absorption bands ranged between 600–665 nm, which was a range of 0.2 eV on an energy scale. In contrast, the first ligand-centered reduction potentials spanned a range of –0.80 to –1.59 V, a difference of 0.79 V, and the second formazanate-based reduction was perturbed by a similar amount across the series. This suggested that the HOMO and LUMO are similarly stabilized when electron-withdrawing groups were introduced, with the HOMO→LUMO gap fairly constant across the series. Consistent with this notion, the oxidation potentials, which were usually irreversible and admittedly less well-defined than the reduction potentials, behaved similarly to the reduction potentials and were anodically shifted by a large amount when electron-withdrawing groups were introduced.

2.2.5 TD-DFT calculations

In order to understand the electronic structure, density functional theory (DFT) calculations were employed for the platinum formazanate complexes. DFT-optimized geometries of the cyclometalated platinum formazanate complexes were good matches for the crystal structures, and the "dragonfly" shape of the formazanate was reproduced.[39] Time-dependent density functional theory (TD-DFT) computations characterized the key electronic transitions of two 1,3,5-triphenylformazanate (FzH,H) models: an unfluorinated complex **6** Pt(ppy) ($Fz^{H,H}$) and a fluorinated derivative **7** Pt(F_2ppy) ($Fz^{H,H}$). Figure 2.9 shows the simulated absorption spectra generated from the TD-DFT results.

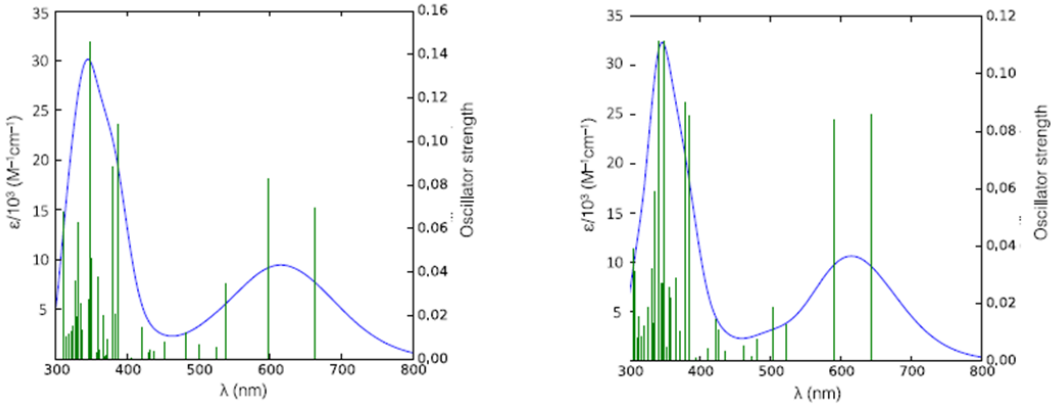

Figure 2.9. simulated absorption spectra for complexes 6 ($PtppyFz^{H,H}$, left) and 7 ($PtF_2ppyFz^{H,H}$, right) computed at B97D/Def2-SVPP//B97D/Def2-TZVPP. Both spectra were generated in the Gaussum 3.0 program, based on TD-DFT results obtained from Gaussian 09.

A HOMO→LUMO transition dominates the one-electron, low-energy excitation of both **6** (86% weight) and **7** (87% weight), and the computed wavelengths (**6**: 677 nm, **7**: 658 nm) agree well with the experimental optical spectra of **2b**. This HOMO→LUMO transition is best described as a formazanate-centered π→π* excitation with some Pt

charge transfer character mixed in. Also, DFT calculations on model complexes **6** and **7** reveal LUMOs that are almost exclusively localized on the formazanate ligand, also suggesting the formazanate as the site of the first reduction event.

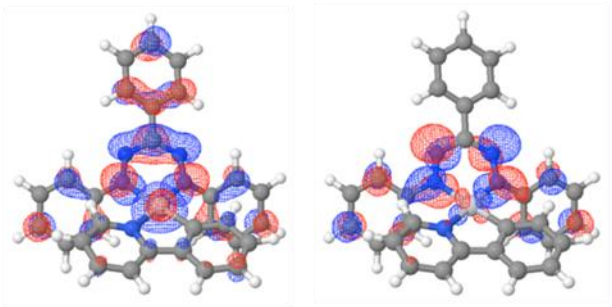

Figure 2.10. Computed HOMO and LUMO contour plots for model complex 6 and 7.

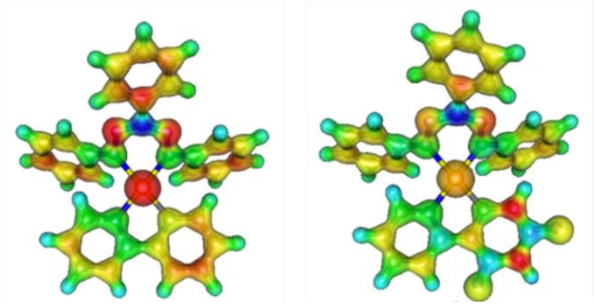

Figure 2.11. Computed MEP plots for the model complexes, 6 and 7, employing the Molekel program (isosurface values were set to 0.1 for illustrative purpose).

As shown in Figure 2.10 the HOMO and LUMO orbitals of **6** showed substantial mixing of the platinum orbitals with the formazanate π-system. Population analyses showed that the HOMO for both **6** and **7** exhibited a ca. 15% contribution from the Pt-centered orbitals (primarily dz2), while the LUMO displayed only ca. 2% Pt character. Direct comparisons of the molecular electrostatic potential (MEP) maps of **6** and **7** (Figure 2.11) revealed that fluorination modestly reduces the electrostatic potential of the Pt center (**6**: V(Pt) = −399.12 V, **7**: V(Pt) = −398.93 V) as well as the nitrogen atoms at

the 2- (**6**: V(N2) = −499.69 V, **7**: V(N2) = −499.53 V) and 4- (**6**: V(N4) = −499.61 V, **7**: V(N4) = −499.54 V) positions of the 1,2,4,5-tetraazapentadienyl core.

2.2.6 Spectroelectrochemistry

To further investigate the nature of the electrochemical features, we investigated the one- and two electron reduction chemistry by UV−vis spectroelectrochemistry. For complex **1a**, electrolysis at −1.8 V vs Fc^+/Fc, which elicits the first reduction event, gave rise to the spectral changes shown in the left side Figure 2.12. The band at 440 nm was minimally affected by reduction. The low-energy absorption band, occurring at 657 nm in this solvent (acetonitrile), disappeared, and new bands at 559 and 950 nm grew in. Reduction of complex **1a** at −2.3 V vs Fc^+/Fc induced a second reduction of the complex. This second reduction resulted in less substantial spectral changes, depicted in the right side of Figure 2.12.

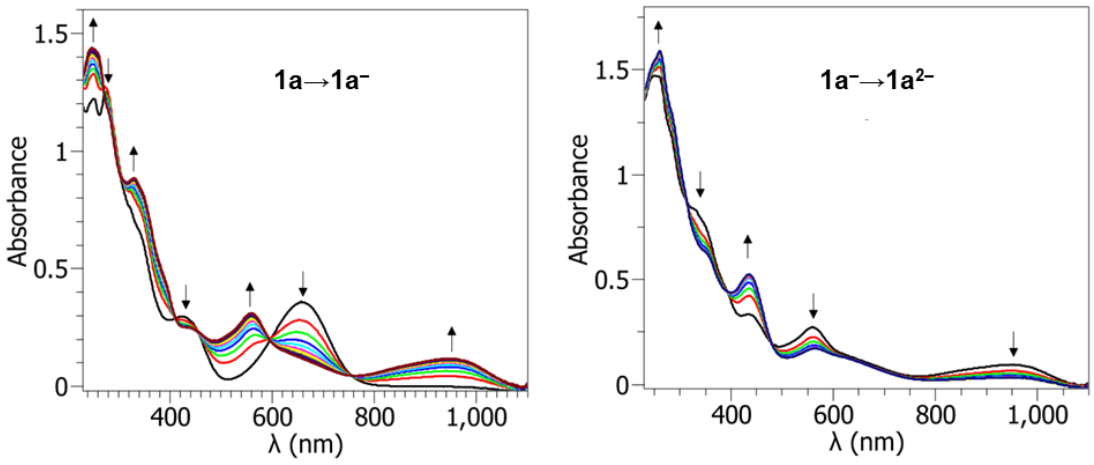

Figure 2.12. UV-vis NIR spectroelectrochemistry of complex **1a** in MeCN with 0.1 M NBu_4PF_6. The applied potential (vs. Fc^+/Fc) was −1.8 V for the first reduction and −2.3 V for the second reduction.

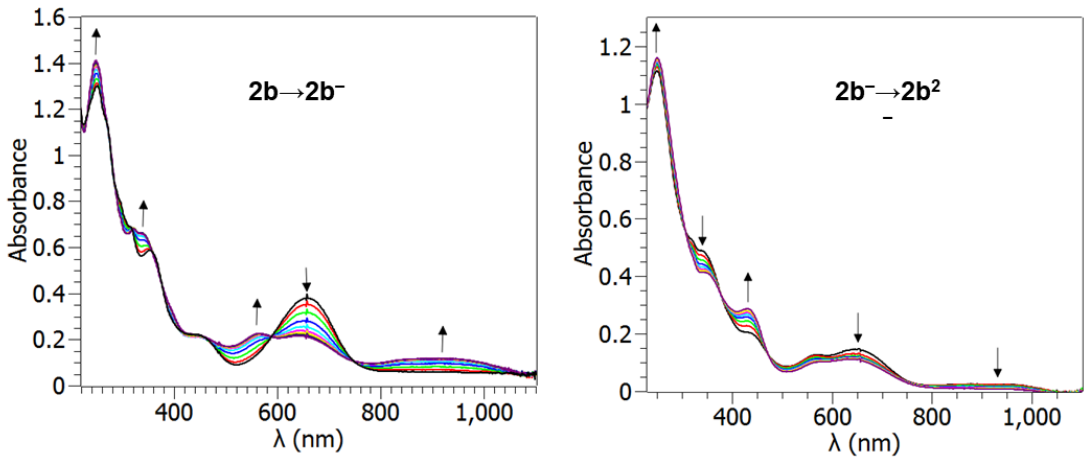

Figure 2.13. UV-vis NIR spectroelectrochemistry of complex **2b** in MeCN with 0.1 M NBu_4PF_6. The applied potential (vs. Fc^+/Fc) was −1.8 V for the first reduction and −2.3 V for the second reduction.

The low-energy transitions attributed to $\mathbf{1a^{\bullet-}}$ diminish slightly in intensity during the second reduction, whereas the band that occurred at 425 nm in **1a** shifted to 435 nm and intensified significantly in the two-electron reduced complex $\mathbf{1a^{2-}}$. Spectroelectrochemistry was also performed on complex **2b**, as shown in Figure 2.13, with a nearly identical outcome to that of complex **1a**. These new features upon applying external potential were entirely consistent with a one-electron reduced formazanate and are qualitatively similar to the absorption bands in other compounds featuring formazanate-derived radical ligands. As described previously, one-electron reduction of zinc[40] and boron[24] formazanate complexes gives rise to two new absorption bands, which resemble the absorption bands of verdazyl radicals. The two new bands flank the π⟶π* band of the closed-shell, monoanionic formazanate,[27] with one growing at higher energy, and one appearing at lower energy. The absorption bands we observed for $\mathbf{1a^{\bullet-}}$ and $\mathbf{2b^{\bullet-}}$, which contained a one-electron reduced verdazyl-type ligand, were substantially red-shifted from those of zinc or boron formazanates and verdazyl radicals, much in the same

manner as the HOMO→LUMO absorption in neutral **1**−**5** undergoes a significant red-shift upon coordination to platinum.

2.3 Conclusion

In this work, we have presented a thorough study of the effects of structurally and electronically modified cyclometalating ligands and formazanate ligands on the properties of heteroleptic platinum complexes containing one of each ligand. A general synthesis was introduced that allows the complexes to form at lower temperature and in shorter times, with moderate to high yields for all complexes. Intense visible absorptions were observed in all complexes and assigned as almost entirely formazanate based π→π* transitions with small Pt-d orbital contribution. A second visible absorption band, assigned to a Pt(d)→C^N(π*) MLCT, could be independently controlled by the structure of the cyclometalating ligand. It was observed that by altering the C^N ligand, and to a lesser extent the formazanate, the absorption properties of these complexes can be tuned, and in some cases panchromatic absorption over the entire visible range was possible. The facile redox chemistry of formazanates was retained in this heteroleptic series, with ligand-based reductions covering a wide range of potentials. The presence of electron withdrawing groups caused anodic shifts in the redox potential, with cathodic shifts noted in with electron-donating groups. The present work implies that the redox and optical properties of cyclometalated Pt formazanate complexes can be tuned extensively by independently varying the C^N and formazanate ligands. These investigations motivate continued pursuits to expand the coordination chemistry of the formazanate ligand class to other third-row transition metals, discover new binding modes and structural motifs

involving formazanate ligands and heavy transition metals, and study their unique redox and photophysical properties.

2.4 Experimental section

2.4.1 Materials

Reactions were carried out in a nitrogen atmosphere using standard Schlenk techniques. Solvents, starting materials, and reagents were of commercial origin and used without further purification, unless stated otherwise below. Dichloromethane and toluene for UV-vis spectroscopy and acetonitrile for electrochemical measurements were dried by the method of Grubbs,[41] passing through dual alumina columns on a commercial solvent purification system (SPS). The acetonitrile was further dried by storage over 3A molecular sieves. Tetrabutylammonium hexafluorophosphate ($TBAPF_6$) was recrystallized from hot ethanol and ferrocene was sublimed at ambient pressure before use in electrochemical experiments. $CDCl_3$ for NMR spectroscopy was stored over potassium carbonate and molecular sieves to remove acidic impurities and moisture. The ligands 3-*p*-methoxyphenyl-1,5-di-*p*-tolylformazan ($Fz^{Me,OMe}$), 1,3,5-tri-*p*-methoxyphenylformazan ($Fz^{OMe,OMe}$), and 3-*p*-cyanophenyl-1,5-di-*p*-tolylformazan ($Fz^{Me,PhCN}$) were prepared by the method of Hicks *et. al*.[39,40] The ligands 3-cyano-1,5-di-p tolylformazan ($Fz^{Me,CN}$), and 3-cyano-1,5-dicyanophenylformazan ($Fz^{CN,CN}$) were prepared by following literature procedures.[25] The platinum precursors $[Pt(ppy)(\mu\text{-}Cl)]_2$ (ppy = 2-phenylpyridine), $[Pt(F_2ppy)(\mu\text{-}Cl)]_2$ (F_2ppy = 2-(2,4-difluorophenyl)pyridine), $[Pt(bt)(\mu\text{-}Cl)]_2$ (bt = 2-phenylbenzothiazole), and $[Pt(pq)(\mu\text{-}Cl)_2]$ (pq = 1-phenylisoquinoline) were prepared as previously described, using conventional heating

and a 1:1 mole ratio of K_2PtCl_4 and the C^N ligand.[42] (*Note*: Many other references describe the syntheses of these dimers, using >2 eq. of C^N with K_2PtCl_4. We have found, as reported in the referenced synthetic procedure, that using excess C^N ligand leads to the formation of substantial amounts of monomeric Pt(κ_2-C^N)(κ_1-N-C^N)(Cl) as a side product.)

2.4.2 Physical Methods

NMR spectra were recorded at room temperature using a JEOL ECA-600 NMR spectrometer. UV–vis absorption spectra were recorded in CH_2Cl_2 solutions in screw-capped quartz cuvettes using an Agilent Cary 60 UV–vis spectrophotometer. Cyclic voltammetry (CV) measurements were performed with a CH Instruments 602E potentiostat interfaced with a nitrogen glovebox via wire feedthroughs. Samples were dissolved in acetonitrile with 0.1 M $TBAPF_6$ as a supporting electrolyte. A 3 mm diameter glassy carbon working electrode, a platinum wire counter electrode, and a silver wire pseudo-reference electrode were used. Potentials were referenced to an internal standard of ferrocene. Spectroelectrochemistry measurements were executed in thin-layer quartz cuvettes, using a patterned "honeycomb" electrode from Pine Research Instrumentation and a silver wire pseudo-reference. Solutions were thoroughly sparged with argon prior to measurement, and spectra were recorded on a Cary 8354 diode array spectrophotometer. Elemental analyses were performed by Midwest Microlab, LLC, and Atlantic Microlab, Inc.

2.4.3 Synthesis

Pt(ppy)(Fz^{Me,OMe}) (1a). [Pt(ppy)(μ-Cl)]$_2$ (100 mg, 0.130 mmol) , Fz^{Me,OMe} (93 mg, 0.26 mmol) and sodium carbonate hydrate (110 mg, 1.04 mmol) were combined in MeOH (12 mL) and the mixture was deoxygenated by bubbling with nitrogen. The mixture was refluxed at 65 ˚C and a color change was observed from deep purple to bright green over the course of refluxing for 16 h. Reaction completion was confirmed from TLC. The methanol was removed via rotary evaporation, and the product was taken up in dichloromethane. The mixture was filtered through a short silica column, eluting with dichloromethane until all of the green color had passed through. The solution was taken to dryness in vacuo. A spectroscopically pure green microcrystalline solid was obtained by adding pentane to a concentrated THF solution. Yield 133.6 mg (70%). Material satisfactory for elemental analysis required recrystallization from CH_2Cl_2/pentane. The crystalline material was spectroscopically and electrochemically indistinguishable from the as-isolated powder. ^{1}H NMR (400 MHz, $CDCl_3$) δ: 8.19 (d, *J* = 8.7 Hz, 2H, ArH), 8.14 (d, *J* = 8.2 Hz, 3H, ArH), 8.00 (d, *J* = 6.8 Hz, 2H, ArH), 7.58–7.67 (m, 2H, ArH), 7.43 (d, *J* = 6.8 Hz, 1H, ArH), 7.15 (d, *J* = 8.4 Hz, 2H, ArH), 7.10 (d, *J* = 8.0 Hz, 2H, ArH), 6.93–6.99 (m, 3H, ArH), 6.80 (t, *J* = 7.2 Hz, 1H, ArH), 6.72 (d, *J* = 6.8 Hz, 1H, ArH), 6.68 (t, *J* = 6.8 Hz, 1H, ArH), 3.87 (s, 3H, OCH_3), 2.38 (s, 6H, CH_3). ^{13}C{^{1}H} NMR: δ 168.5, 159.9, 153.8, 151.1, 150.9, 150.6, 148.0, 145.9, 138.4, 136.86, 136.84, 136.6, 130.1,129.8, 129.2, 129.1, 126.4, 125.8, 124.7, 123.6, 123.0, 121.0, 118.5, 113.7, 55.5, 21.3, 21.2. IR (solid): 3020 (m), 2951 (m), 2924 (m), 2908 (m), 2831 (m), 1607 (s), 1584 (m), 1510 (s), 1494 (s), 1482 (s), 1439 (m), 1427 (m), 1389 (m) cm^{-1}.

Anal. Calcd for $C_{33}H_{29}N_5OPt$: C, 56.09; H, 4.14, N, 9.91. Found: C, 56.32, H, 4.41, N, 9.63.

Pt(F_2ppy)($Fz^{Me,OMe}$) (1b). Prepared by the general method described above for complex **1a**, using 100 mg of $[Pt(F_2ppy)(\mu\text{-}Cl)]_2$ and 85 mg of $Fz^{Me,OMe}$. Yield: 151 mg (85.7%). Recrystallization from CH_2Cl_2/pentane gave the product as **3**·0.5CH_2Cl_2, evident from ^{1}H NMR spectra of the crystals and combustion analysis data. ^{1}H NMR (400 MHz, $CDCl_3$) δ: 8.15–8.19 (m, 3H, ArH), 8.06 (d, J = 8.2 Hz, 2H, ArH), 7.96–8.01 (m, 3H, ArH), 7.69 (t, J = 7.8 Hz, 1H, ArH), 7.11–7.16 (m, 4H, ArH), 6.97–7.01 (m, 2H, ArH), 6.66–6.69 (m, 1H, ArH), 6.37–6.43 (m, 1H, ArH), 6.20 (dd, J = 9.6, 2.4 Hz, 1H, ArH), 3.87 (s, 3H, OCH_3), 2.40 (s, 3H, CH_3), 2.38 (s, 3H, CH_3). $^{13}C\{^1H\}$ NMR: 165.1 (d, J_{CF} = 7.4 Hz), 162.1 (dd, J_{CF} = 343, 12 Hz), 160.4 (dd, J_{CF} = 346, 12 Hz), 160.0, 153.9, 152.8 (d, J_{CF} = 5.9 Hz), 151.0, 150.4, 150.2, 138.9, 137.3, 136.8, 129.9, 129.7, 129.6, 129.2, 126.4, 125.7, 124.7, 122.2 (d, J_{CF} = 21 Hz), 120.9, 118.7 (d, J_{CF} = 16 Hz), 113.8, 99.6 (t, J_{CF} = 27 Hz), 55.5, 21.24, 21.21. IR (solid): 3077 (m), 3023 (m), 3004 (m), 2950 (m), 2922 (m), 2855 (m), 2838 (m), 1601 (s), 1571 (s), 1560 (s), 1513 (s), 1497 (s), 1480 (s), 1427 (s), 1407 (s) cm^{-1}. Anal. Calcd for $C_{33}H_{27}F_2N_5OPt$·0.5CH_2Cl_2: C, 51.25; H, 3.59, N, 8.92. Found: C, 51.44, H, 3.55, N, 8.58.

Pt(bt)($Fz^{Me,PhOMe}$) (1c). $[Pt(bt)(\mu\text{-}Cl)]_2$ (50 mg, 0.056 mmol), $Fz^{Me,PhOMe}$ (41 mg, 0.11 mmol), and triethylamine (45 mg, 0.45 mmol) were combined in dichloromethane (8 mL) and the mixture was refluxed at 40 – 45 °C and a color change was observed from deep purple to bright green over the course of refluxing for 8 h. Reaction completion was confirmed from TLC. The mixture was filtered through a short silica column, eluting

with dichloromethane until all of the green color had passed through. The solution was taken to dryness in vacuo. The product was purified by column chromatography (hexane/ethyl acetate gradient eluent, neutral alumina) and recrystallization (THF/pentane) to afford green crystalline powder. Yield: 52 mg (59%). ^{1}H NMR (400 MHz, $CDCl_3$) δ: 7.97–8.21 (m, 6H, ArH), 7.67 (d, *J* = 7.3 Hz, 1H, ArH), 7.44–7.58 (m, 2H, ArH), 7.12–7.22 (m, 1H, ArH), 6.91–7.11 (m, 8H, ArH), 6.79 (d, *J* = 3.6 Hz, 2H, ArH), 3.89 (s, 3H, OCH_3), 2.37 (s, 3H, CH_3), 2.21 (s, 3H, CH_3). $^{13}C\{^{1}H\}$ NMR (125 MHz, $CDCl_3$): 182.9, 160.0,155.0, 152.6, 150.5, 150.0, 149.0, 142.5, 137.0, 136.8, 136.0, 30.3, 130.0, 129.8, 129.6, 128.9, 126.6, 126.4, 125.7, 125.0, 124.5, 124.3, 123.7, 121.9, 121.2, 113.7, 21.14. IR (Solid): 3056 (m), 2997 (m), 2916 (m), 2840 (m), 1607 (s), 1580 (s), 1566 (s), 15552 (s), 1514(s), 1495 (s), 1447 (s), 1440 (s), 1410 (s), 1394 (s) cm^{-1}. Anal. Calcd for $C_{35}H_{29}N_5OPtS$: C, 55.11; H, 3.83, N, 9.18. Found: C, 54.53, H, 3.87, N, 8.99.

Pt(pq)(Fz^{Me,PhOMe}) (1d). Prepared by the general method described above for complex **1c**, using $[Pt(pq)(\mu\text{-}Cl)]_2$ (100 mg, 0.114 mmol), Fz^{Me,PhOMe} (82 mg, 0.23 mmol), and triethylamine (93 mg, 0.91 mmol). The product was purified by column chromatography (hexane/ethyl acetate gradient eluent, neutral alumina) and recrystallization (THF/pentane) to afford dark blue crystalline powder. Yield: 120 mg (69%). ^{1}H NMR (600 MHz, $CDCl_3$) δ: 8.12 (d, *J* = 8.9 Hz, 3H, ArH), 8.06 (d, *J* = 7.6 Hz, 1H, ArH), 7.91 (d, *J* = 7.6 Hz, 2H, ArH), 7.73–7.83 (m, 3H, ArH), 7.58 (d, *J* = 7.6 Hz, 1H, ArH), 7.47–7.54 (m, 1H, ArH), 7.13–7.22 (m, 2H, ArH), 7.06 (d, *J* = 8.9 Hz, 2H, ArH), 6.95–7.03 (m, 3H, ArH), 6.83 (d, *J* = 7.6 Hz, 1H, ArH), 6.73–6.79 (m, 1H, ArH),

6.68 (d, *J* = 7.6 Hz, 2H, ArH), 3.91 (s, 3H, OCH_3), 2.33 (s, 3H, CH_3), 2.06 (s, 3H, CH_3). $^{13}C\{^1H\}$ NMR (151 MHz, $CDCl_3$): 169.0, 160.0, 154.0, 152.6, 151.6, 151.3, 147.3, 138.6, 137.4, 136.5, 135.8, 130.3, 130.2, 128.8, 128.6, 128.5, 127.2, 126.7, 126.6., 126.5, 126.1, 125.9, 124.4, 124.0, 123.3, 116.4, 113.8, 21.11, 20.88. IR (Solid): 3016 (m), 2988 (m), 2924 (m), 2833 (m), 1604 (s), 1578 (s), 1547 (s), 1511 (s), 1493 (s), 1450 (s), 1437 (s), 1392 (s) cm^{-1}. Anal. Calcd for $C_{37}H_{31}N_5OPt$: C, 58.72; H, 4.13, N, 9.25. Found: C, 58.91, H, 4.32, N, 9.74.

Pt(ppy)($Fz^{OMe,OMe}$) (2a). Prepared by the general method described above for complex **1a**, using 100 mg of $[Pt(ppy)(\mu\text{-}Cl)]_2$ and 101 mg of $Fz^{OMe,OMe}$. Yield: 189 mg (94.0%). ^1H NMR (400 MHz, $CDCl_3$) δ: 8.14–8.25 (m, 5H, ArH), 7.96–8.00 (m, 2H, ArH), 7.58-7.67 (m, 2H, ArH), 7.43 (d, *J* = 7.6 Hz, 1H, ArH), 6.79–6.98 (m, 8H, ArH), 6.66–6.74 (m, 2H, ArH), 3.87 (s, 3H, OCH_3), 3.84 (s, 3H, OCH_3), 3.83 (s, 3H, OCH_3). $^{13}C\{^1H\}$ NMR: 168.6, 159.9, 158.6, 158.4, 153.8, 151.0, 148.1, 147.1, 146.5, 146.0, 138.5, 136.9, 132.4, 130.3, 129.4, 127.0, 126.4, 125.9, 123.7, 123.0, 121.2, 118.6, 114.5, 113.7, 55.79, 55.76, 55.6. IR (solid): 3045 (m), 3000 (m), 2951 (m), 2928 (m), 2907 (m), 2834 (m), 1597 (s), 1582 (s), 1509 (s), 1495 (s), 1483 (s), 1459 (s), 1438 (s) cm^{-1}. Anal. Calcd for $C_{33}H_{29}N_5O_3Pt$: C, 53.66; H, 3.96, N, 9.48. Found: C, 53.68, H, 3.91, N, 9.39.

Pt(F_2ppy)($Fz^{OMe,OMe}$) (**2b**). Prepared by the general method described above for complex **1a**, using 100 mg of $[Pt(F_2ppy)(\mu\text{-}Cl)]_2$ and 93 mg of $Fz^{OMe,OMe}$. Yield: 148 mg (80.4%). ^1H NMR (400 MHz, $CDCl_3$) δ: 8.19–8.22 (m, 3H, ArH), 8.14 (d, *J* = 9.2 Hz, 2H, ArH), 7.97–7.99 (m, 3H, ArH), 7.66–7.70 (m, 1H, ArH), 6.97–7.00 (m, 2H, ArH), 6.85–6.91 (m, 4H, ArH), 6.68–6.72 (m, 1H, ArH), 6.38–6.44 (m, 1H, ArH), 6.23 (dd, *J* =

9.2, 2.2 Hz, 1H, ArH), 3.87 (s, 3H, OCH_3), 3.83 (s, 6H, OCH_3). $^{13}C\{^1H\}$ NMR: 165.2 (d, J_{CF} = 5.9 Hz), 162.2 (dd, J_{CF} = 347, 13 Hz), 160.5 (dd, J_{CF} = 352, 12 Hz), 160.0, 158.9, 158.5, 153.8, 152.9 (d, J_{CF} = 5.9 Hz), 150.9, 146.3, 146.1, 139.0, 129.8, 129.6, 126.9, 126.4, 125.8, 122.3 (d, J_{CF} = 19 Hz), 121.0, 118.7 (d, J_{CF} = 18 Hz), 114.5, 113.83, 113.75, 99.6 (t, J_{CF} = 27 Hz), 55.74, 55.71, 55.5. IR (solid): 3070(m), 3043 (m), 3006 (m), 2938 (m), 2911 (m), 2836 (m), 1598 (s), 1574 (s), 1514 (s), 1494 (s), 1481 (s), 1464 (s), 1451 (s), 1434 (s), 1405 (s) cm^{-1}. Anal. Calcd for $C_{33}H_{27}F_2N_5O_3Pt$: C, 51.16; H, 3.51, N, 9.04. Found: C, 50.98, H, 3.53, N, 8.90.

Pt(bt)($Fz^{OMe,PhOMe}$) (2c). Prepared by the general method described above for complex **1c**, using $[Pt(bt)(\mu\text{-}Cl)]_2$ (100 mg, 0.113 mmol), $Fz^{OMe,PhOMe}$ (88 mg, 0.23 mmol), and triethylamine (91 mg, 0.90 mmol). The product was purified by column chromatography (hexane/ethyl acetate gradient eluent, neutral alumina) and recrystallization (THF/pentane) to afford green crystalline powder. Yield: 80 mg (45%). ^1H NMR (400 MHz, $CDCl_3$) δ: 8.19 (d, *J* = 8.7 Hz, 2H, ArH), 8.02–8.14 (m, 4H, ArH), 7.67 (d, *J*= 7.8 Hz, 1H, ArH), 7.51 (dd, *J*= 8.0, 14 Hz, 2H, ArH), 7.18 (t, *J*= 7.8 Hz, 1H, ArH), 6.92–7.07 (m, 4H, ArH), 6.76–6.88 (m, 4H, ArH), 6.71 (d, *J*= 9.1 Hz, 2H, ArH), 3.89 (s, 3H, OCH_3), 3.81 (s, 3H, OCH_3), 3.70 (s, 3H, OCH_3). $^{13}C\{^1H\}$ NMR (151 MHz, $CDCl_3$): 182.8, 160.0, 158.5, 157.8, 154.8, 150.1, 148.5, 148.7, 146.5, 142.5, 137.0, 130.3, 130.1, 129.1, 126.6, 126.5, 125.1, 124.5, 123.7, 122.0, 121.1, 114.3, 113.7, 113.5, 55.65, 55.59, 55.47. IR (Solid): 2964 (m), 2903 (m), 2825 (m), 1637 (m), 1599 (s), 1580 (s), 1558 (s), 1511 (s), 1496 (s), 1437 (s), 1412 (m), 1392 (s) cm^{-1}. Anal. Calcd for $C_{35}H_{29}N_5O_3PtS$: C, 52.89; H, 3.68, N, 8.81. Found: C, 52.16, H, 3.78, N, 8.74.

Pt(pq)(Fz^{OMe,PhOMe}) (2d). Prepared by the general method described above for complex **1c**, using [Pt(pq)(μ-Cl)]$_2$ (100 mg, 0.114 mmol), Fz^{OMe,PhOMe} (89 mg, 0.23 mmol), and triethylamine (93 mg, 0.91 mmol) to afford dark blue crystalline powder. Yield: 109 mg (61%). ^{1}H NMR (400 MHz, $CDCl_3$) δ: 8.02–8.18 (m, 4H, ArH), 7.97 (d, *J* = 8.2 Hz, 2H, ArH), 7.86 (d, *J* = 9.2 Hz, 2H, ArH), 7.78 (d, *J* = 9.2 Hz, 1H, ArH), 7.60 (d, *J* = 7.3 Hz, 1H, ArH), 7.47–7.54 (m, 1H, ArH), 7.15–7.24 (m, 2H, ArH), 7.05–7.12 (m, 2H, ArH), 6.96–7.03 (m, 1H, ArH), 6.68–6.89 (m, 4H, ArH), 6.43 (d, *J*= 9.6 Hz, 2H, ArH), 3.92 (s, 3H, OCH_3), 3.79 (s, 3H, OCH_3), 3.60 (s, 3H, OCH_3). ^{13}C{^{1}H} NMR (151 MHz, $CDCl_3$): 169.0, 160.0, 158.3, 157.7, 154.0, 152.7, 147.7, 147.5, 147.2, 147.1, 138.1, 137.4, 130.3, 128.7, 127.3, 126.7, 126.6, 126.0, 125.1, 124.5, 123.4, 116.4, 113.7, 113.6, 113.3, 55.6, 55.52, 55.50. IR (Solid): 3049 (m), 3002 (m), 2995 (m), 2832 (m), 1596 (s), 1579 (s), 1547 (s), 1513 (s), 1495 (s), 1461 (s), 1451 (s), 1439 (s), 1390 (s) cm^{-1}. Anal. Calcd for $C_{37}H_{31}N_5O_3Pt$: C, 56.34; H, 3.96, N, 8.88. Found: C, 56.34, H, 4.11, N, 9.17.

Pt(ppy)(Fz^{Me,PhCN}) (3a). Prepared by the general method described above for complex **1c**, using [Pt(ppy)(μ-Cl)]$_2$ (50 mg, 0.065 mmol), Fz^{Me,PhCN} (46 mg, 0.13 mmol) and triethylamine (55 mg, 0.52 mmol) to afford pure green microcrystalline solid. Yield: 144 mg (78%). ^{1}H NMR (600 MHz, $CDCl_3$) δ: 8.09–8.08 (m, 6H, ArH), 8.02 (d, *J* = 6.2 Hz, 1H, ArH), 7.69 (d, *J* = 8.3 Hz, 2H, ArH), 7.64–7.67 (m, 1H, ArH), 7.59 (d, *J* = 7.6 Hz, 1H, ArH), 7.41 (d, *J* = 8.3 Hz, 1H, ArH), 7.18 (d, *J* = 7.6 Hz, 2H, ArH), 7.13 (d, *J* = 7.6 Hz, 2H, ArH), 6.95 (t, *J* = 7.6 Hz, 1H, ArH), 6.78 (t, *J* = 7.6 Hz, 1H, ArH), 6.62–6.67 (m, 2H, ArH), 2.39 (s, 6H, CH_3). ^{13}C{^{1}H} NMR (151 MHz, $CDCl_3$) δ: 168.5, 152.0,

150.8. 150.2, 146.9, 145.9, 141.9, 138.7, 137.8, 137.6, 136.7, 132.0, 130.3, 130.0, 129.3, 129.2, 125.9, 124.9, 124.7, 124.0, 123.0, 121.1, 119.8, 119.0, 118.6, 110.2, 21.29, 21.25. IR (Solid): 3014 (m), 2919 (m), 2857 (m), 2260 (m), 1603 (s), 1585 (s), 1546 (s), 1496(s), 1481 (s), 1438 (s), 1427 (s), 1383 (s) cm^{-1}. Anal. Calcd for $C_{33}H_{26}N_6Pt$: C, 56.49; H, 3.73, N, 11.98. Found: C, 56.60, H, 4.04, N, 12.29.

Pt(F_2ppy)($Fz^{Me,PhCN}$) (3b). Prepared by the general method described above for complex **1c**, using $[Pt(F_2ppy)(\mu\text{-}Cl)]_2$ (50 mg, 0.059 mmol), $Fz^{Me,PhCN}$ (42 mg, 0.12 mmol), and triethylamine (48 mg, 0.47 mmol) to afford green crystalline powder. Yield: 78 mg (89%). ^{1}H NMR (400 MHz, $CDCl_3$) δ: 8.04–8.17 (m, 7H, ArH), 7.99 (d, *J* = 8.7 Hz, 1H, ArH), 7.66–7.74 (m, 3H, ArH), 7.17 (dd, *J* = 8.0, 14.2 Hz, 4H, ArH), 6.65–6.71 (m, 1H, ArH), 6.64–6.72 (m, 1H, ArH), 6.11 (dd, *J* = 9.6, 2.3 Hz, 1H, ArH), 2.46 (s, 3H, CH_3) 2.40 (s, 3H, CH_3). $^{13}C\{^1H\}$ NMR (151 MHz, $CDCl_3$) δ: 165.1 (d, J_{CF} = 7.4 Hz), 162.3 (dd, J_{CF} = 11.8, 255.8 Hz), 160.0 (dd, J_{CF} = 13.3, 259.5 Hz), 152.1, 151.7 (d, J_{CF} = 7.8 Hz), 150.9, 150.2, 149,8, 141.5, 139.2, 138.3, 137.8, 130.1, 129.6, 129.3, 125.8, 125.0, 124.8, 122.3, (d, J_{CF} = 20 Hz), 121.0, 119.7, 118.6 (d, J_{CF} = 19 Hz), 110.5, 99.9 (t, J_{CF} = 26 Hz), 21.3, 21.2. ^{19}F NMR (564 MHz, $CDCl_3$) ^{19}F NMR (564 MHz, $CDCl_3$) δ: –107.09 (q, *J* = 9.6 Hz, 1F), –111.09 (t, *J* = 11.3 Hz, 1F). IR (Solid): 3080 (m), 3017 (m), 2920 (m), 2859 (m), 2224 (m), 1604 (s), 1576 (s), 1561 (s), 1497 (s), 1481 (s), 1429 (s), 1407 (s) cm^{-1}. Anal. Calcd for $C_{33}H_{24}F_2N_6Pt.0.2CH_2Cl_2$: C, 52.84; H, 3.26, N, 11.20. Found: C, 53.05, H, 3.50, N, 11.49.

Pt(bt)($Fz^{Me,PhCN}$) (3c). Prepared by the general method described above for complex **1c**, using $[Pt(bt)(\mu\text{-}Cl)]_2$ (100 mg, 0.113 mmol), $Fz^{Me,PhCN}$ (80 mg, 0.23 mmol),

and triethylamine (91 mg, 0.90 mmol) to afford green crystalline powder. The product was purified by column chromatography (hexane/ethyl acetate gradient eluent, neutral alumina) and recrystallization (THF/pentane). Yield: 81 mg (47%). ^{1}H NMR (400 MHz, $CDCl_3$) δ: 8.22 (d, *J* = 6.9 Hz, 2H, ArH), 8.14 (d, *J* = 8.2 Hz, 2H, ArH), 8.01 (d, *J* = 7.8 Hz, 2H, ArH), 7.71–7.77 (m, 2H, ArH), 7.68 (d, *J* = 7.8 Hz, 1H, ArH), 7.50–7.56 (m, 1H, ArH), 7.38 (d, *J* = 8.7 Hz, 1H, ArH), 7.15–7.22 (m, 1H, ArH), 7.09 (d, *J* = 7.8 Hz, 2H, ArH), 6.95–7.03 (m, 4H, ArH), 6.66–6.83 (m, 2H, ArH), 2.38 (s, 3H, CH_3), 2.22 (s, 3H, CH_3). ^{13}C{^{1}H} NMR (151 MHz, $CDCl_3$): 183.1, 153.2, 152.3, 150.5, 149.1, 148.6, 142.5, 141.5, 137.7, 136.8, 132.1, 130.2, 130.1, 29.1, 126.4, 125.3, 125.1, 124.6, 12.0, 122.1, 120.8, 119.8, 110.6, 21.22, 21.15. IR (Solid): 3058 (m), 3019 (m), 2916 (m), 2854 (m), 2221 (s), 1603 (s), 1580 (s), 1552 (s), 1495 (s), 1471 (s), 1448 (s), 1410 (s), 1381 (s) cm^{-1}. Anal. Calcd for $C_{35}H_{26}N_6PtS$: C, 55.48; H, 3.46, N, 11.09. Found: C, 55.05, H, 3.75, N, 11.43.

Pt(pq)(Fz^{Me,PhCN}) (3d). Prepared by the general method described above for complex **1c**, using $[Pt(pq)(\mu\text{-}Cl)]_2$ (50 mg, 0.057 mmol), Fz^{Me,PhCN} (40 mg, 0.11 mmol), and triethylamine (46 mg, 0.46 mmol) to afford dark green crystalline powder. Yield: 69 mg (81%). ^{1}H NMR (400 MHz, $CDCl_3$) δ: 8.23–8.30 (m, 2H, ArH), 8.16 (d, *J*= 8.2 Hz, 1H, ArH), 7.93–7.99 (d, 1H, ArH), 7.89 (d, *J*= 8.2 Hz, 2H, ArH), 7.73–7.84 (m, 5H, ArH), 7.49–7.62 (m, 2H, ArH), 7.15–7.23 (m, 2H, ArH), 6.96–7.07 (m, 3H, ArH), 6.72 (dd, *J*= 5.9, 19 Hz, 4H, ArH), 2.35 (s, 3H, CH_3), 2.08 (s, 3H, CH_3). ^{13}C{^{1}H} NMR (151 MHz, $CDCl_3$): 169.1, 152.2, 151.7, 151.4, 151.2, 147.5, 147.1, 142.0, 139.0, 137.4, 137.3, 136.8, 132.1, 10.4, 130.2, 128.9, 128.8, 128.6, 127.3, 126.7, 126.1, 126.0, 125.2,

124.6, 124.1, 123.7, 119.9, 119.0, 116.4, 124.6, 123.7, 119.9, 119.0, 116.4, 110.4, 21.12,20.93. IR (Solid): 3048 (m), 2917 (m), 2855 (m), 2220 (m), 1602 (s), 1578 (s), 1548 (s), 1515 (s), 1495 (s), 1448 (s), 1425 (s), 1382 (s) cm^{-1}. Anal. Calcd for $C_{37}H_{28}N_6Pt$: C, 59.12; H, 3.75, N, 11.18. Found: C, 58.87, H, 3.94, N, 11.83.

Pt(ppy)($Fz^{Me,CN}$) (4a). Prepared by the general method described above for complex **1c**, using $[Pt(ppy)(\mu\text{-}Cl)]_2$ (100 mg, 0.130 mmol), $Fz^{Me,CN}$ (72 mg, 0.26 mmol), and triethylamine (105 mg, 1.04 mmol) to afford greenish blue crystalline powder. Yield: 129 mg (80%). ^{1}H NMR (400 MHz, $CDCl_3$) δ: 7.91–8.10 (m, 4H, ArH), 7.77 (d, *J* = 5.5 Hz, 1H, ArH), 7.51–7.71 (m, 2H, ArH), 7.34–7.45 (m, 1H, ArH), 7.15 (dd, *J* = 8.2, 24.73 Hz, 4H, ArH), 6.87–6.99 (m, 1H, ArH), 6.65–6.78 (m, 1H, ArH), 6.55–6.64 (m, 1H, ArH), 6.40 (d, *J* = 7.3 Hz, 1H, ArH), 2.40 (s, 3H, CH_3), 2.39 (s, 3H, CH_3). $^{13}C\{^1H\}$ NMR (151 MHz, $CDCl_3$): 168.4, 150.7, 150.4, 149.3, 145.9, 145.0, 139.0, 136.7, 134.0, 130.1, 129.2, 129.1, 126.0, 124.8, 124.3, 123.0, 121.0, 118.7, 118.4, 21.33, 21.28. IR (Solid): 3048 (m), 3029 (m), 2918 (m), 2857 (m), 2227 (m), 1608 (s), 1584 (s), 1564 (s), 1499 (s), 1483 (s), 1438 (s), 1427 (s) cm^{-1}. Anal. Calcd for $C_{27}H_{22}N_6Pt$: C, 51.84; H, 3.54, N, 13.43. Found: C, 52.12, H, 3.72, N, 13.29.

Pt(F2ppy)(FzMe,PhCN) (4b). Prepared by the general method described above for complex **1c**, using $[Pt(F_2ppy)(\mu\text{-}Cl)]_2$ (50 mg, 0.059 mmol), $Fz^{Me,PhCN}$ (42 mg, 0.12 mmol), and triethylamine (48 mg, 0.47 mmol) to afford green crystalline powder. Yield: 78 mg (89%). ^{1}H NMR (400 MHz, CDCl3) δ: 8.04−8.17 (m, 7H, ArH), 7.99 (d, *J* = 8.7 Hz, 1H, ArH), 7.66−7.74 (m, 3H, ArH), 7.17 (dd, *J* = 8.0, 14.2 Hz, 4H, ArH), 6.65−6.71 (m, 1H, ArH), 6.64−6.72 (m, 1H, ArH), 6.11 (dd, *J* = 9.6, 2.3 Hz, 1H, ArH), 2.46 (s, 3H,

CH3) 2.40 (s, 3H, CH3). $^{13}C\{^{1}H\}$ NMR (151 MHz, $CDCl_3$) δ: 165.1 (d, J_{CF} = 7.4 Hz), 162.3 (dd, J_{CF} = 11.8, 255.8 Hz), 160.0 (dd, J_{CF} = 13.3, 259.5 Hz), 152.1, 151.7 (d, J_{CF} = 7.8 Hz), 150.9, 150.2, 149,8, 141.5, 139.2, 138.3, 137.8, 130.1, 129.6, 129.3, 125.8, 125.0, 124.8, 122.3, (d, J_{CF} = 20 Hz), 121.0, 119.7, 118.6 (d, J_{CF} = 19 Hz), 110.5, 99.9 (t, J_{CF} = 26 Hz), 21.3, 21.2. ^{19}F NMR (564 MHz, $CDCl_3$) δ: −107.09 (q, J = 9.6 Hz, 1F), −111.09 (t, J = 11.3 Hz, 1F). IR (Solid): 3080 (m), 3017 (m), 2920 (m), 2859 (m), 2224 (m), 1604 (s), 1576 (s), 1561 (s), 1497 (s), 1481 (s), 1429 (s), 1407 (s) cm−1. Anal. Calcd for $C_{33}H_{24}F_2N_6Pt.0.2CH_2Cl_2$: C, 52.84; H, 3.26, N, 11.20. Found: C, 53.05, H, 3.50, N, 11.49.

Pt(bt)($Fz^{Me,CN}$) (4c). Prepared by the general method described above for complex **1c**, using $[Pt(bt)(\mu\text{-}Cl)]_2$ (50 mg, 0.057 mmol), $Fz^{Me,CN}$ (32 mg, 0.11 mmol), and triethylamine (46 mg, 0.46 mmol) to afford green crystalline powder. Yield: 37 mg (48%). ^{1}H NMR (600 MHz, $CDCl_3$) δ: 7.97 (d, J = 8.2 Hz, 2H, ArH), 7.83 (d, J = 7.6 Hz, 2H, ArH), 7.61 (d, J = 8.2 Hz, 1H, ArH), 7.46 (d, J = 7.6 Hz, 1H, ArH), 7.02–7.18 (m, 4H, ArH), 6.86–7.01 (m, 4H, ArH), 6.69 (t, J = 7.6 Hz, 1H, ArH), 6.41 (d, J = 8.2 Hz, 1H, ArH), 2.37 (s, 3H, CH_3), 2.17 (s, 3H, CH_3). $^{13}C\{^{1}H\}$ NMR (151 MHz, $CDCl_3$): 183.0, 151.5, 150.2,147.9, 147.5, 142.6, 139.0, 138.5, 136.8, 134.8, 129.8, 129.7, 129.1, 126.4, 126.0, 125.2, 124.7, 124.5, 124.4, 122.1, 120.3, 118.3, 21.26, 21.15. IR (Solid): 3060 (m), 3026 (m), 2917 (m), 2855 (m), 2227 (s), 1581 (m), 1566 (m), 15551(m), 1498 (s), 1470 (s), 1447 (s), 1411 (s) cm^{-1}. Anal. Calcd for $C_{29}H_{22}N_6PtS$: C, 51.10; H, 3.25, N, 12.23. Found: C, 51.46, H, 3.48, N, 12.24.

Pt(pq)($Fz^{Me,CN}$) (4d). Prepared by the general method described above for complex **1c**, using $[Pt(pq)(\mu\text{-}Cl)]_2$ (100 mg, 0.114 mmol), $Fz^{Me,CN}$ (63 mg, 0.23 mmol), and triethylamine (92 mg, 0.91 mmol) to afford dark blue crystalline powder. Yield: 127 mg (82%). ^{1}H NMR (400 MHz, $CDCl_3$) δ: 8.14 (d, *J* = 8.7 Hz, 1H, ArH), 7.71–7.84 (m, 4H, ArH), 7.63 (d, *J* = 8.2 Hz, 2H, ArH), 7.45–7.59 (m, 2H, ArH), 7.12–7.23 (m, 2H, ArH), 6.92–7.08 (d, 3H, ArH), 6.58–6.73 (m, 3H, ArH), 6.41–6.58 (m, 1H, ArH), 2.35 (s, 3H, CH_3), 2.06 (s, 3H, CH_3). $^{13}C\{^1H\}$ NMR (151 MHz, $CDCl_3$) δ: 169.1, 150.8, 150.4, 150.3, 147.7, 146.8, 139.4, 138.6, 138.1, 137.3, 134.0, 130.8, 128.9, 128.8, 128.5, 127.3, 126.5, 126.2, 125.3, 124.6, 124.2, 124.1, 118.5, 116.3, 21.22, 20.94. IR (Solid): 3047 (m), 3023 (m), 2922 (m), 2223 (s), 1604 (s), 1590 (s), 1580 (s), 1566 (s), 1515 (s), 1498 (s), 1451 (s), 1437 (s), 1428 (s), 1411 (s) cm^{-1}. Anal. Calcd for $C_{31}H_{24}N_6Pt$: C, 55.11; H, 3.58, N, 12.44. Found: C, 54.56, H, 3.73, N, 12.28.

Pt(ppy)($Fz^{CN,CN}$) (5a). Prepared by the general method described above for complex **1c**, using $[Pt(ppy)(\mu\text{-}Cl)]_2$ (50 mg, 0.065 mmol), $Fz^{CN,CN}$ (39 mg, 0.13 mmol), and triethylamine (53 mg, 0.520 mmol) to afford greenish blue crystalline powder. Yield: 37 mg (74%). ^{1}H NMR (400 MHz, $CDCl_3$) δ: 8.19–8.33 (m, 4H, ArH), 7.56–7.82 (m, 7H, ArH), 7.38–7.46 (m, 1H, ArH), 6.92–7.04 (m, 1H, ArH), 6.63–6.79 (m, 2H, ArH), 6.18–6.32 (m, 1H, ArH). $^{13}C\{^1H\}$ NMR (151 MHz, $CDCl_3$): 168.5, 156.2, 154.6, 150.2, 146.0, 145.2, 143.3, 140.0, 136.2, 135.7, 135.1, 133.5, 132.7, 129.5, 126.8, 125.5, 125.1, 123.5, 121.4, 119.2, 118.2, 118.1, 116.6, 112.4, 112.1. IR (Solid): 3093 (m), 3065 (m), 3042 (m), 2233 (s), 2220 (s), 1609 (s), 1595 (s), 1585 (s), 1560 (s), 1489 (s), 1439

(s), 1420 (s) cm^{-1}. Anal. Calcd for $C_{27}H_{16}N_8Pt$: C, 50.08; H, 2.49, N, 17.30. Found: C, 49.83, H, 2.69, N, 17.11.

Pt(F_2ppy)($Fz^{CN,CN}$) (5b). Prepared by the general method described above for complex **1c**, using $[Pt(F_2ppy)(\mu\text{-}Cl)]_2$ (50 mg, 0.059 mmol), $Fz^{CN,CN}$ (36 mg, 0.12 mmol), and triethylamine (53 mg, 0.52 mmol) to afford greenish blue crystalline powder. Yield: 45 mg (71%). ^{1}H NMR (400 MHz, $CDCl_3$) δ: 8.17–8.32 (m, 4H, ArH), 8.04 (d, *J* = 8.2 Hz, 1H, ArH), 7.60–7.84 (m, 6H, ArH), 6.68–6.79 (m, 1H, ArH), 6.38–6.53 (m, 1H, ArH), 5.74 (dd, *J*= 2.3, 9.2Hz, 1H, ArH). $^{13}C\{^1H\}$ NMR (151 MHz, $CDCl_3$) δ: 165.2 (d, J_{CF} = 19.2 Hz), 161.8 (dd, J_{CF} = 6.0, 309.7 Hz), 160.1 (dd, J_{CF} = 11.8, 319.4 Hz), 154.6, 154.2, 150.3, 147.3, 140.5, 135.8, 133.6, 123.8, 129.7, 126.8, 125.5, 122.8 (d, J_{CF} = 20.7 Hz), 121.3, 118.6 (d, J_{CF} = 20.7 Hz), 117.9, 116.5, 112.8, 112.3, 101.3 (t, *J* = 26.6 Hz). ^{19}F NMR (564 MHz, $CDCl_3$) δ: –105.17 (q, *J* = 9.4 Hz, 1F), –109.56 (t, *J* = 11.0 Hz, 1F). IR (Solid): 3139 (m), 3091 (m), 3059 (m), 2228 (s), 1715 (s), 1597 (s), 1577 (s), 1564 (s), 1526 (s), 1488 (s), 1427 (s), 1412 (s), 1375 (s) cm^{-1}. Anal. Calcd for $C_{27}H_{14}F_2N_8Pt.0.4CH_2Cl_2$: C, 45.87; H, 2.08, N, 15.62. Found: C, 46.14, H, 2.36, N, 15.25.

2.4.4 X-ray crystallography details

Single crystals of **1a**, **1b**, **2a**, **2c**, **3a**, **3d**, **4a** – **4c**, and **5b** were grown by layering concentrated CH_2Cl_2 solutions with pentane or diffusing pentane into concentrated THF or $CHCl_3$ solution. Crystals were mounted on a Bruker Apex II three-circle diffractometer using MoKα radiation (λ = 0.71073 Å). The data were collected at 213(2) K (**1a**) or 123(2) K and were processed and refined within the APEXII software.

Structures were solved by direct methods in SHELXS and refined by standard difference Fourier techniques in the program SHELXL.[43] Hydrogen atoms were placed in calculated positions using the standard riding model and refined isotropically. All non-hydrogen atoms were refined anisotropically. The crystal of **1a** was found to be partially desolvated; one dichloromethane was modeled as half-occupied, and a second was modeled as a two-part disorder about a special position with total one-half occupancy. The structure of **1b** contained a heavily disordered solvent molecule, likely dichloromethane, which was removed using the SQUEEZE function within Platon. The structure of **5b** included a disordered CH_2Cl_2 molecule, modeled as two-part positional disorder. Distance restraints (SADI) were used for all 1,2 and 1,3 distances within the disordered parts, and rigid bond restraints SIMU and DELU were employed for the thermal displacement parameters. Crystallographic details are summarized in Tables 2.7–2.10. All of the crystal structures were solved by Dr. Thomas S. Teets, Department of Chemistry at University of Houston.

Table 2.6. Summary of crystallographic data for complexes **1a**, **1b** and **2a**

	1a·0.375CH_2Cl_2	**1b·CH_2Cl_2**	**2a**
Chemical formula	$C_{33.38}H_{29.75}Cl_{0.75}N_5OPt$	$C_{33}H_{27}F_2N_5OPt$	$C_{34}H_{31}Cl_2N_5O_3Pt$
M_r	738.55	742.68	823.63
Crystal system, space group	Monoclinic, $P2_1/c$	Triclinic, $P\bar{1}$	Monoclinic, $P2_1/c$
a, *b*, *c* (Å)	15.2681 (11), 23.2426 (15), 17.6927 (12)	11.104 (3), 11.535 (3), 13.956 (4)	16.384 (4), 11.205 (3), 17.922 (4)
a, b, g (°)	90.2117 (12)	95.274 (3), 100.098 (3), 113.620 (3)	90, 105.605 (3), 90
V (Å^3)	6278.6 (7)	1586.0 (7)	3168.9 (13)
Z	8	2	4
m (mm^{-1})	4.57	4.47	4.64
Crystal size (mm)	0.30 × 0.15 × 0.10	0.25 × 0.25 × 0.15	0.50 × 0.35 × 0.10
T_{min}, T_{max}	0.517, 0.746	0.608, 0.746	0.533, 0.746
No. of measured, independent and observed [I > 2s(I)] reflections	47399, 17145, 13872	10339, 7686, 7270	19810, 7957, 6663
R_{int}	0.014	0.013	0.027
(sin q/l)$_{max}$ (Å^{-1})	0.735	0.691	0.690
$R[F^2 > 2s(F^2)]$, $wR(F^2)$, S	0.035, 0.101, 1.10	0.023, 0.057, 1.04	0.032, 0.097, 1.10
No. of reflections	17145	7686	7957
No. of parameters	781	382	409
Dρ$_{max}$, Dρ$_{min}$ (e Å^{-3})	3.05, -2.45	2.68, -1.13	3.67, -1.83
No. of restraints	43		

Table 2.7. Summary of crystallographic data for complexes **2c**, **3a** and **3d**

	2c	**3a**	**3d•**$CHCl_3$
CCDC	1843720	1843715	1843716
Chemical formula	$C_{35}H_{28}N_5O_3PtS$	$C_{33}H_{26}N_6Pt$	$C_{38}H_{29}Cl_3N_6Pt$
M_r	793.77	701.69	871.11
Crystal system, space group	Orthorhombic, *Pbca*	Triclinic, $P\bar{1}$	Monoclinic, $P2_1/c$
a, *b*, *c* (Å)	18.589 (7), 14.609 (6), 22.553 (8)	7.907 (2), 11.456 (3), 15.692 (5)	10.9414 (11), 11.8155 (12), 26.524 (3)
α, β, γ (°)	90, 90, 90	105.324 (3), 94.331 (4), 101.480 (4)	90, 91.3728 (13), 90
V (Å^3)	6125 (4)	1331.1 (7)	3428.0 (6)
Z	4.70	2	4
μ (mm^{-1})	0.25 × 0.16 × 0.10	5.31	4.37
Crystal size (mm)	0.598, 0.746	0.30 × 0.22 × 0.10	0.49 × 0.19 × 0.10
T_{min}, T_{max}	35665, 7008, 5659	0.514, 0.746	0.406, 0.746
No. of measured, independent and observed [$I > 2\sigma(I)$] reflections	0.031	5805, 5805, 5692	20998, 7911, 7269
R_{int}	0.649	0.026	0.025
$(\sin\theta/\lambda)_{max}$ (Å^{-1})	0.046, 0.121, 1.05	0.657	0.652
$R[F^2 > 2\sigma(F^2)]$, $wR(F^2)$, *S*	7008	0.030, .079, 1.03	0.020 0.061, 1.15
No. of reflections	409	5805	7911

Table 2.7. Continued

No. of parameters	0	364	435
No. of restraints	$w = 1/[\sigma^2(F_o^2) + (0.0495P)^2 + 72.9711P]$ where $P = (F_o^2 + 2F_c^2)/3$	0	0
	9.40, -1.66	$w = 1/[\square^2(F_o^2) + (0.0442P)^2 + 1.1815P]$ where $P = (F_o^2 + 2F_c^2)/3$	$w = 1/[\square^2(F_o^2) + (0.0325P)^2 + 0.0162P]$ where $P = (F_o^2 + 2F_c^2)/3$
$\Delta\rho_{max}$, $\Delta\rho_{min}$ (e Å^{-3})		1.73, -2.16	0.92, -1.07

Table 2.8. Summary of crystallographic data for complexes **4a** and **4b**

	4a•0.5CH_2Cl_2	**4b**
CCDC	1843717	1843718
Chemical formula	$C_{27.50}H_{23}ClN_6Pt$	$C_{27}H_{20}F_2N_6Pt$
M_r	668.06	661.58
Crystal system, space group	Monoclinic, $P2_1/c$	Orthorhombic, $Pca2_1$
a, b, c (Å)	21.211 (4), 8.0689 (16), 28.976 (6)	18.619 (6), 10.857 (3), 23.626 (7)
α, β, γ (°)	90, 90.001 (3), 90	90, 90, 90
V (Å^3)	4959.4 (17)	4776 (3)
Z	8	8
μ (mm^{-1})	5.80	5.92
Crystal size (mm)	0.52 × 0.32 × 0.25	0.35 × 0.15 × 0.05
T_{min}, T_{max}	0.350, 0.746	0.428, 0.746
No. of measured, independent and observed [$I > 2\sigma(I)$] reflections	27789, 11357, 9730	55383, 10755, 10002
R_{int}	0.039	0.036
$(\sin\theta/\lambda)_{max}$ (Å^{-1})	0.649	0.649
$R[F^2 > 2\sigma(F^2)]$, $wR(F^2)$, S	0.059, 0.140, 1.10	0.023, 0.054, 1.07
No. of reflections	11357	10755
No. of parameters	644	654
No. of restraints	0	1
	$w = 1/[\square^2(F_o^2) + (0.0576P)^2 + 73.9261P]$ where $P = (F_o^2 + 2F_c^2)/3$	$w = 1/[\sigma^2(F_o^2) + (0.0274P)^2 + 2.8423P]$ where $P = (F_o^2 + 2F_c^2)/3$
$\Delta\rho_{max}$, $\Delta\rho_{min}$ (e Å^{-3})	4.21, -2.53	2.73, -1.14
Absolute structure		Refined as an inversion twin.
Absolute structure parameter		0.225 (7)

Table 2.9. Summary of crystallographic data for complexes **4c** and **5b**

	4c	**5b**•0.5CH_2Cl_2
CCDC	1843719	1843721
Chemical formula	$C_{29}H_{22}N_6PtS$	$C_{27.50}H_{16}ClF_2N_8Pt$
M_r	681.67	727.02
Crystal system, space group	Triclinic, $P\bar{1}$	Monoclinic, $C2/c$
a, b, c (Å)	7.666 (3), 11.976 (5), 14.925 (6)	24.497 (2), 15.2716 (13), 13.5103 (12)
α, β, γ (°)	103.388 (4), 95.779 (4), 106.856 (4)	90, 91.5658 (12), 90
V (Å^3)	1254.8 (9)	5052.4 (8)
μ (mm^{-1})	2	5.71
Crystal size (mm)	5.71	0.43 × 0.14 × 0.05
T_{min}, T_{max}	0.16 × 0.08 × 0.06	0.434, 0.746
No. of measured, independent and observed [$I > 2\sigma(I)$] reflections	0.541, 0.746	15573, 5792, 5343
R_{int}	35223, 5533, 5352	0.023
$(\sin\theta/\lambda)_{max}$ (Å^{-1})	0.021	0.651
$R[F^2 > 2\sigma(F^2)]$, $wR(F^2)$, S	0.641	0.019, 0.048, 1.05
No. of reflections	0.014, 0.037, 1.14	5792
No. of parameters	5533	367
No. of restraints	336	21
	0	$w = 1/[\sigma^2(F_o^2) + (0.0214P)^2 + 8.820P]$ where $P = (F_o^2 + 2F_c^2)/3$
$\Delta\rho_{max}$, $\Delta\rho_{min}$ (e Å^{-3})	$w = 1/[\sigma^2(F_o^2) + (0.0117P)^2 + 1.9398P]$ where $P = (F_o^2 + 2F_c^2)/3$	1.00, -1.00
	1.78, -0.51	

2.4.5 Computational details

Geometry optimizations and time-dependent density functional theory (TD-DFT) computations for **6** and **7** were performed at the B97/Def2-TZVPP level employing Gaussian09. For TD-DFT, only the lowest-energy excited state was computed at the B97/Def2-TZVPP level, whereas the full simulated spectrum shown in Figure 2.9 was computed at B97D/Def2-SVPP// B97D/Def2-TZVPP. Molecular electrostatic potential (MEP) maps were computed at B97/Def2-SVPP//B97/Def2-TZVPP and plotted with the Molekel program. The optimized geometries of both **6** and **7** exhibited a characteristic "dragonfly" shape and match well with the crystal structures of **1**–**5**. TD-DFT computations quantified the HOMO → LUMO transition oscillator strengths and composition of the one-electron excitation transitions. TD-DFT calculations were done by Dr. Judy Wu, Department of Chemistry at University of Houston.

2.5 References

(1) Nineham, A. W. "The Chemistry of Formazans and Tetrazolium Salts." *Chem. Rev.* **1955**, *55*, 355–483.

(2) Szymczyk, M.; El-Shafei, A.; Freeman, H. S. "Design, Synthesis, and Characterization of New Iron-Complexed Azo Dyes." *Dyes Pigments* **2007**, *72*, 8–15.

(3) Gruden, C. L.; Fevig, S.; Abu-Dalo, M.; Hernandez, M. "5-Cyano-2,3-Ditolyl Tetrazolium Chloride (CTC) Reduction in a Mesophilic Anaerobic Digester: Measuring Redox Behavior, Differentiating Abiotic Reduction, and Comparing FISH Response as an Activity Indicator." *J. Microbiol. Methods* **2003**, *52*, 59–68.

(4) Frederiks, W. M.; Marle, J. van; Oven, C. van; Comin-Anduix, B.; Cascante, M. "Improved Localization of Glucose-6-Phosphate Dehydrogenase Activity in Cells with 5-Cyano-2, 3-Ditolyl-Tetrazolium Chloride as Fluorescent Redox Dye Reveals Its Cell Cycle-Dependent Regulation." *J. Histochem. Cytochem.* **2006**, *54*, 47–52.

(5) Irving, H.; Gill, J. B.; Cross, W. R. “423. The Structure of Some Di-(3-Methyl-1,5-Diarylformazyl)-Nickel(II) Complexes.” *J. Chem. Soc. Resumed* **1960**, *0*, 2087–2095.

(6) Dale, D. “The X-Ray Crystallographic Determination of the Structure of Di-[3-Methyl-1(or 5)-Phenyl-5(or 1)-p-Tolylformazyl]Nickel(II).” *J. Chem. Soc. Inorg. Phys. Theor.* **1967**, *0*, 278–287.

(7) Budesinsky, B.; Svecova, J. “Hydrogen and Metal Complexes of Some 3-Cyanoformazans.” *Inorg. Chem.* **1971**, *10*, 313–317.

(8) Siedle, A. R.; Pignolet, L. H. “Formazanylpalladium Compounds. Synthesis and Structure of Bis(1,3,5-Tri-p-Tolylformazanyl)Palladium.” *Inorg. Chem.* **1980**, *19*, 2052–2056.

(9) Kawamura, Y.; Yamauchi, J.; Ohya-Nishiguchi, H. “Spectroscopic and Structural Characterization of Formazanyl Copper Complexes.” *Bull. Chem. Soc. Jpn.* **1993**, *66*, 3593–3599.

(10) Gilroy, J. B.; Patrick, B. O.; McDonald, R.; Hicks, R. G. “Transition Metal Complexes of 3-Cyano- and 3-Nitroformazans.” *Inorg. Chem.* **2008**, *47*, 1287–1294.

(11) Pavlova, I. S.; Pervova, I. G.; Belov, G. P.; Khasbiullin, I. I.; Slepukhin, P. A. “Ethylene Oligomerization Mediated by Iron Formazanates and Organoaluminum Compounds.” *Pet. Chem.* **2013**, *53*, 127–133.

(12) Gilroy, J. B.; Ferguson, M. J.; McDonald, R.; Hicks, R. G. “Synthesis and Characterization of Palladium Complexes of 3-Nitroformazans.” *Inorganica Chim. Acta* **2008**, *361*, 3388–3393.

(13) Hong, S.; Hill, L. M. R.; Gupta, A. K.; Naab, B. D.; Gilroy, J. B.; Hicks, R. G.; Cramer, C. J.; Tolman, W. B. “Effects of Electron-Deficient β-Diketiminate and Formazan Supporting Ligands on Copper(I)-Mediated Dioxygen Activation.” *Inorg. Chem.* **2009**, *48*, 4514–4523.

(14) Hong, S.; Gupta, A. K.; Tolman, W. B. “Intermediates in Reactions of Copper(I) Complexes with N-Oxides: From the Formation of Stable Adducts to Oxo Transfer.” *Inorg. Chem.* **2009**, *48*, 6323–6325.

(15) Broere, D. L. J.; Mercado, B. Q.; Lukens, J. T.; Vilbert, A. C.; Banerjee, G.; Lant, H. M. C.; Lee, S. H.; Bill, E.; Sproules, S.; Lancaster, K. M.; et al. “Reversible Ligand-Centered Reduction in Low-Coordinate Iron Formazanate Complexes.” *Chem. – Eur. J.* **2018**, *24*, 9417–9425.

(16) Broere, D. L. J.; Mercado, B. Q.; Holland, P. L. “Selective Conversion of CO2 into Isocyanate by Low-Coordinate Iron Complexes.” *Angew. Chem. Int. Ed.* **2018**, *57*, 6507–6511.

(17) Travieso-Puente, R.; Broekman, J. O. P.; Chang, M.-C.; Demeshko, S.; Meyer, F.; Otten, E. “Spin-Crossover in a Pseudo-Tetrahedral Bis(Formazanate) Iron Complex.” *J. Am. Chem. Soc.* **2016**, *138*, 5503–5506.

(18) Protasenko, N. A.; Poddel’sky, A. I.; Bogomyakov, A. S.; Fukin, G. K.; Cherkasov, V. K. “Heteroligand O-Semiquinonato-Formazanato Cobalt Complexes.” *Inorg. Chem.* **2015**, *54*, 6078–6080.

(19) Protasenko, N. A.; Poddel’sky, A. I.; Bogomyakov, A. S.; Starikov, A. G.; Smolyaninov, I. V.; Berberova, N. T.; Fukin, G. K.; Cherkasov, V. K. “The Chemical and Electrochemical Reduction of Heteroligand O-Semiquinonato-Formazanato Cobalt Complexes.” *Inorganica Chim. Acta* **2019**, *489*, 1–7.

(20) Barbon, S. M.; Price, J. T.; Reinkeluers, P. A.; Gilroy, J. B. “Substituent-Dependent Optical and Electrochemical Properties of Triarylformazanate Boron Difluoride Complexes.” *Inorg. Chem.* **2014**, *53*, 10585–10593.

(21) Barbon, S. M.; Staroverov, V. N.; Gilroy, J. B. “Effect of Extended π Conjugation on the Spectroscopic and Electrochemical Properties of Boron Difluoride Formazanate Complexes.” *J. Org. Chem.* **2015**, *80*, 5226–5235.

(22) Hesari, M.; Barbon, S. M.; Staroverov, V. N.; Ding, Z.; Gilroy, J. B. “Efficient Electrochemiluminescence of a Readily Accessible Boron Difluoride Formazanate Dye.” *Chem. Commun.* **2015**, *51*, 3766–3769.

(23) Hesari, M.; Barbon, S. M.; Mendes, R. B.; Staroverov, V. N.; Ding, Z.; Gilroy, J. B. “Structural Tuning of Boron Difluoride Formazanate Electrochemiluminescence Mediated by Tri- *n* -Propylamine.” *J. Phys. Chem. C* **2018**, *122*, 1258–1266.

(24) Chang, M.-C.; Otten, E. “Synthesis and Ligand-Based Reduction Chemistry of Boron Difluoride Complexes with Redox-Active Formazanate Ligands.” *Chem. Commun.* **2014**, *50*, 7431–7433.

(25) Barbon, S. M.; Reinkeluers, P. A.; Price, J. T.; Staroverov, V. N.; Gilroy, J. B. “Structurally Tunable 3-Cyanoformazanate Boron Difluoride Dyes.” *Chem. – Eur. J.* **2014**, *20*, 11340–11344.

(26) Mondol, R.; Snoeken, D. A.; Chang, M.-C.; Otten, E. “Stable, Crystalline Boron Complexes with Mono-, Di- and Trianionic Formazanate Ligands.” *Chem. Commun.* **2017**, *53*, 513–516.

(27) Chang, M.-C.; Dann, T.; Day, D. P.; Lutz, M.; Wildgoose, G. G.; Otten, E. “The Formazanate Ligand as an Electron Reservoir: Bis(Formazanate) Zinc Complexes Isolated in Three Redox States.” *Angew. Chem. Int. Ed.* **2014**, *53*, 4118–4122.

(28) Meriwether, L. S.; Breitner, E. C.; Sloan, C. L. “The Photochromism of Metal Dithizonates.” *J. Am. Chem. Soc.* **1965**, *87*, 4441–4448.

(29) Petersen, R. L.; McFarland, J. T.; Watters, K. L. “Resonance Raman Study of Metal-Formazans: A Model for Complexes of Metalloenzymes with Chelate Inhibitors.” *Bioinorg. Chem.* **1978**, *9*, 355–367.

(30) Zhang, H.-Y.; Sun, W.-X.; Wu, Q.-A.; Zhangb, H.-Q.; Chen, Y.-Y. “Study on 1,5-Bis(2-Carboxyphenyl)-3-Phenylformazan and Its Complexes.” *Synth. React. Inorg. Met.-Org. Chem.* **2000**, *30*, 571–582.

(31) Bait, S.; Meuldijk, J.; Renkema, W. E. “Square Planar Complexes of Nickel(II), Palladium(II) and Platinum(II) with 1-(2-Hydroxyphenyl)-3,5-Diphenylformazan.” *Transit. Met. Chem.* **1980**, *5*, 357–361.

(32) Balt, S.; Meuldijk, J. “Solvent Effects in Square Planar Complexes: Kinetics of Substitution at 1-(2-Hydroxyphenyl)-3,5-(Diphenylformazanato)-Platinum(II) Complexes.” *Inorganica Chim. Acta* **1981**, *47*, 217–223.

(33) Chang, M.-C.; Roewen, P.; Travieso-Puente, R.; Lutz, M.; Otten, E. “Formazanate Ligands as Structurally Versatile, Redox-Active Analogues of β-Diketiminates in Zinc Chemistry.” *Inorg. Chem.* **2015**, *54*, 379–388.

(34) Schorn, W.; Grosse-Hagenbrock, D.; Oelkers, B.; Sundermeyer, J. “Formazanido Complexes of Heavier Group 13 Elements Aluminium, Gallium, and Indium.” *Dalton Trans.* **2016**, *45*, 1201–1207.

(35) Brooks, J.; Babayan, Y.; Lamansky, S.; Djurovich, P. I.; Tsyba, I.; Bau, R.; Thompson, M. E. “Synthesis and Characterization of Phosphorescent Cyclometalated Platinum Complexes.” *Inorg. Chem.* **2002**, *41*, 3055–3066.

(36) Bronner, C.; Baudron, S. A.; Hosseini, M. W.; Strassert, C. A.; Guenet, A.; Cola, L. D. “Dipyrrin Based Luminescent Cyclometallated Palladium and Platinum Complexes.” *Dalton Trans.* **2009**, *39*, 180–184.

(37) Barbon, S. M.; Buddingh, J. V.; Maar, R. R.; Gilroy, J. B. “Boron Difluoride Adducts of a Flexidentate Pyridine-Substituted Formazanate Ligand: Property Modulation via Protonation and Coordination Chemistry.” *Inorg. Chem.* **2017**, *56*, 12003–12011.

(38) Barbon, S. M.; Novoa, S.; Bender, D.; Groom, H.; Luyt, L. G.; Gilroy, J. B. “Copper-Assisted Azide–Alkyne Cycloaddition Chemistry as a Tool for the Production of Emissive Boron Difluoride 3-Cyanoformazanates.” *Org. Chem. Front.* **2017**, *4*, 178–190.

(39) Kabir, E.; Wu, C.-H.; Wu, J. I.-C.; Teets, T. S. “Heteroleptic Complexes of Cyclometalated Platinum with Triarylformazanate Ligands.” *Inorg. Chem.* **2016**, *55*, 956–963.

(40) Gilroy, J. B.; McKinnon, S. D. J.; Koivisto, B. D.; Hicks, R. G. “Electrochemical Studies of Verdazyl Radicals.” *Org. Lett.* **2007**, *9*, 4837–4840.

(41) Pangborn, A. B.; Giardello, M. A.; Grubbs, R. H.; Rosen, R. K.; Timmers, F. J. “Safe and Convenient Procedure for Solvent Purification.” *Organometallics* **1996**, *15*, 1518–1520.

(42) Godbert, N.; Pugliese, T.; Aiello, I.; Bellusci, A.; Crispini, A.; Ghedini, M. “Efficient, Ultrafast, Microwave-Assisted Syntheses of Cycloplatinated Complexes.” *Eur. J. Inorg. Chem.* **2007**, *2007*, 5105–5111.

(43) Sheldrick, G. M. “A Short History of *SHELX*.” *Acta Crystallogr. A* **2008**, *64*, 112–122.

Chapter 3

Formazanate Complexes of Bis-cyclometalated Iridium.

Portions of this work have been submitted for publication:

Kabir, E.; Mu, G.; Momtaz, D. A.; Bryce, N.; Teets, T. S. Submitted

3.1 Introduction

The coordination chemistry of formazans, which are a class of chromophoric conjugated organic molecules with a 1,2,4,5-tetraazapentadienyl core, has been long been investigated with transition metals and main group metals. The nitrogen-rich redox active formazans have also been intensively studied in the fields of bioinorganic chemistry[1,2] and catalysis,[3–5] and a few successful applications have emerged over time in biomedical assays, textile dyes, and colorimetric indicators of cell activity.[6–9] The monoanionic form of formazans (referred to as "formazanates") have become a well-known N-chelating ligand class in recent years, structurally analogous to the ubiquitous β-diketiminate ligand class but with redox activity at much more accessible potentials and strong visible absorption, primarily because of LUMOs that are significantly stabilized relative to β-diketiminates.[10–13] The growing interest in formazanate coordination complexes is largely due to the ligand-based redox processes, which can facilitate multielectron redox behavior,[14] bond activation,[15] and excited-state charge separation. In particular, the stabilized LUMOs in formazanates result in relatively stable reduced products, greatly expanding the redox chemistry of these complexes in small-molecule activation and other contexts.[16–18]

Complexes of first-row transition metals with formazanates have been extensively reported,[5,19] including copper complexes which mediate oxygen activation.[20,21] Ligand-based redox chemistry of low-coordinated iron complexes,[22–25] and bis-chelated zinc complexes have affirmed the versatility of redox active formazanate ligands.[17,26] Unique magnetic properties were demonstrated in heteroleptic cobalt and bis(formazanate) iron

complexes.[26–28] Formazanate complexes of group 14 elements and ruthenium highlight the redox non-innocence of some classes of formazanate complexes.[16,29] Furthermore, boron chelates of formazanates not only exhibit tunable redox properties but are also in many cases photoluminescent,[30–35] finding applications as cell-imaging agents,[32,36] electrochemiluminescence emitters,[37,38] multifunctional polymers,[39,40] and precursors to a wide range of BN heterocycles.[41,42]

In spite of these numerous examples, coordination complexes of formazans with third-row transition metals remain rare. Dithizonate complexes with a formazan-like core were described where coordination of sulfur to the metal was observed.[43] Complexes of dianionic aryl formazanate ligands which involve *o*-phenoxy or *o*-benzoate donors were found to be coordinated in a tridentate fashion with a few heavy transition metals but none of them were extensively characterized or analyzed for further studies.[44–47] Since the strong orbital overlap between radially extended 5d orbitals and the formazanate π system could perturb the inherent redox and optical properties of the formazanates and the 5d metal center could promote formazanate-centered triplet photophysics, our group began investigating third-row transition metal complexes of formazanates. We have expanded the coordination chemistry of formazanates a series of heteroleptic platinum complexes[48,49] and accessed homoleptic azo-iminate platinum complexes[50] via hydrogenative cleavage of formazans.

In this work, we describe a diverse set of cyclometalated iridium(III) formazanate complexes. Cyclometalated iridium(III) compounds have been extensively studied in a number of contexts,[51–55] primarily due to their good thermal and photostability, relatively

short phosphorescence lifetime, and high photoluminescence quantum yields. Although the synthetic chemistry of cyclometalated iridium(III) formazanates largely parallels that of our previous cyclometalated platinum(II) formazanate series,[48,49] moving from platinum(II) to iridium(III) allows us to evaluate the effects of coordination geometry and d-electron count on the structural chemistry, redox properties, and optical properties of 5d metal formazanates. We describe 18 new cyclometalated iridium(III) formazanate complexes of the type $Ir(C^N)_2$(formazanate) (C^N = cyclometalating ligands). These neutral complexes feature four different cyclometalating ligands and six structurally and electronically varied triaryl- and diarylformaznates. A general synthetic route is presented here and 8 of 18 compounds are structurally characterized by single crystal X-ray diffraction, which reveals two distinct coordination modes for the formazanate. The substitution patterns on the formazanate strongly influence the observed ligand-centered redox potentials, with subtle influences from the C^N ligand that suggest some degree of mixing between iridium d-orbitals and formazanate π orbitals. The UV-vis absorption spectra show intense bands from the contributions of both formazanates and Ir-C^N fragments, and solvatochromic studies assist in the assignment of these features. This work demonstrates that alteration of the C^N and formazanate ligands offers two layers of control over the redox and optical properties of neutral iridium formazanate complexes.

3.2 Results and discussion

3.2.1 General synthesis

Scheme 1 depicts the general synthetic procedure of the series of 18 heteroleptic cyclometalated iridium formazanate complexes of the type Ir(C^N)$_2$(formazanate). Compounds are numbered based on the identity of the C^N ligand, with the associated letter designating the structure of the formazanate ancillary ligand. Two cyclometalating ligands, 2-phenylpyridine (ppy) and 2-(2,4-difluorophenyl)pyridine (F_2ppy), were partnered with all six formazanates studied here (**Fza–Fzf**), to produce products **1a–1f** and **2a–2f**, while the other two C^N ligands, 2-phenylbenzothiazole (bt) and 1-phenylisoquinoline(piq), were used to prepare a smaller subset of complexes (**3a**, **3b**, **3e**, **3f**, **4a**, and **4f**).

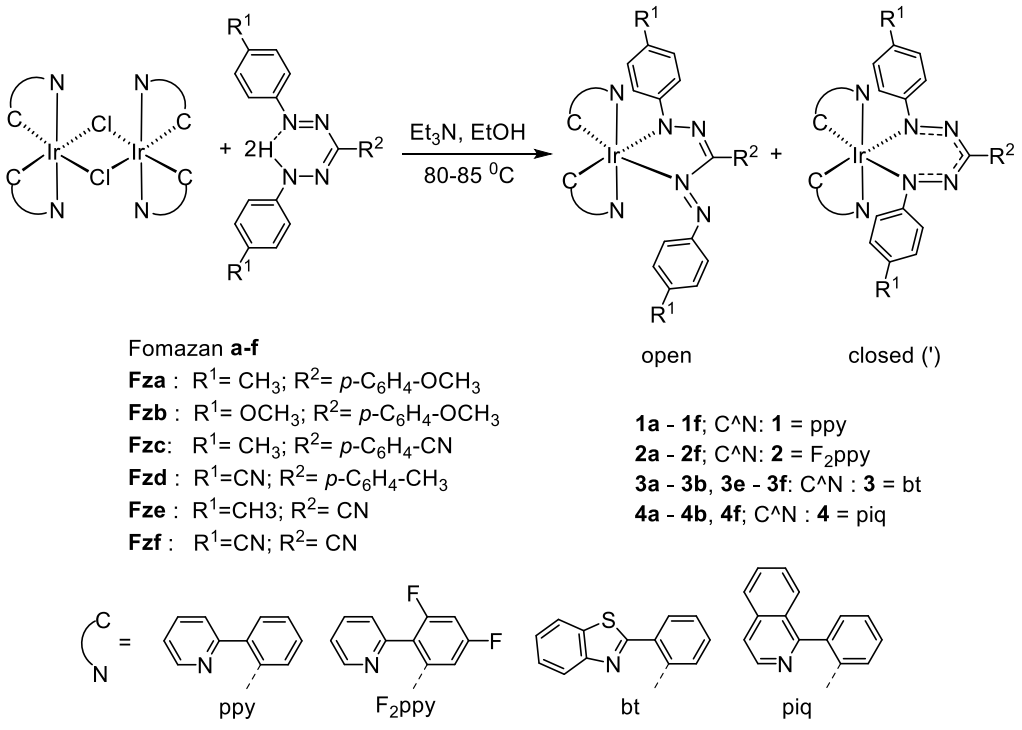

Scheme 1.1. General synthesis of complexes **1**–**4**.

The chloro-bridged dimers $[Ir(C\hat{}N)_2(\mu\text{-}Cl)]_2$ were treated with a stoichiometric amount of free formazan in ethanol in the presence of excess triethylamine, by refluxing for 20–36 h. The reaction was general and tolerated a variety of electronically modified formazans, which include different combinations of electron-donating ($-CH_3$, $-OCH_3$) and electron-withdrawing (-CN) substituents at either the azo aryl substituent (R^1) or at the central position of backbone (R^2). Reactions involving triarylformazanates (**Fza–d**) showed a distinct color change from purple (free formazan) to dark green or blue upon coordination of the formazanate to iridium. In contrast, in reactions involving diarylformazanates the color of the product was almost identical to the free formazan and were most conveniently monitored by TLC. The isolated yields varied from 43–80% across the series. NMR analysis of crude reaction mixtures indicated the possibility of two isomeric products. In particular, some of the complexes with electron-donating substituents on the formazanate, **1a**, **1b**, **3a**, **3b**, and **4a**, as well as **1c'** ($R^2 = p\text{-}C_6H_4\text{-}CN$), initially showed the presence of two products in their ^1H NMR spectra, one with apparent C_2 symmetry and one with C_1 symmetry. As unequivocally determined by X-ray crystallography (see below), these features are attributed to two different binding modes of the formazanate, one that involves a five-member chelate ring "open" form, binding through the 1- and 4-positions of the formazanate core, and other is the more typical six-member chelate "closed" form, binding through the 1- and 5- positions and denoted by a prime symbol (′). Varying the reaction solvents (dichloromethane, tetrahydrofuran) and temperature did not significantly alter the isomeric ratio, and prolonged heating of isolated mixtures of isomers did not lead to significant interconversion. Chromatographic purification was not effective as both isomers are similar in polarity. Recrystallization of

the above-mentioned products was generally a good approach for purifying the mixtures, allowing **3a**, **3b**, and **4a** to be isolated as the C_1-symmetric "open" form with only trace amount of the "closed" isomer present. In contrast, in the C^N = ppy series recrystallization allowed isolation of **1b′** and **1c′** exclusively as the C_2-symmetric "closed" isomer, whereas **1a** was isolated as a mixture of isomers after repeated recrystallization attempts. The remaining triarylformazanate iridium complexes were all isolated in the five-member chelate conformation, as were all diarylformazanate complexes prepared from **Fze** and **Fzf**. To summarize, 15 of the 18 complexes were isolated in pure form as the five-member chelate "open" form, whereas only **1b′** and **1c′** were obtained in the "closed" form and **1a/1a'** was isolated as a mixture of both isomers. All of the compounds are air and moisture stable and were fully characterized by ^{1}H, $^{13}C\{^{1}H\}$ and ^{19}F (for **2a**–**2f**) NMR spectroscopy and elemental analysis, which establish identity and bulk purity. NMR spectroscopy was especially useful for distinguishing the two isomers, with the C_2-symmetric "closed" isomer displaying chemical equivalency of the C^N ligands and the two R^1 substituents on the formazanate.

3.2.2 X-ray Crystallography

The structures of **1c'**, **1d**, **2a**, **2c**, **2c′**, **2d**, **2e**, **3a**, and **4a** were confirmed by single-crystal X-ray diffraction, are shown in Figure 3.1. Formazanate bond lengths and angles are summarized in Table 3.1 with refinement details collected in Tables 3.1–3.2. The iridium metal center resides in the center of distorted octahedral coordination geometry with two C^N ligands and one formazanate.

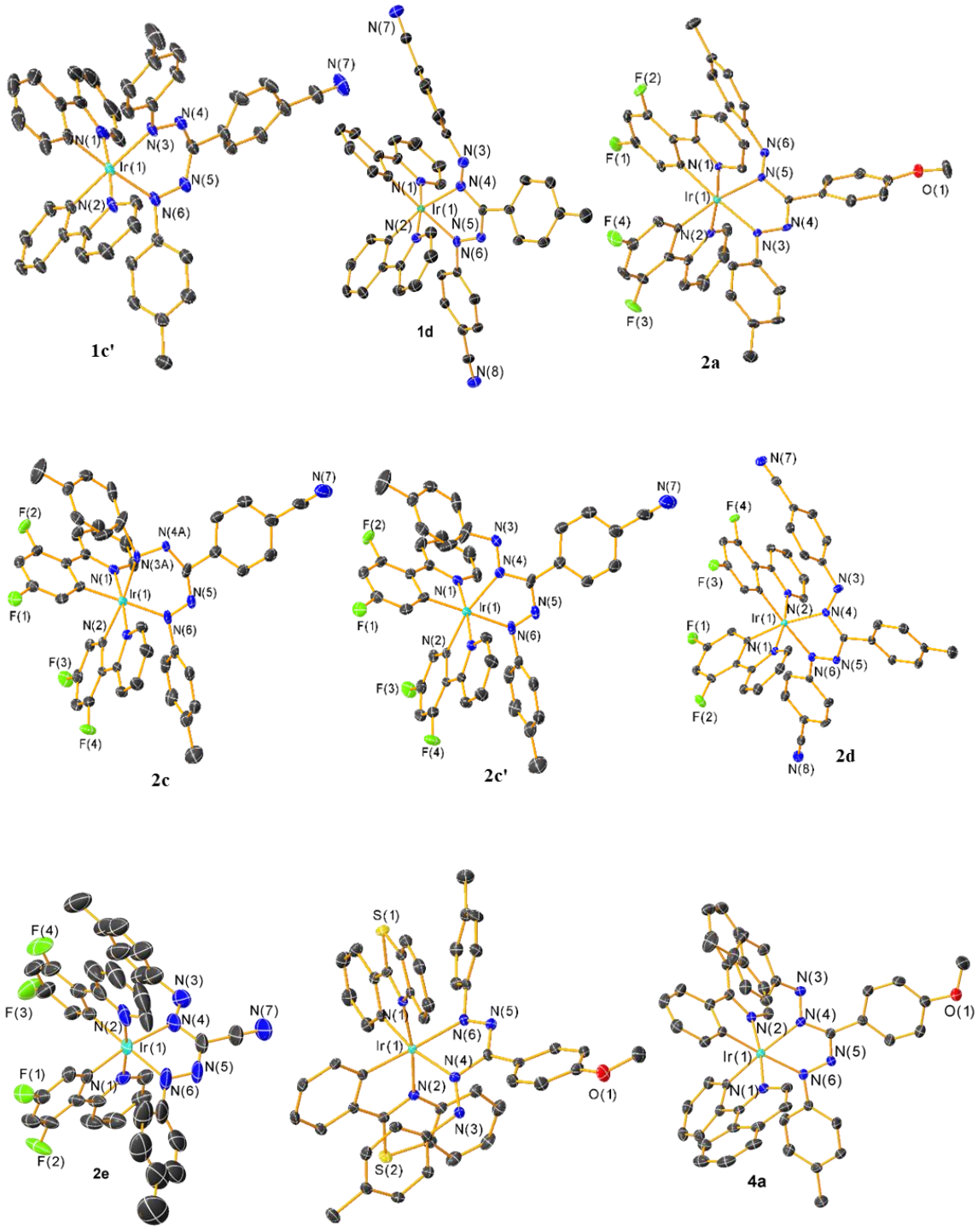

Figure 3.1. X-ray crystal structure of complexes **1c, 1d**, **2a**, **2c**, **2c'**, **2d**, **2e**, **3a**, and **4a**. Hydrogen atoms and solvated molecules are omitted for clarity. Ellipsoids are shown at the 50% probability level.

Table 3.1. Summary of crystallographic bond lengths (Å) and angles (deg) for complexes **1c'**, **1d**, **2a**, **2c**, and **2c'**

	1c′	**1d**	**2a**[a]	**2c**[b]	**2c′**[b]
d (Ir–N3/4)[c]	2.173(3)	2.208(8)	2.161(4)	2.210(5)	2.142(9)
d (Ir–N6)	2.127(3)	2.119(8)	2.125(4)	2.110(3)	2.110(3)
d (N3–N4)	1.309(4)	1.318(11)	1.313(5)	1.285(7)	1.325(12)
d (N4–C1)	1.344(5)	1.376(12)	1.383(5)	1.400(6)	1.418(10)
d (N5–C1)	1.363(5)	1.333(12)	1.328(6)	1.349(5)	1.349(5)
d (N5–N6)	1.294(4)	1.314(11)	1.313(5)	1.297(4)	1.297(4)
∠N(3/4)–Ir–N(6)[d]	82.45(11)	74.1(3)	74.53(14)	70.50(15)	94.5(3)

[a] Average of two crystallographically independent molecules. [b] Both isomers disordered in the same crystal structure. [c] Formazanate Ir–N distance. Relevant distance is Ir–N3 for "closed" isomers **1c′** and **2c′**, and Ir–N4 for the rest. [d] Formazanate N–Ir–N chelate angle. Relevant angle is ∠N(3)–Ir–N(6) for "closed" isomers **1c′** and **2c′**, and ∠N(4)–Ir–N(6) for the rest.

In all cases, the nitrogen atoms of C^N ligands are in a trans position relative to each other. The Ir–C bond distances (2.014(7)–2.033(4) Å) and Ir–N bond distances involving the C^N ligands (2.036(17)–2.091(8) Å) of all complexes are similar to those of the previously re-ported cyclometalated Ir complexes.[51,52] Complex **1c′** crystallized with the formazanate exclusively in the six-membered chelate "closed" form, whereas in **2c** both isomers were present, modeled as a two-part disorder with 71% of the "open" form (**2c**) and 29% of the "closed" form (**2c′**). As shown in Table 3.1 and Figure 3.1, the binding mode of the formazanate ("open" vs. "closed") has little influence on the Ir–N (formazanate) bond distances, which range between 2.103(7) and 2.210(3) Å and are significantly longer than those in other formazanate chelate complexes (1.809–2.090 Å).[16,17,25–27,48,49] The different chelating modes of formazanates, however, impact the bond distances within the formazanate core critically. For both cases of **1c′** and **2c′**, which include the "closed" form of the formazanate, full π delocalization within the

formazanate is indicated. The two N–N and two N–C distances are nearly equal and intermediate between single and double bonds. In contrast, for "open form" formazanate chelating complexes, in many cases there are alternating short and long bond distances in the formazanate core, which is particularly apparent in the structures of **2d**, **2e**, **3a**, and **4a**. In these cases, the N(3)–N(4) distances exterior to the five-member chelate ring are shorter than the N(5)–N(6) distances in the chelate ring, and the N(4)–C(1) distance is significantly longer than N(5)–C(1). This pattern of bond distances is consistent with less π delocalization in the "open" form, which in the localized limit consists of alternating single and double bonds, as shown in the structure diagram in Scheme 3.1. Unsurprisingly, the other major structural difference between the "open" and "closed" forms is the chelate angles of formazanates, which for the "open" forms range between 74.10(3) and 74.45(9)° (∠N(4)–Ir–N(6)), except **2c** which has an abnormally small chelate angle (70.50(15)°).

Table 3.2. Summary of crystallographic bond lengths (Å) and angles (deg) for complexes **1c'**, **1d**, **2a**, **2c**, and **2c'**

	2d	**2e**	**3a**	**4a**
d (Ir–N3/4)[a]	2.152(2)	2.155(6)	2.1545(18)	2.192(3)
d (Ir–N6)	2.135(3)	2.103(7)	2.1234(17)	2.153(3)
d (N3–N4)	1.278(3)	1.263(11)	1.292(2)	1.309(5)
d (N4–C1)	1.418(4)	1.397(11)	1.404(3)	1.378(5)
d (N5–C1)	1.315(4)	1.314(12)	1.332(3)	1.330(6)
d (N5–N6)	1.348(3)	1.304(8)	1.322(2)	1.322(5)
∠N(3/4)–Ir–N(6)[b]	74.45(9)	75.6(3)	73.88(7)	73.62(13)

[a] Formazanate Ir–N distance. Relevant distance is Ir–N3 for "closed" isomers **1c′** and **2c′**, and Ir–N4 for the rest. [b] Formazanate N–Ir–N chelate angle. Relevant angle is ∠N(3)–Ir–N(6) for "closed" isomers **1c′** and **2c′**, and ∠N(4)–Ir–N(6) for the rest.

The formazanate bite angles are larger for the C_2-symmetric isomers, observed to be 82.45(11)° in **1c** and 94.5(3)° in **2c′**. There does not appear to be any systematic dependence of the key structural metrics on the presence of electron-withdrawing or electron-donating groups on the formazanate periphery. The observation of both structure types ("open" and "closed") suggests that the two structures are similar in energy, though overall the "open" isomer seems to be favored. This observation stands in contrast to many previously described platinum(II) formazanates, where only the "closed" binding mode was observed.[48,49] The covalent radii of platinum and iridium are quite similar,[56] so we don't think the preference for a five-member chelate is because iridium(III) is smaller than platinum(II), nor are there any obvious electronic differences between the two isomers (see description of UV-vis and electrochemistry below). We propose that the "open" binding mode relieves steric pressure in these complexes, avoiding close approaches of the formazanate N-aryl substituent with the aryl rings of the cyclometalating ligand. In previously characterized bis-cyclometalated iridium β-diketiminate complexes from our group, we noted a close stacking arrangement of the N-aryl groups and the cyclometalated aryl groups,[57,58] which is avoided in **1c′** ("closed" isomer) by a buckling of the formazanate backbone. In contrast, in all of the "open"-form structures presented here, except in **2c** where the two isomers are disordered, the aryl substituent at the iridium-bound N(6) is safely away from the steric congestion of the cyclometalating ligands, oriented orthogonal to the nearest cyclometalated aryl ring in a cleft between the two C^N ligands. Thus, the crystallo-graphic evidence suggests that it is steric effects that are likely responsible for the "open" chelate conformation most of these complexes adopt.

3.2.3 UV-vis absorption spectroscopy

UV–vis absorption spectra of all cyclometalated iridium formazanate complexes were recorded and Table 3.3 represents the summarized absorption data in tetrahydrofuran (THF). Figure 3.2 displays spectra of the complexes **1a**–**1f**, **2a**–**2f**, **3a**–**3d**, and **4a**–**4f**. None of the complexes are photoluminescent in the visible region at room temperature or 77 K. All of the complexes described here are highly colored, appearing green or bluish green for the triarylformazanate complexes and greenish brown to dark red for the diarylformazanates complexes. These iridium formazanate compounds display low-energy absorption bands between 525–677 nm with extinction coefficients between 2200–13000 $M^{-1}cm^{-1}$ in the visible range of the spectrum, which is assigned as a formazanate ligand-centered $\pi \rightarrow \pi^*$ transition primarily involving HOMO and LUMO orbitals. As shown in Table 3.2 these low-energy absorption maxima are nearly identical for all of the triarylformazanate complexes **1a**/**1b'**, **2a**/**2b**, **3a**/**3b** and **4a**, ranging from 628–639 nm for these complexes which have electron-donating substituents at both the R^1 and R^2 position of the formazanate scaffold. Complex **1a** was isolated as a mixture of "open" and "closed" isomers but no significant spectral differences were observed by comparing this with the other **Fza** complexes that existed exclusively in the "open" configuration. The position of the low-energy absorption band depended strongly on the identity of the substituents at the central R^2 position of the formazanate backbone. Placing the electron withdrawing 4-cyanophenyl group in the R^2 position (**Fzc**) caused a hypsochromic shift of ~27–38 nm (715–989 cm^{-1}) in the low-energy absorption maximum for complexes **1c'** and **2c** relative to the respective **Fza** and **Fzb** complexes.

Table 3.3. Summary of UV-vis absorption data recorded in tetrahydrofuran (THF) at room temperature

	λ / nm (ε × 10^{-3} / $M^{-1}cm^{-1}$)
1a/1a'	265 (53), 480 (6.7), 633 (13)
1b'	261 (25), 463 (3.6), 630 (3.2)
1c'	264 (71), 387 (42), 602 (8.7)
1d	270 (17), 370[a] (6.8), 677 (4.6)
1e	260 (30), 380[a] (8.0), 476 (5.8), 554 (6.6)
1f	258 (33), 342 (10), 401[a] (7.9), 520 (7.5)
2a	250 (34), 347[a] (13), 445 (3.2), 628 (8.6)
2b	252 (27), 454 (2.9), 639 (7.5)
2c	251 (52), 390 (18), 601 (10)
2d	260a (38), 313[a] (23), 360[a] (17), 655 (10)
2e	250 (28), 300 (14), 454[a] (4.2), 551 (6.5)
2f	261 (15), 353[a] (5.4), 532 (3.5)
3a	320 (43), 410[a] (11), 630 (12)
3b	262 (36), 319 (39), 635 (10)
3e	263 (34), 319 (36), 382[a] (18), 443[a] (14), 578 (2.2)
3f	266 (38), 321 (36), 384[a] (13), 443 (12), 596 (6.7)
4a	293 (51), 349[a] (29), 435[a] (9.0), 638 (9.4)
4f	285 (44), 343 (26), 403 (14), 443 (13), 525[a] (10)

[a] Shoulder.

In contrast, this low-energy absorption band was red-shifted for complexes **1d** (677 nm) and **2d** (655 nm), when the 4-cyanophenyl substituent was on the formazanate nitrogen atoms, i.e. R^1 = CN. As shown in Table 3.2, replacing the aryl group at the R^2 position with a cyano group in diarylformazanate (**Fze** and **Fzf**) complexes resulted in a significant blue-shift, with the low-energy absorption maximum occurring between 520 nm (**1f**) and 578 nm (**3e**) in this subset of complexes. This significant blue-shift in the

formazanate π→π* transition was likely a result of the decreased conjugation in the diarylformazanate analogues. Additionally, higher-energy absorption bands were observed in the near-UV and visible regions which were dependent on the identity of the cyclometalated ligands, characteristic of Ir(d)→π* metal-to-ligand charge transfer (MLCT) bands along with a slight dependence on the N-aryl substituents of the formazanate ligands.

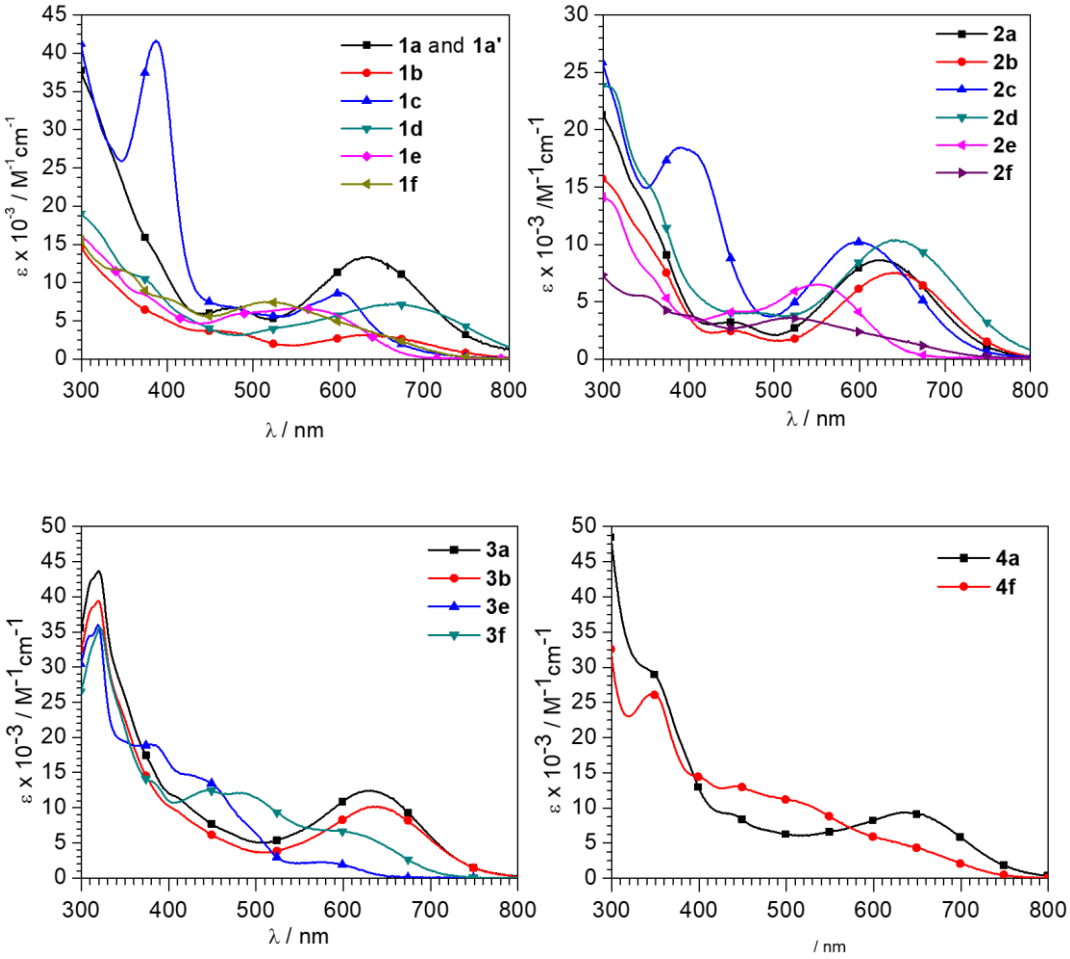

Figure 3.2. Overlaid electronic absorption spectra of **1a**–**1f** (top), **2a**–**2f** (top), **3a**, **3b**, **3e**, **3f**, **4a**, and **4f** (bottom). Spectra were recorded in tetrahydrofuran (THF) solution in room temperature. Data was collected in intervals of 1 nm, and symbols are included on each plot are to help distinguish the overlaid spectra.

Table 3.4. Summary of UV-vis absorption maxima for spectra recorded in tetrahydrofuran (THF), toluene, and MeOH

	λ (nm)		
	THF	Toluene	MeOH
$Ir(ppy)_2$**(Fza) (1a)**	265, 480, 633	478, 635	262, 472, 631
$Ir(ppy)_2$**(Fzb) (1b)**	261, 463, 630	468, 633	258, 459, 630
$Ir(ppy)_2$**(Fzc) (1c)**	264, 387, 602	385, 605	260, 387, 599
$Ir(ppy)_2$**(Fzd) (1d)**	270, 374[a], 673	271, 374[a], 677	269, 370[a], 674
$Ir(ppy)_2$**(Fze) (1e)**	260, 380[a], 476, 554	380[a], 478, 565	378[a], 477, 553
$Ir(ppy)_2$**(Fzf) (1f)**	258, 342, 401[a], 520	349, 402[a], 527	258, 341, 400[a], 512
$Ir(F_2ppy)_2$**(Fza) (2a)**	250, 347[a], 445, 628	346[a], 452, 632	249, 344[a], 453, 628
$Ir(F_2ppy)_2$**(Fzb) (2b)**	252, 454, 639	452, 651	260, 451, 646
$Ir(F_2ppy)_2$**(Fzc) (2c)**	251, 390, 601	387, 606	390, 605
$Ir(F_2ppy)_2$**(Fzd) (2d)**	260[a], 313[a], 360[a], 655	315[a], 361[a], 656	312[a], 357[a], 640
$Ir(F_2ppy)_2$**(Fze) (2e)**	250, 300, 454[a], 551	302, 455[a], 554	300, 454[a], 547
$Ir(F_2ppy)_2$**(Fzf) (2f)**	261, 353[a], 532	354[a], 545	261, 347[a], 524
$Ir(bt)_2$**(Fza) (3a)**	320, 410[a], 630	319, 412[a], 636	318, 403[a], 476[a], 639
$Ir(bt)_2$**(Fzb) (3b)**	262, 319, 635	320, 637	261, 307, 636
$Ir(bt)_2$**(Fze) (3e)**	263, 319, 382[a], 443[a], 578	321, 383[a], 451[a], 580	318, 378, 438[a], 572
$Ir(bt)_2$**(Fzf) (3f)**	266, 321, 384[a], 443, 596	323, 384[a], 450, 597	320, 378[a], 439, 595
$Ir(piq)_2$**(Fza) (4a)**	293, 349[a], 435[a], 638	293, 348[a], 437[a], 637	288, 344[a], 431[a], 637
$Ir(piq)_2$**(Fzf) (4f)**	285, 343, 403, 443, 525[a]	346, 406, 446, 526[a]	283, 343, 436, 522[a]

[a]= shoulder

These bands typically overlapped with other high-energy absorption features, likely localized π→π* transitions, though in general F_2ppy-ligated complexes **2a**–**f** displayed MLCT bands at the shortest wavelengths, with piq complexes having MLCT bands at the longest wavelength, consistent with many other cyclometalated iridium complexes.[59] Complexes of formazan (R^2 = 4-cyanophenyl) displayed a distinct absorption at ~400 nm, which was not observed in other members of the series and is likely attributed to a transition localized on the 4-cyanophenyl substituent. In many complexes, particularly in the bt (**3**) and piq series (**4**), the high-energy absorption features overlapped with low-energy formazanate-centered bands, giving rise to panchromatic visible absorption, as observed for previously reported pq-ligated platinum formazanate compounds.[49]

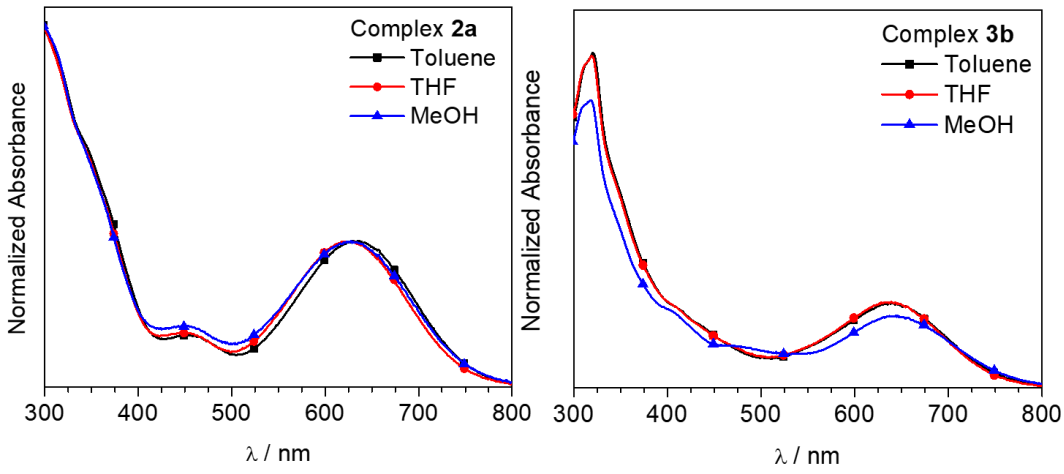

Figure 3.3. Electronic absorption spectra of complex **2a** and **3b**, recorded in toluene, tetrahydrofuran (THF), and MeOH at room temperature. The spectra are normalized to the low-energy absorption maximum.

UV-vis spectra were also recorded in three solvents of varying polarity (toluene, THF, and MeOH), representative spectra for two complexes **2a** and **3b** were shown in Figure 3.3. Summary of the solvatochromic data is tabulated in Table 3.3 and only slight

solvatochromic shifts of <10 nm were observed for the low-energy absorption bands in all cyclometalated iridium formazanate complexes, further supporting the assignment of this band as a ligand-localized π→π* transition with minimal charge-transfer character. Taken together, these results show the UV-vis absorption features of the iridium formazanate complexes depend on the location and identity of the substituents on the formazan scaffold as well as the cyclometalating ligand. Changing substituents at the R^1 and R^2 position of the formazanate ligand allows predictive control over the formazanate-based low energy π → π* transition, which spans a relatively broad range of 520–677 nm in this series of complexes.

3.2.4 Electrochemistry of new complexes

The electrochemical properties of complexes **1**–**4** were investigated by cyclic voltammetry (CV) experiments, and the results are summarized in Table 3.5 with the voltammograms shown in Figures 3.4. The compounds displayed both oxidation and reduction features in their cyclic voltammograms. Ligand-centered reductions which occur at mild potential are generally one of the most important features of coordinated formazanate complexes, and these features are discussed here along with the Ir^{IV}/Ir^{III} oxidation waves. The first reduction wave for all complexes was assigned as a formazanate-centered one electron reduction which occurs in the range of −1.22 to −1.98V (all potentials referenced to the ferrocenium/ferrocene couple). The F_2ppy series (**2a**–**f**) provides the best insight into the effect of the formazanate structure on the redox properties, since this series includes all six formazanate ligands studied here and all of them bind exclusively in the five-member chelate “open” form in these analogues.

Table 3.5. Summary of electrochemical data for complexes **1**–**4**

	CV in CH_2Cl_2	
	Ir^{IV} / Ir^{III} E^{ox} (V)	Fz-centered E^{red} (V)
1a/1a'	−0.02	−1.96[a]
1b'	−0.10	−1.97[a]
1c'	0.23	−1.95
1d	0.37	−1.41
1e	0.55	−1.61, −2.10[a]
1f	0.86	−1.26, − 1.70
2a	0.08	−1.83[a]
2b	−0.02	−1.89[a]
2c	0.23	−1.79[a]
2d	0.51	−1.31, −1.78
2e	0.70	−1.50, −1.94[a]
2f	1.15	−1.22, −1.71
3a	0.01	−1.98[a]
3b	−0.06	−1.95[a]
3e	0.68[a]	−1.72
3f	0.97	−1.29, −1.74
4a	0.01	−1.96[a]
4f	0.83[a]	−1.27, −1.68

[a] Irreversible wave. $E_{p,c}$ or $E_{p,a}$ is reported.

As the data in Figure 3.4 and Table 3.5 shows, the redox potentials in **2a**–**c** followed the trend expected from the electron donating/withdrawing attributes of the substituents, although the effects were modest. Moving from **2a** to **2b**, where the R^1 substituent was changed from CH_3 to a more electron-donating OCH_3, resulted in a cathodic (negative) shift of the reduction potential by 60 mV. Similarly, comparing **2a** to **2c**, where the *p*-C_6H_4-OCH_3 R^2 substituent was replaced with the more electron-withdrawing *p*-cyanophenyl, we noted a 40 mV anodic (positive) shift in the reduction potential. A much

more dramatic change in potential occurred when electron-withdrawing cyano substituents were added to the R^1 position, with the potential in **2d** more positive than that of **2a** by over 500 mV. Similarly, large effects were observed in **2e** and **2f**, where the R^2 aryl substituent is replaced with a cyano group, resulting in comparatively mild formazanate based reduction potentials, in particular in **2f** ($R^1 = R^2 = CN$, $E_{red} = -1.22$ V). Similar substituent effects were observed in the other members of the series with different cyclometalating ligands.

Effects of the cyclometalating ligand on the reduction potentials were modest, and in general the observed reduction potential was mainly determined by the substituent pattern on the formazanate. Fluorination of the phenylpyridine ligand caused an overall anodic shift (~100 mV on average) for complexes **2a**–**2f** (Figure 3.4) if we compare them with the set **1a**–**1f**, but complexes with C^N = bt or piq had very similar potentials to their ppy analogues, at parity of formazanate structure. In addition, the potentials for the complexes that were isolated as the "closed" isomer (**1b′** and **1c′**) or as a mixture of isomers (**1a**) were all very similar to the other members of the series with the same formazanate structure, suggesting that the formazanate-centered LUMO energy and corresponding redox potential depend little on the binding mode of the formazanate. All of the complexes here (except **3e** and **4f**) also displayed a formal Ir^{IV}/Ir^{III} redox couple which has slight dependence on the identity of the C^N ligand but highly sensitive to the identity of the formazanate ligands. Electron rich complexes **1a**/**1b**, **2a**/**2b**, **3a**/**3b**, and **4a** oxidized at similar potentials across the series, and again the isomeric form of the complex did not appear to have a large effect on the observed potential (Table 3.5). The

oxidation potential of these seven complexes were very near the Fc^+/Fc potential and again had a slight dependence on the formazanate substituents, with the most electron-rich **Fzb** complexes being easiest to oxidize.

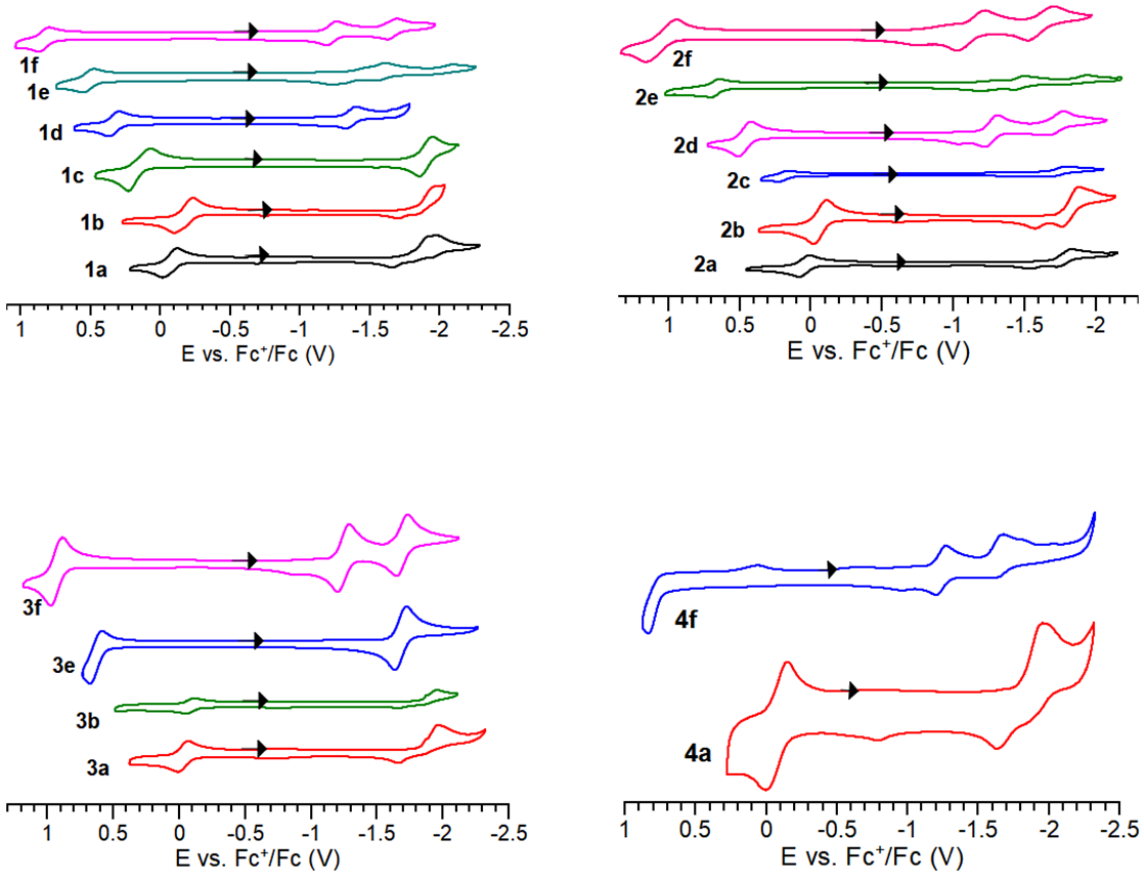

Figure 3.4. Overlaid cyclic voltammograms of complexes **1a**–**1f** (top), **2a**–**2f** (top), **3a**, **3b**, **3e**, **3f**, **4a**, and **4f** (bottom). CVs were recorded in CH_2Cl_2 with 0.1 M NBu_4PF_6 supporting electrolyte, using a glassy carbon working electrode and a scan rate of 0.1 V/s. The arrows indicate the scan direction. Concentrations were not carefully controlled, and currents are low in some of plots because of the limited solubility of some of the compounds in CH_2Cl_2.

Addition of cyano substituents in the remaining complexes rendered the complexes more difficult to oxidize, with shifts in potential that were qualitatively similar

to those discussed above for the reduction potentials. The four **Fzf** complexes, where $R^1 = R^2 = CN$, have the most positive oxidation potentials (≥ 0.83 V), and the complexes where only one of the R^1 and R^2 positions includes a cyano group (**Fzc**–**e**) have Ir^{IV}/Ir^{III} potentials intermediate between the most electron-rich and electron-poor members of the series. As with the reduction potentials, the C^N ligands exerted a modest effect on the formally Ir^{IV}/Ir^{III} couple, with F_2ppy complexes being the most difficult to oxidize for a given formazanate ligand. We note that although this oxidation potential can be formally classified as Ir^{IV}/Ir^{III}, and in typical cyclometalated iridium complexes the HOMO included significant Ir dπ character,[60] the strong dependence of this potential on the formazanate structure implies that the HOMO in the complexes described here is also primarily formazanate ligand-centered, like the LUMO. Consistent with this supposition, previously reported platinum formazanate complexes from our group,[48] as well as cyclometalated iridium complexes with structurally analogous β-diketiminate ancillary ligands,[58] both have HOMOs that are almost exclusively formazanate or β-diketiminate-centered, with minor contribution from the metal.

One other noteworthy insight to come out of this work is the effect of the metal center and coordination geometry on the formazanate-centered optical transitions and redox properties. Our group has also prepared an extensive series of cyclometalated platinum formazanate complexes,[49] using many of the same cyclometalating ligands and formazanates used in this work (except for **Fzd**, and piq, which we did not use to prepare any platinum complexes). In the UV-vis absorption spectra, in every case the low-energy formazanate π→π* transition was significantly blue-shifted in the iridium complexes, by

at least 23 nm (767 cm^{-1}) and as much as 122 nm (3650 cm^{-1}) when comparing **1f** to its platinum congener. In the cyclic voltammograms, the formazanate-centered reduction potentials were substantially different as well, cathodically (negatively) shifted by at least 290 mV and as many as 500 mV in the iridium complexes. We do note that some of the reduction waves in the iridium complexes were irreversible, which makes these comparisons less quantitatively meaningful, but even in cases where both the platinum and iridium analogues have well-behaved, reversible reductions of the iridium complex was more difficult to reduce by a substantial margin. Although the electrochemical oxidation of the platinum complexes tended to not be as well-behaved and we have not investigated it thoroughly, we can compare some complexes and we find that the iridium complexes were in general easier to oxidize, although the oxidation potentials were not as sensitive to the identity of the metal as the reduction potentials, in all cases differing by <200 mV. Taken together, these observations indicated that, compared to cyclometalated platinum formazanate complexes, the iridium analogues have destabilized HOMO and LUMO energies and larger HOMO–LUMO gaps. The significant differences between the formazanate-centered properties in platinum and iridium complexes underscores the importance of d-orbital overlap with the formazanate in determining frontier orbital energies, an emerging theme in our work on formazanate 5d metal complexes.

3.3 Conclusion

In this work, we disclose the first examples of cyclometalated iridium formazanate complexes prepared by a general synthetic strategy and a thorough study of the electronic modification of the formazanate ligand on the electrochemical and photophysical properties is also presented. Structural elucidation of the complexes reveals two distinct binding modes for the formazanate, with the typical six-membered chelate form and an unusual five-membered "open" structure both observed. Systematic comparison of different cyclometalated and formazanate ligands reveals that the redox potentials are much more sensitive to the identity of the substituents on the formazanate backbone. The UV-vis absorption features prove some predictable control of photophysical properties by tuning the formazanate and cyclometalated ligands independently. In future works, we plan to continue our exploration of 5d metal formazanate complexes, further underscoring the effects of the metal identity, oxidation state, and coordination geometry on the formazanate-derived redox and optical properties.

3.4 Experimental Section

3.4.1 Materials

Reactions were carried out in a nitrogen atmosphere using standard Schlenk techniques. Solvents, starting materials, and reagents were of commercial origin and used without further purification, unless stated otherwise below. Tetrahydrofuran (THF) and toluene for UV-vis spectroscopy, and acetonitrile and dichloromethane (DCM) for electrochemical measurements were dried by the method of Grubbs,[61] passing through dual alumina columns on a commercial solvent purification system (SPS). The

acetonitrile was further dried by storage over 3A molecular sieves. Tetrabutylammonium hexafluorophosphate (TBAPF6) was recrystallized from hot ethanol and ferrocene was sublimed at ambient pressure before use in electrochemical experiments. $CDCl_3$ and CD_3CN for NMR spectroscopy was stored over potassium carbonate and molecular sieves to remove acidic impurities and moisture. The ligands 3-*p*-methoxyphenyl-1,5-di-*p*-tolylformazan (**Fza**), 1,3,5-tri-*p*-methoxyphenylformazan (**Fzb**) and 3-*p*-cyanophenyl-1,5-di-*p*-tolylformazan (**Fzc**), and 3-*p*-tolyl-1,5-di-*p*-cyanophenylformazan (**Fzd**) were prepared by the method of Hicks et al.[62] The ligands 3-cyano-1,5-di-*p*-tolylformazan (**Fze**) and 3-cyano-1,5-di-*p*-cyanophenylformazan (**Fzf**) were prepared by following the literature procedures.[30] The iridium precursors $[Ir(ppy)_2(\mu\text{-}Cl)]_2$ (ppy = 2-phenylpyridine), $[Ir(F_2ppy)_2(\mu\text{-}Cl)]_2$ (F_2ppy = 2-(2,4-difluorophenyl)pyridine), $[Ir(bt)_2(\mu\text{-}Cl)]_2$ (bt = 2-phenylbenzothiazole), and $[Ir(piq)_2(\mu\text{-}Cl)]_2$ (piq = 1-phenylisoquinoline) were prepared by a modified version of the well-known Nonoyama procedure.[63,64]

3.4.2 Physical Methods

NMR spectra were recorded at room temperature using a JEOL ECA-600, ECA-500, or ECA-400 NMR spectrometer. UV–vis absorption spectra were recorded in THF, toluene, and MeOH solutions in screw-capped 1 cm quartz cuvettes using an Agilent Cary 8454 UV–vis spectrophotometer. Cyclic voltammetry (CV) measurements were performed with a CH Instruments 602E potentiostat interfaced with a nitrogen glovebox via wire feedthroughs. Samples were dissolved in dichloromethane (CH_2Cl_2) with 0.1 M $TBAPF_6$ as a supporting electrolyte. A 3 mm diameter glassy carbon working electrode, a platinum wire counter electrode, and a silver wire pseudo-reference electrode were used.

Potentials were referenced to an internal standard of ferrocene. The bulk purity for all complexes is established by Elemental analysis, performed by Atlantic Microlab, Inc.

3.4.3 Synthesis

$Ir(ppy)_2(Fza)$ (1a/1a′). $[Ir(ppy)_2(\mu\text{-}Cl)]_2$ (101 mg, 0.0942 mmol) and **Fza** (67 mg, 0.19 mmol) were combined in ethanol (15 mL) with excess triethylamine (0.10 mL), and the mixture was deoxygenated under the protection of N_2. The mixture was refluxed for 24 h and the color changed from red to green. The reaction completion was confirmed by TLC and presence of the product as two isomers were observed on the TLC plate. Solvent was removed using rotary evaporation and the product was re-dissolved in ethyl acetate to filter through neutral alumina in order to remove insoluble impurities. After removing ethyl acetate, column chromatography (hexane / ethyl acetate gradient eluent, neutral alumina) was performed to purify the product but attempts to separate the isomers using chromatography was not successful. Both isomers were eluted together from the column, which were recrystallized (THF / pentane) later to get dark green solid. NMR analysis suggests a ca. 2:1 ratio of the "open" (**1a**) and "closed" (**1a′**) isomers, which results in very similar integration values for the resonances associated with each isomer. As such, clear assignment of the peaks was not possible, and integration values for the ^1H NMR peaks are not provided. The spectrum is shown in Figure S2 with relative integration values shown. Yield: 83 mg (51%). ^1H NMR (400 MHz, $CDCl_3$) δ: 8.70 (d, *J* = 5.6 Hz, ArH), 8.63 (d, *J* = 5.6 Hz, ArH) 8.43 (d, *J* = 6.0 Hz, ArH), 7.93 (d, *J* = 7.8 Hz, ArH), 7.58–7.87 (m, ArH), 7.30 (d, *J* = 7.8 Hz, ArH), 7.20 (dd, *J* = 5.9 Hz, ArH), 6.94–7.11 (m, ArH), 6.86 (d, *J* = 7.8 Hz, ArH), 6.73 (t, *J* = 7.3 Hz, ArH), 6.47–6.69 (m, ArH),

6.12–6.38 (m, ArH), 5.94 (d, *J* = 7.8 Hz, ArH), 5.57 (d, *J* = 7.8 Hz, ArH), 3.80 (s, OCH_3, both isomers coincident), 2.12 (s, CH_3), 2.10 (s, CH_3), 2.04 (s, CH_3). $^{13}C\{^1H\}$ NMR (151 MHz, $CDCl_3$) δ: 169.3, 168.5, 167.5, 158.8, 158.6, 158.2, 156.9, 154.7, 153.7, 152.4, 152.2, 151.8, 150.1, 149.6, 149.0, 143.7, 143.5, 142.8, 136.8, 136.7, 136.5, 134.4, 134.3, 134.2, 133.8, 133.2, 131.1, 130.2, 129.6, 129.0, 128.8, 128.5, 128.3, 127.6, 127.4, 125.6, 123.8, 123.7, 123.4, 122.2, 121.9, 121.5, 121.3, 120.6, 120.1, 119.3, 119.0, 118.9, 118.7, 113.4, 55.47, 55.4, 20.94, 20.85. Anal. Calcd for $C_{44}H_{38}IrN_6O$: C, 61.52; H, 4.46; N, 9.78. Found: C, 61.69; H, 4.47; N, 9.76.

Ir(ppy)$_2$(Fzb) (1b′). The title compound was prepared by the general method described above for complex **1a/1a',** using $[Ir(ppy)_2(\mu\text{-}Cl)]_2$ (50 mg, 0.047 mmol) and **Fzb** (37 mg, 0.094 mmol). The product was isolated as a mixture of isomer and recrystallized later (CH_2Cl_2/ pentane) to get a dark green solid. Yield: 36 mg (43%). We were unable to obtain satisfactory elemental analysis for this compound, but the NMR spectrum provide evidence for bulk purity. The minor impurity peaks in the ^1H NMR spectrum arise from a small amount of the "open" isomer **1b** present in the isolated product. ^1H NMR (400 MHz, $CDCl_3$) δ: 8.70 (d, *J* = 5.5 Hz, 2H, ArH), 7.82 (d, *J* = 8.7 Hz, 2H, ArH), 7.60–7.71 (m, 4H, ArH), 7.21–7.28 (m, 2H, ArH), 6.95–7.03 (m, 2H, ArH), 6.86 (d, *J* = 8.7 Hz, 2H, ArH), 6.65 (t, *J* = 7.3 Hz, 2H, ArH), 6.51–6.61 (m, 6H, ArH), 6.18–6.32 (m, 6H, ArH), 3.80 (s, 3H, OCH_3), 3.62 (s, 6H, OCH_3). $^{13}C\{^1H\}$ NMR (151 MHz, $CDCl_3$) δ: 168.5, 158.3, 156.8, 154.8, 150.0, 149.0, 148.9, 143.7, 136.9, 134.3, 133.8, 130.1, 128.9, 125.6, 124.6, 123.7, 121.5, 120.7, 118.8, 113.4, 113.1, 112.2, 55.47, 55.21.

Ir(ppy)$_2$(Fzc) (1c′). [Ir(ppy)$_2$(μ-Cl)]$_2$ (54 mg, 0.05 mmol) and **Fzc** (34 mg, 0.10 mmol) were combined in ethanol (10 mL) with excess triethylamine (0.1 mL), and the mixture was deoxygenated under the protection of N_2. The mixture was refluxed for 36 h and the color changed from red to green. The reaction completion was confirmed by TLC. Solvent was removed using rotary evaporation and the product was re-dissolved in minimum amount of ethyl acetate. After that column chromatography (hexane / ethyl acetate gradient eluent, neutral alumina) was performed to purify the product, which was crystallized by vapor diffusion of pentane into a concentrated CH_2Cl_2 solution. Yield: 43 mg (50%). ^{1}H NMR (500 MHz, $CDCl_3$) δ: 8.68 (d, *J* = 5.5 Hz, 2H, ArH), 7.98 (d, *J* = 8.6 Hz, 2H, ArH), 7.69–7.74 (m, 2H, ArH), 7.65 (d, *J* = 7.9 Hz, 2H, ArH), 7.52 (d, *J* = 8.6 Hz, 2H, ArH), 7.18–7.20 (m, 2H, ArH), 7.05 (ddd, *J* = 7.2, 5.8, 1.2 Hz, 2H, ArH), 6.61–6.65 (m, 2H, ArH), 6.57 (dd, *J* = 7.4, 1.1 Hz, 2H, ArH), 6.53 (d, *J* = 8.1 Hz, 4H, ArH), 6.44 (d, *J* = 8.4 Hz, 4H, ArH), 6.17 (d, *J* = 7.0 Hz, 2H, ArH), 2.11 (s, 6H, CH_3). ^{13}C{^{1}H} NMR (151 MHz, $CDCl_3$) δ: 168.5, 153.8, 153.7, 149.7, 146.8, 146.0, 143.5, 137.2, 134.9, 133.7, 131.7, 129.0, 127.6, 124.1, 123.7, 123.1, 121.8, 120.9, 120.4, 119.0, 107.6, 20.9. Anal. Calcd for $C_{44}H_{34}N_7Ir$: C, 61.95, H, 4.02, N, 11.49. Found: C, 62.04, H, 4.00, N, 11.36.

Ir(ppy)$_2$(Fzd) (1d). The title compound was prepared by the general method described above for complex **1c',** using [Ir(ppy)$_2$(μ-Cl)]$_2$ (54 mg, 0.050 mmol) and **Fzd** (37 mg, 0.10 mmol). Yield: 62 mg (72%). ^{1}H NMR (500 MHz, $CDCl_3$) δ: 8.46 (d, *J* = 5.7 Hz, 1H, ArH), 8.34 (d, *J* = 5.6 Hz, 1H, ArH), 7.83–7.88 (m, 1H, ArH), 7.82 (d, *J* = 7.2 Hz, 1H, ArH), 7.73 (d, *J* = 8.3 Hz, 2H, ArH), 7.72 (dd, *J* = 7.1, 1.3 Hz, 1H, ArH), 7.68

(d, *J* = 7.2 Hz, 1H, ArH), 7.33 (dd, *J* = 7.9, 1.0 Hz, 1H, ArH), 7.25 (d, *J* = 8.1 Hz, 1H, ArH), 7.20 (s, 2H, ArH), 7.18 (s, 2H, ArH), 7.10 (d, *J* = 8.9 Hz, 4H, ArH), 6.87 (d, *J* = 8.6 Hz, 2H, ArH), 6.79 (td, *J* = 7.6, 1.2 Hz, 1H, ArH), 6.68–6.74 (m, 2H, ArH), 6.40 (td, *J* = 7.5, 1.1 Hz, 1H, ArH), 6.35 (d, *J* = 8.2 Hz, 2H, ArH), 5.91 (dd, *J* = 7.8, 0.9 Hz, 1H, ArH), 5.63–5.67 (m, 1H, ArH), 2.37 (s, 3H, CH_3). $^{13}C\{^1H\}$ NMR (151 MHz, $CDCl_3$) δ: 168.9, 167.4, 161.3, 160.4, 157.0, 155.9, 155.3, 151.6, 149.1, 148.3, 147.2, 143.4, 142.6, 138.3, 137.6, 137.5, 132.1, 132.0, 130.7, 130.5, 130.2, 129.7, 129.1, 128.9, 124.3, 124.2, 122.6, 122.5, 122.3, 122.2, 121.1, 120.5, 119.8, 119.5, 119.4, 108.3, 105.7, 21.5. Anal. Calcd for $C_{44}H_{31}N_8Ir$: C, 61.17, H, 3.62, N, 12.97. Found: C, 61.03, H, 3.68, N, 12.72.

Ir(ppy)$_2$(Fze) (1e). The title compound was prepared by the general method described above for complex **1c',** using $[Ir(ppy)_2(\mu\text{-}Cl)]_2$ (54 mg, 0.050 mmol) and **Fze** (28 mg, 0.10 mmol). Yield: 47 mg (60%). ^1H NMR (500 MHz, $CDCl_3$) δ: 8.37 (d, *J* = 5.5 Hz, 1H, ArH), 8.27 (d, *J* = 5.4 Hz, 1H, ArH), 7.78–7.83 (m, 1H, ArH), 7.76 (d, *J* = 7.7 Hz, 1H, ArH), 7.68–7.72 (m, 1H, ArH), 7.65 (d, *J* = 7.9 Hz, 1H, ArH), 7.27 (s, 1H, ArH), 7.19 (d, *J* = 7.4 Hz, 1H, ArH), 7.12–7.16 (m, 1H, ArH), 7.05–7.09 (m, 1H, ArH), 6.82 (d, *J* = 8.5 Hz, 2H, ArH), 6.74 (td, *J* = 7.5, 0.8 Hz, 1H, ArH), 6.67 (d, *J* = 7.8 Hz, 3H, ArH), 6.59 (t, *J* = 7.8 Hz, 1H, ArH), 6.38 (d, *J* = 8.0 Hz, 2H, ArH), 6.30 (t, *J* = 7.8 Hz, 1H, ArH), 6.22 (d, *J* = 8.1 Hz, 2H, ArH), 5.89 (d, *J* = 7.5 Hz, 1H, ArH), 5.55 (d, *J* = 7.5 Hz, 1H, ArH), 2.13 (s, 3H, CH_3), 2.04 (s, 3H, CH_3). $^{13}C\{^1H\}$NMR (151 MHz, $CDCl_3$) δ: 168.8, 167.2, 167.2, 153.7, 151.2, 150.6, 150.4, 149.7, 148.1, 143.4, 142.6, 137.4, 136.4, 136.3, 135.2, 132.0, 130.9, 129.9, 129.4, 128.5, 128.3, 124.0, 123.9, 122.6, 122.3, 122.1,

121.9, 120.1, 120.1, 119.2, 119.2, 116.2, 21.0, 21.0. Anal. Calcd for $C_{38}H_{30}N_7Ir$: C, 58.75, H, 3.89, N, 12.62. Found: C, 58.90, H, 3.89, N, 12.42.

Ir(ppy)$_2$(Fzf) (1f). The title compound was prepared by the general method described above for complex **1c',** using $[Ir(ppy)_2(\mu\text{-}Cl)]_2$ (54 mg, 0.050 mmol) and **Fzf** (30 mg, 0.10 mmol). Yield: 41 mg (52%). ^{1}H NMR (500 MHz, CD_3CN) δ: 8.40 (d, *J* = 5.6 Hz, 1H, ArH), 8.26 (d, *J* = 5.5 Hz, 1H, ArH), 7.97 (t, *J* = 7.1 Hz, 1H, ArH), 7.91 (d, *J* = 8.0 Hz, 1H, ArH), 7.85 (t, *J* = 7.8 Hz, 1H, ArH), 7.76 (d, *J* = 8.0 Hz, 1H, ArH), 7.32 (d, *J* = 7.7 Hz, 1H, ArH), 7.28 (dd, *J* = 7.6, 4.3 Hz, 2H, ArH), 7.20–7.24 (m, 1H, ArH), 7.17 (d, *J* = 8.7 Hz, 2H, ArH), 7.00 (d, *J* = 8.5 Hz, 2H, ArH), 6.98 (d, *J* = 8.7 Hz, 2H, ArH), 6.75 (t, *J* = 7.0 Hz, 1H, ArH), 6.69 (dd, *J* = 10.7, 4.2 Hz, 1H, ArH), 6.66 (dd, *J* = 11.5, 4.2 Hz, 1H, ArH), 6.49 (d, *J* = 8.4 Hz, 2H, ArH), 6.40 (t, *J* = 6.9 Hz, 1H, ArH), 5.83 (d, *J* = 7.6 Hz, 1H, ArH), 5.60 (d, *J* = 7.5 Hz, 1H, ArH). ^{13}C{^{1}H}NMR (151 MHz, CD_3CN) δ: 167.7, 166.1, 155.3, 154.2, 152.5, 151.5, 150.5, 146.8, 144.0, 143.2, 138.8, 138.8, 137.9, 137.2, 132.2, 132.0, 130.6, 129.9, 129.4, 124.4, 124.1, 123.9, 123.5, 123.0, 122.6, 121.1, 120.6, 120.1, 119.7, 118.7, 118.64, 114.6, 110.1, 108.1. Anal. Calcd for $C_{38}H_{24}N_9Ir$: C, 57.13, H, 3.03, N, 15.78. Found: C, 57.30, H, 3.18, N, 15.56.

Ir(F$_2$ppy)$_2$(Fza) (2a). The title compound was prepared by the general method described above for complex **1c',** using $[Ir(F_2ppy)_2(\mu\text{-}Cl)]_2$ (61 mg, 0.050 mmol) and **Fza** (36 mg, 0.10 mmol). Yield: 76 mg (82%). ^{1}H NMR (500 MHz, CD_3CN) δ: 8.57 (d, *J* = 4.3 Hz, 1H, ArH), 8.44 (d, *J* = 4.5 Hz, 1H, ArH), 8.17 (d, *J* = 6.9 Hz, 1H, ArH), 8.03 (d, *J* = 6.9 Hz, 1H, ArH), 7.92 (d, *J* = 8.1 Hz, 2H, ArH), 7.78–7.85 (m, 1H, ArH), 7.71 (td, *J* = 8.0, 1.2 Hz, 1H, ArH), 7.11 (ddd, *J* = 7.3, 5.9, 1.4 Hz, 1H, ArH), 7.08 (ddd, *J* = 7.3, 5.9,

1.4 Hz, 1H, ArH), 6.88 (dd, *J* = 7.0, 3.0 Hz, 4H, ArH), 6.71 (d, *J* = 6.7 Hz, 2H, ArH), 6.51 (d, *J* = 6.5 Hz, 2H, ArH), 6.27 (ddd, *J* = 12.3, 9.1, 2.3 Hz, 1H, ArH), 6.15 (d, *J* = 5.9 Hz, 2H, ArH), 6.06 (ddd, *J* = 12.5, 9.3, 2.3 Hz, 1H, ArH), 5.41 (dd, *J* = 7.0, 1.8 Hz, 1H, ArH), 5.11 (dd, *J* = 7.0, 1.8 Hz, 1H, ArH), 3.81 (s, 3H, OCH_3), 2.15 (s, 3H, CH_3), 2.13 (s, 3H, CH_3). $^{13}C\{^1H\}$NMR (126 MHz, CD_3CN) δ: 165.8 (d, J_{CF} = 5.3 Hz), 164.2 (d, J_{CF} = 5.5 Hz), 163.5 (d, J_{CF} = 10.2 Hz), 163.3, 161.7 (d, J_{CF} = 9.8 Hz), 161.0 (d, J_{CF} = 7.7 Hz), 159.8 (d, J_{CF} = 5.2 Hz), 158.8, 158.4, 154.2, 152.2, 151.8, 151.6, 149.8, 137.9, 137.7, 135.1, 133.9, 130.2, 128.6, 128.2, 127.5, 127.2, 126.9, 123.2 (d, J_{CF} = 15.9 Hz), 122.9 (d, J_{CF} = 16.4 Hz), 122.5, 122.2, 121.7, 120.4, 113.9(d, J_{CF} = 12.5 Hz), 113.5, 113.0 (d, J_{CF} = 13.8 Hz), 97.7 (t, J_{CF} = 26.8 Hz), 95.9 (t, J_{CF} = 27.1 Hz), 55.4, 20.9, 20.6. ^{19}F NMR (470 MHz, CD_3CN) δ: −107.6 (dd, *J* = 19.0, 9.2 Hz, 1F), −109.4 (dd, *J* = 18.9, 9.4 Hz, 1F), −110.2 (t, *J* = 12.4 Hz, 1F), −111.1 (t, *J* = 11.4 Hz, 1F). Anal. Calcd for $C_{44}H_{33}N_6F_4OIr$: C, 56.83, H, 3.58, N, 9.04. Found: C, 56.76, H, 3.67, N, 8.90.

Ir(F_2ppy)$_2$(Fzb) (2b). The title compound was prepared by the general method described above for complex **1c',** using $[Ir(F_2ppy)_2(\mu\text{-}Cl)]_2$ (61 mg, 0.050 mmol) and **Fzb** (39 mg, 0.10 mmol). Yield: 53 mg (55%). ^1H NMR (500 MHz, CD_3CN) δ: 8.58–8.62 (m, 1H, ArH), 8.46 (d, *J* = 5.5 Hz, 1H, ArH), 8.13 (d, *J* = 8.6 Hz, 1H, ArH), 7.99 (d, *J* = 8.4 Hz, 1H, ArH), 7.93–7.97 (m, 1H, ArH), 7.83 (dd, *J* = 11.7, 5.1 Hz, 1H, ArH), 7.68 (d, *J* = 9.0 Hz, 2H, ArH), 7.29 (t, *J* = 7.3 Hz, 1H, ArH), 7.24 (t, *J* = 6.6 Hz, 1H, ArH), 6.88 (d, *J* = 9.0 Hz, 2H, ArH), 6.72 (d, *J* = 9.0 Hz, 2H, ArH), 6.41 (d, *J* = 6.9 Hz, 2H, ArH), 6.38–6.42 (m, 1H, ArH), 6.30 (d, *J* = 9.1 Hz, 2H, ArH), 6.21 (d, *J* = 8.1 Hz, 2H, ArH), 6.06–6.12 (m, 1H, ArH), 5.43 (dd, *J* = 7.6, 3.5 Hz, 1H, ArH), 5.21 (dd, *J* = 8.9, 2.4 Hz, 1H,

ArH), 3.77 (s, 3H, OCH_3), 3.62 (s, 3H, OCH_3), 3.60 (s, 3H, OCH_3). ^{13}C {^1H} NMR (126 MHz, CD_3CN) δ: 164.9 (d, J_{CF} = 7.1 Hz), 163.2 (d, J_{CF} = 7.4 Hz), 162.4 (d, J_{CF} = 5.2 Hz), 161.7 (d, J_{CF} = 12.1 Hz), 161.6 (d, J_{CF} = 13.8 Hz), 161.5, 159.7 (d, J_{CF} = 4.7 Hz), 159.6 (d, J_{CF} = 3.9 Hz), 158.8, 158.4, 157.5, 156.5, 154.7 (d, J_{CF} = 6.3 Hz), 151.8, 150.8, 148.1, 147.6, 138.7, 138.6, 130.5, 127.7, 127.4, 123.5, 123.3 (d, J_{CF} = 19.9 Hz), 123.1, 123.0, 122.7 (d, J_{CF} = 20.4 Hz), 121.8, 114.1(d, J_{CF} = 16.5 Hz), 113.1, 112.9, 112.8, 112.6, 97.31, 96.16, 55.0, 54.9, 54.8. ^{19}F NMR (470 MHz, CD_3CN) δ: −109.5 (dd, *J* = 18.8, 9.4 Hz, 1F), −111.2 (q, *J* = 9.5 Hz, 1F), −111.7 (t, *J* = 11.8 Hz, 1F), −111.8 (t, *J* = 11.8 Hz, 1F). Anal. Calcd for $C_{44}H_{33}N_6F_4O_3Ir$: C, 54.94, H, 3.46, N, 8.74. Found: C, 54.76, H, 3.51, N, 8.57.

Ir(F_2ppy)$_2$(Fzc) (2c). The title compound was prepared by the general method described above for complex **1c',** using [Ir(F_2ppy)$_2$(μ-Cl)]$_2$ (61 mg, 0.050 mmol) and **Fzc** (34 mg, 0.10 mmol). Yield: 67 mg (73%). ^1H NMR (500 MHz, $CDCl_3$) δ: 8.48 (d, *J* = 5.9 Hz, 1H, ArH), 8.40 (d, *J* = 6.5 Hz, 1H, ArH), 8.18 (d, *J* = 8.4 Hz, 3H, ArH), 8.03 (d, *J* = 9.2 Hz, 1H, ArH), 7.85 (t, *J* = 7.8 Hz, 1H, ArH), 7.74 (t, *J* = 7.8 Hz, 1H, ArH), 7.57 (d, *J* = 8.4 Hz, 2H, ArH), 7.14 (t, *J* = 6.6 Hz, 1H, ArH), 7.11 (t, *J* = 6.6 Hz, 1H, ArH), 6.80 (d, *J* = 8.4 Hz, 2H, ArH), 6.73 (d, *J* = 8.4 Hz, 2H, ArH), 6.56 (d, *J* = 8.2 Hz, 2H, ArH), 6.23–6.31 (m, 1H, ArH), 6.18 (d, *J* = 7.8 Hz, 2H, ArH), 6.06–6.12 (m, 1H, ArH), 5.37 (dd, *J* = 8.7, 2.3 Hz, 1H, ArH), 5.11 (dd, *J* = 8.6, 2.3 Hz, 1H, ArH), 2.17 (s, 3H, CH_3), 2.15 (s, 3H, CH_3). $^{13}C\{^1H\}$NMR (151 MHz, $CDCl_3$) δ: 165.7 (d, J_{CF} = 5.5 Hz), 164.1 (d, J_{CF} = 4.7 Hz), 163.6 (d, J_{CF} = 2.4 Hz), 160.6, 160.0 (d, J_{CF} = 4.2 Hz), 155.8, 153.0 (d, J_{CF} = 5.8 Hz), 151.5, 151.3, 151.1, 149.6, 138.5, 138.1, 138.0, 136.0, 134.9, 131.9, 128.7, 128.3,

128.3, 127.3, 127.2, 123.4, 123.2, 123.1, 122.7, 122.5, 121.9, 120.3, 119.7, 113.9 (d, J_{CF} = 13.2 Hz), 113.4, 112.9 (d, J_{CF} = 13.9 Hz), 109.3, 97.99 (t, J_{CF} = 26 Hz), 96.41, 96.24, 21.0, 20.7. ^{19}F NMR (470 MHz, $CDCl_3$) δ: −107.2 (dd, *J* = 15.1, 7.4 Hz, 1F), −108.9 (dd, *J* = 15.0, 7.4 Hz, 1F), −110.0 (t, *J* = 9.2 Hz, 1F), −110.6 (t, *J* = 9.1 Hz, 1F). Anal. Calcd for $C_{44}H_{30}N_7F_4Ir$: C, 57.13, H, 3.27, N, 10.60. Found: C, 57.14, H, 3.42, N, 10.46.

Ir(F$_2$ppy)$_2$(Fzd) (2d). The title compound was prepared by the general method described above for complex **1c',** using $[Ir(F_2ppy)_2(\mu\text{-}Cl)]_2$ (61 mg, 0.050 mmol) and **Fzd** (37 mg, 0.10 mmol). Yield: 75 mg (80%). ^{1}H NMR (500 MHz, $CDCl_3$) δ: 8.41 (d, *J* = 5.8 Hz, 1H, ArH), 8.37 (d, *J* = 5.7 Hz, 1H, ArH), 8.21 (d, *J* = 8.4 Hz, 1H, ArH), 8.08 (d, *J* = 8.3 Hz, 1H, ArH), 7.93 (t, *J* = 7.9 Hz, 1H, ArH), 7.79 (t, *J* = 7.9 Hz, 1H, ArH), 7.72 (dd, *J* = 8.1, 1.6 Hz, 2H, ArH), 7.14–7.22(m, 6H, ArH), 7.12 (dd, *J* = 8.8, 1.9 Hz, 2H, ArH), 7.03–7.06 (m, 2H, ArH), 6.35 (d, *J* = 8.8 Hz, 3H, ArH), 6.23 (dd, *J* = 12.1, 9.4 Hz, 1H, ArH), 5.35–5.40 (m, 1H, ArH), 5.15–5.19 (m, 1H, ArH), 2.37 (s, 3H, CH_3). ^{13}C{^{1}H}NMR (151 MHz, $CDCl_3$) δ: 165.5 (d, J_{CF} = 7.0 Hz), 164.0, 163.8 (d, J_{CF} = 7.5 Hz), 162.0 (dd, J_{CF} = 17.4, 11.9 Hz), 161.7 (d, J_{CF} = 7.7 Hz), 161.0, 160.1, 160.0, 159.0 (d, J_{CF} = 6.0 Hz), 156.5, 155.6, 152.0 (d, J_{CF} = 6.8 Hz), 151.6, 149.2, 138.7, 138.7, 132.3, 131.5, 129.8, 129.1, 129.0, 127.4, 127.1, 123.7 (d, J_{CF} = 19.8 Hz), 123.4 (d, J_{CF} = 19.8 Hz), 123.0, 122.9, 122.0, 120.7, 119.5, 118.6, 114.2 (d, J_{CF} = 17.8 Hz), 112.9 (d, J_{CF} = 18.0 Hz), 109.0, 106.8, 98.8 (t, J_{CF} = 26.6 Hz), 97.6 (t, J_{CF} = 26.6 Hz), 21.5. ^{19}F NMR (470 MHz, $CDCl_3$) δ: −105.8 (dd, *J* = 8.6, 10 Hz, 1F), −107.0 (dd, *J* = 8.6, 10 Hz, 1F), −108.7 (t, J = 11 Hz, 1F), −109.2 (t, *J* = 10 Hz, 1F). Anal. Calcd for $C_{44}H_{27}N_8F_4Ir$: C, 56.46, H, 2.91, N, 11.97. Found: C, 56.22, H, 3.13, N, 11.70.

Ir(F_2ppy)$_2$(Fze) (2e). The title compound was prepared by the general method described above for complex **1c',** using [Ir(F_2ppy)$_2$(μ-Cl)]$_2$ (61 mg, 0.050 mmol) and **Fze** (28 mg, 0.10 mmol). Yield: 46 mg (54%). ^{1}H NMR (400 MHz, $CDCl_3$) δ: 8.32 (d, *J* = 5.6 Hz, 1H), 8.27 (d, *J* = 5.7 Hz, 1H, ArH), 8.16 (d, *J* = 8.7 Hz, 1H, ArH), 8.03 (d, *J* = 9.1 Hz, 1H, ArH), 7.89 (t, *J* = 7.9 Hz, 1H, ArH), 7.79 (t, *J* = 7.9 Hz, 1H, ArH), 7.20–7.24 (m, 1H, ArH), 7.13Ą7.19 (m, 1H, ArH), 6.72 (s, 4H, ArH), 6.56 (d, *J* = 8.0 Hz, 2H, ArH), 6.24–6.33 (m, 1H, ArH), 6.20 (d, *J* = 8.0 Hz, 2H, ArH), 6.05–6.15 (m, 1H, ArH), 5.34 (d, *J* = 6.7 Hz, 1H, ArH), 5.06 (d, *J* = 8.6 Hz, 1H, ArH), 2.17 (s, 3H, CH_3), 2.13 (s, 3H, CH_3). ^{13}C{^{1}H}NMR (151 MHz, $CDCl_3$) δ: 166.3, 163.7 (d, J_{CF} = 6.7 Hz), 161.9 (t, J_{CF} = 11.7 Hz), 161.6 (d, J_{CF} = 12.3 Hz), 159.9, 157.7 (d, J_{CF} = 6.5 Hz), 151.8, 151.7 (d, J_{CF} = 7.2 Hz), 151.2, 150.3, 149.9, 149.8, 138.6, 137.0, 136.1, 128.7, 128.3, 127.8, 127.3, 127.0, 123.4, 123.3 (d, J_{CF} = 20.4 Hz), 123.1, 122.8 (d, J_{CF} = 39.7 Hz), 122.3, 121.9, 120.1, 115.5, 114.2 (d, J_{CF} = 17.0 Hz), 113.0 (d, J_{CF} = 16.8 Hz), 98.4 (t, J_{CF} = 27.0 Hz), 96.7 (t, J_{CF} = 25.5 Hz), 21.0, 20.8. ^{19}F NMR (470 MHz, $CDCl_3$) δ: −106.7 (dd, *J* = 19.1, 9.1 Hz, 1F), −108.4 (dd, *J* = 19.1, 9.4 Hz, 1F), −109.7 (t, *J* = 11.6 Hz, 1F), −110.2 (t, *J* = 11.6 Hz, 1F). Anal. Calcd for $C_{38}H_{26}N_7F_4Ir$: C, 53.77, H, 3.09, N, 11.55. Found: C, 53.75, H, 3.26, N, 11.62.

Ir(F_2ppy)$_2$(Fzf) (2f). The title compound was prepared by the general method described above for complex **1c',** using [Ir(F_2ppy)$_2$(μ-Cl)]$_2$ (61 mg, 0.050 mmol) and **Fzf** (30 mg, 0.10 mmol). Yield: 51 mg (58%). ^{1}H NMR (500 MHz, CD_3CN) δ: 8.44 (d, *J* = 5.1 Hz, 1H, ArH), 8.31 (d, *J* = 6.5 Hz, 1H, ArH), 8.14 (d, *J* = 8.4 Hz, 1H, ArH), 8.04 (t, *J* = 8.1 Hz, 1H, ArH), 8.00 (d, *J* = 8.4 Hz, 1H, ArH), 7.92 (t, *J* = 8.0 Hz, 1H, ArH), 7.35

(ddd, *J* = 7.4, 5.8, 1.4 Hz, 1H, ArH), 7.29–7.32 (m, 1H, ArH), 7.26–7.29 (m, 2H, ArH), 7.21 (d, *J* = 8.7 Hz, 2H, ArH), 6.92 (d, *J* = 6.8 Hz, 2H, ArH), 6.54 (d, *J* = 8.4 Hz, 2H, ArH), 6.42 (ddd, *J* = 12.6, 9.3, 2.3 Hz, 1H, ArH), 6.29 (ddd, *J* = 12.7, 9.4, 2.3 Hz, 1H, ArH), 5.37 (dd, *J* = 8.7, 2.4 Hz, 1H, ArH), 5.18 (dd, *J* = 8.7, 2.4 Hz, 1H, ArH). $^{13}C\{^{1}H\}$NMR (151 MHz, CD_3CN) δ: 163.8 (d, J_{CF} = 7.2 Hz), 163.3, 162.3 (d, J_{CF} = 6.6 Hz), 161.6 (d, J_{CF} = 12.5 Hz), 161.1, 159.5 (d, J_{CF} = 3.8 Hz), 156.7 (d, J_{CF} = 6.9 Hz), 154.8, 154.1, 152.1, 151.2, 150.4, 139.8 (d, J_{CF} = 15.9 Hz), 137.7, 132.3, 132.1, 131.7, 127.6, 124.5, 124.2, 123.8 (d, J_{CF} = 19.8 Hz), 123.6, 123.5 (d, J_{CF} = 20.1 Hz), 123.0, 121.0, 118.5, 118.2, 114.4, 114.1, 112.9, 110.6, 108.8, 98.7 (t, J_{CF} = 27.1 Hz), 97.4 (t, *J* = 27.2 Hz). ^{19}F NMR (470 MHz, CD_3CN) δ: −107.8 (dd, *J* = 19.1, 9.2 Hz, 1F), −109.4 (dd, *J* = 19.0, 9.4 Hz, 1F), −110.6 (t, *J* = 11.4 Hz, 1F), −110.7 (t, *J* = 11.6 Hz, 1F). Anal. Calcd for $C_{38}H_{20}N_9F_4Ir$: C, 52.41, H, 2.31, N, 14.48. Found: C, 52.34, H, 2.59, N, 14.23.

Ir(bt)$_2$(Fza) (3a). The title compound was prepared by the general method described above for complex **1a/1a',** using $[Ir(bt)_2(\mu\text{-}Cl)]_2$ (51 mg, 0.039 mmol) and **Fza** (37 mg, 0.10 mmol). The dark green solid product was isolated as a mixture of isomer where the major product was the five-member chelate with a trace amount of six-member chelate evident from ^{1}H NMR data (Figure S32). Yield: 35 mg (47%). ^{1}H NMR (500 MHz, $CDCl_3$) δ: 7.97–8.03 (m, 2H, ArH), 7.71–7.91 (m, 4H, ArH), 7.32–7.51 (m, 4H, ArH), 7.22 (d, *J* = 7.5 Hz, 1H, ArH), 7.02 (d, *J* = 8.0 Hz, 1H, ArH), 6.78–6.84 (m, 2H, ArH), 6.72 (t, *J* = 7.4 Hz, 1H, ArH), 6.53–6.67 (m, 2H, ArH), 6.32–6.52 (m, 9H, ArH), 6.19 (d, *J* = 8.0 Hz, 1H, ArH), 6.12 (d, *J* = 8.0 Hz, 1H, ArH), 3.76 (s, 3H, CH_3), 2.09 (s 3H, CH_3), 2.08 (s, 3H, CH_3). $^{13}C\{^{1}H\}$ NMR (101 MHz, $CDCl_3$) δ: 181.5, 179.8, 161.7,

150.2.150.0, 149.2, 140.0, 139.5, 133.4, 131.5, 131.3, 131.0, 130.9, 130.0, 128.1, 128.0, 127.6, 127.4, 126.1, 125.6, 125.4, 123.6, 122.8, 122.4, 121.7, 121.1, 120.6, 119.7, 113.5, 55.36, 21.05, 20.89. Anal. Calcd for $C_{48}H_{37}IrN_6OS_2$: C, 59.42; H, 3.84; N, 8.66. Found: C, 59.44; H, 3.84; N, 8.58.

Ir(bt)$_2$(Fzb) (3b). The title compound was prepared by the general method described above for complex **1a/1a',** using $[Ir(bt)_2(\mu\text{-}Cl)]_2$ (50 mg, 0.039 mmol) and **Fzb** (32 mg, 0.81 mmol). The product was isolated as a mixture of isomers after column chromatography, and recrystallization of the product from a THF/MeOH mixture afforded pure **3b** as a dark green solid. Yield: 39 mg (50%). ^{1}H NMR (400 MHz, $CDCl_3$) δ: 7.95–8.02 (m, 2H, ArH), 7.78–7.89 (m, 2H, ArH), 7.72 (d, *J* = 8.7 Hz, 2H, ArH), 7.34–7.52 (m, 4H, ArH), 7.22–7.29 (m, 1H, ArH), 7.11 (d, *J* = 7.3 Hz, 1H, ArH), 6.82 (d, *J* = 8.7 Hz, 2H, ArH), 6.72 (t, *J* = 7.3 Hz, 1H, ArH), 6.42–6.67 (m, 7H, ArH), 6.09–6.27 (m, 6H, ArH), 3.78 (s, 3H, OCH_3), 3.62 (s, 3H, OCH_3), 3.61 (s, 3H, OCH_3). $^{13}C\{^1H\}$ NMR (151 MHz, $CDCl_3$) δ: 181.4, 179.7, 162.6, 158.5, 157.1, 156.2, 150.1, 149.8, 149.7, 149.2, 147.3, 146.5, 140.7, 140.1, 139.6, 134.2, 133.5, 131.6, 131.3, 131.0, 130.9, 130.0, 129.9, 128.2, 127.7, 126.0, 125.7, 125.5, 124.8, 123.7, 122.9, 122.4, 122.3, 121.7, 121.0, 120.5, 120.4, 113.6, 112.8, 112.6, 112.2, 55.55, 55.36, 55.12. Anal. Calcd for $C_{48}H_{37}IrN_6O_3S_2$: C, 57.53; H, 3.72; N, 8.39. Found: C, 57.22; H, 3.57; N, 7.91.

Ir(bt)$_2$(Fze) (3e). The title compound was prepared by the general method described above for Complex **1c',** using $[Ir(bt)_2(\mu\text{-}Cl)]_2$ (100 mg, 0.0771 mmol) and **Fze** (39 mg, 0.15 mmol). The product was obtained as a reddish green solid. Yield: 45 mg (33%). Elemental analysis returned low percentages for C, H, and N, but the NMR

spectra in Figures S36 and S37 indicate satisfactory bulk purity. ^{1}H NMR (400 MHz, $CDCl_3$) δ: 8.08 (d, *J* = 7.3 Hz, 2H, ArH), 7.80 (d, *J* = 7.8 Hz, 1H, ArH), 7.74 (d, *J* = 7.8 Hz, 1H, ArH), 7.68 (d, *J* = 8.2 Hz, 1H, ArH), 7.38–7.47 (m, 1H, ArH), 6.98–7.34 (m, 10H, ArH), 6.79–6.93 (m, 3H, ArH), 6.72 (d, *J* = 6.8 Hz, 3H, ArH), 6.49–6.54 (m, 1H, ArH), 6.44 (d, *J* = 7.8 Hz, 1H, ArH), 2.33 (s, 3H, CH_3), 2.24 (s, 3H, CH_3). $^{13}C\{^{1}H\}$ NMR (151 MHz, $CDCl_3$) δ: 182.7, 180.0, 178.1, 171.7, 170.8, 150.9, 150.0, 149.9, 141.5, 139.9, 138.7, 138.2, 137.1, 133.0, 132.6, 131.2, 131.1, 130.8, 129.7, 128.5, 127.5, 127.4, 125.8, 125.6, 125.4, 125.3, 124.1, 122.8, 122.2, 121.9, 121.2, 120.8, 119.6, 119.4, 21.34, 21.23. Anal. Calcd for $C_{42}H_{30}IrN_7S_2$: C, 56.74; H, 3.40; N, 11.03. Found: C, 57.70; H, 3.93; N, 10.28.

Ir(bt)$_2$(Fzf) (3f). The title compound was prepared by the general method described above for complex **1c',** using $[Ir(bt)_2(\mu\text{-}Cl)]_2$ (100 mg, 0.0771 mmol) and **Fzf** (46 mg, 0.15 mmol). The product was isolated as a greenish brown solid. Yield: 51 mg (38%). ^{1}H NMR (500 MHz, $CDCl_3$) δ: 7.92–7.99 (m, 2H, ArH), 7.64–7.71 (m, 1H, ArH), 7.41–7.61 (m, 5H, ArH), 7.23–7.30 (m, 1H, ArH), 7.13 (d, *J* = 7.8 Hz, 2H, ArH), 7.01–7.08 (m, 2H, ArH), 6.95 (d, *J* = 8.2 Hz, 2H, ArH), 6.77–6.86 (m, 2H, ArH), 6.69–6.76 (m, 3H, ArH), 6.58–6.66 (m, 3H, ArH), 6.05 (dd, *J* = 7.8, 22.9 Hz, 2H, ArH). $^{13}C\{^{1}H\}$ NMR (126 MHz, $CDCl_3$) δ: 181.6, 180.1, 155.6, 154.8, 152.7, 149.2, 148.4, 146.2, 139.7, 139.4, 139.1, 133.3, 132.0, 131.9, 131.5, 131.3, 131.1, 130.6, 129.1, 128.7, 126.7, 127.7, 126.4, 126.0, 123.7, 123.4, 123.3, 123.2, 122.2, 120.9, 119.2, 119.0, 118.9, 118.6, 114.2, 110.5, 108.7. Anal. Calcd for $C_{42}H_{24}IrN_9S_2.0.25C_4H_8O_2$: C, 55.35; H, 2.80; N, 13.51. Found: C, 55.49; H, 2.67; N, 13.52.

Ir(piq)$_2$(Fza) (4a). The title compound was prepared by the general method described above for complex **1a/1a',** using [Ir(piq)$_2$(μ-Cl)]$_2$ (100 mg, 0.0785 mmol) and **Fza** (63 mg, 0.16 mmol). The product was isolated as a mixture of isomer and recrystallized later (CH_2Cl_2/pentane) to get greenish blue solid. Yield: 74 mg (48%). ^{1}H NMR (400 MHz, $CDCl_3$) δ: 8.65–8.74 (m, 1H, ArH), 8.58–8.64 (m, 1H, ArH), 8.46 (d, *J* = 6.4 Hz, 1H, ArH), 8.32 (d, *J* = 6.4 Hz, 1H, ArH), 7.79–7.93 (m, 5H, ArH), 7.58–7.78 (m, 5H, ArH), 7.37 (d, *J* = 6.4 Hz, 1H, ArH), 7.30 (d, *J* = 6.4 Hz, 1H, ArH), 6.78–6.88 (m, 5H, ArH), 6.45–6.64 (m, 5H, ArH), 6.31–6.43 (m, 3H, ArH), 6.21–6.28 (m, 2H, ArH), 6.14 (d, *J* = 6.4 Hz, 1H, ArH), 5.79 (d, *J* = 8.0 Hz, 1H, ArH), 3.78 (s, 3H, OCH_3), 2.06 (s, 3H, CH_3), 2.02 (s, 3H, CH_3). ^{13}C{^{1}H} NMR (151 MHz, $CDCl_3$) δ: 169.8, 169.4, 168.7, 160.6, 158.7, 158.6, 153.5, 153.3, 152.4, 152.0, 144.8, 144.6, 143.4, 142.7, 136.8, 136.6, 134.5, 134.2, 133.1, 133.0, 131.5, 130.9, 130.2, 129.8, 129.4, 129.3, 128.5, 128.4, 128.2, 127.7, 127.4, 127.2, 127.1, 126.2, 123.6, 122.0, 121.0, 120.6, 120.2, 119.6, 119.1, 113.4, 55.37, 20.87, 20.82. Anal. Calcd for $C_{52}H_{41}IrN_6O.0.2C_5H_{12}$: C, 65.17; H, 4.58; N, 8.60. Found: C, 65.15; H, 4.46; N, 8.50.

Ir(piq)$_2$(Fzf) (4f). The title compound was prepared by the general method described above for complex **1c',** using [Ir(piq)$_2$(μ-Cl)]$_2$ (75 mg, 0.0589 mmol) and **Fzf** (46 mg, 0.12 mmol). The product was isolated as a greenish brown solid. Yield: 60 mg (56%). ^{1}H NMR (600 MHz, $CDCl_3$) δ: 8.63 (dd, *J* = 8.3, 16.2 Hz, 2H, ArH), 8.10 (d, *J* = 6.2 Hz, 1H, ArH), 8.03 (d, *J* = 6.2 Hz, 1H, ArH), 7.93–8.00 (m, 2H, ArH), 7.77–7.91 (m, 5H, ArH), 7.71 (t, *J* = 7.9 Hz, 1H, ArH), 7.52 (d, *J* = 6.9 Hz, 1H, ArH), 7.44 (d, *J* = 6.2 Hz, 1H, ArH), 7.01–7.10 (m, 2H, ArH), 6.86–6.98 (m, 5H, ArH), 6.75–6.83 (m, 1H,

ArH), 6.68 (t, J = 6.9 Hz, 1H, ArH), 6.42–6.52 (m, 3H, ArH), 6.04–6.10 (m, 1H, ArH), 5.82 (d, J = 8.3 Hz, 1H, ArH). $^{13}C\{^{1}H\}$ NMR (151 MHz, $CDCl_3$) δ: 169.1, 168.1, 156.0, 155.2, 153.9, 149.6, 144.7, 144.3, 142.3, 141.6, 138.4, 137.0, 136.9, 133.1, 132.1, 131.9, 131.7, 131.5, 131.2, 130.3, 130.0, 129.8, 129.0, 128.9, 127.8, 127.5, 126.9, 126.8, 126.2, 126.1, 122.9, 122.6, 121.7, 121.5, 121.2, 119.1, 118.7, 114.6, 110.2, 108.5. Anal. Calcd for $C_{46}H_{28}N_9Ir.0.1C_5H_{12}$: C, 60.96; H, 3.11; N, 13.91. Found: C, 60.99; H, 3.18; N, 14.04.

3.4.4 X-ray cryastallographic details

Single crystals of **1c′**, **1d**, **2a**, **2c**, **2d**, **2e**, **3a**, and **4a** were grown by layering concentrated CH_2Cl_2 solutions with pentane or diffusing pentane into concentrated ethyl acetate solution. Crystals were mounted on a Bruker Apex II three-circle diffractometer using MoKα radiation (λ = 0.71073 Å). The data were collected at 123(2) K and was processed and refined within the APEXII software. Structures were solved by direct methods in SHELXS and refined by standard difference Fourier techniques in the program SHELXL.[65] Hydrogen atoms were placed in calculated positions using the standard riding model and refined isotropically. All non-hydrogen atoms were refined anisotropically. Crystallographic details are summarized in Tables 3.6–3.8. All of the crystal structures were solved by Dr. Thomas S. Teets, Department of Chemistry at University of Houston.

Table 3.6. Summary of crystallographic data for **1c′, 1d,** and **2a**

	1c′·0.5CH_2Cl_2	**1d**·CH_2Cl_2	**2a**
CCDC	191336	191337	191338
Crystal data			
Chemical formula	$C_{44.50}H_{35}ClIrN_7$	$C_{45}H_{33}Cl_2IrN_8$	$C_{44}H_{33}F_4IrN_6O$
M_r	895.44	948.89	929.96
Crystal system, space group	Monoclinic, $P2_1/c$	Triclinic, $P\bar{1}$	Monoclinic, $P2_1/c$
a, b, c (Å)	8.3278 (11), 13.6396 (18), 32.927 (4)	7.800 (4), 13.666 (7), 19.338 (10)	13.819 (2), 17.291 (3), 31.180 (5)
α, β, γ (°)	90, 94.820 (2), 90	94.197 (6), 100.672 (6), 100.065 (6)	90, 99.037 (2), 90
V (Å^3)	3726.9 (9)	1982.6 (18)	7358 (2)
Z	4	2	8
μ (mm^{-1})	3.70	3.55	3.70
Crystal size (mm)	0.25 × 0.12 × 0.05	0.25 × 0.10 × 0.08	0.39 × 0.14 × 0.12
Data collection			
T_{min}, T_{max}	0.553, 0.746	0.602, 0.745	0.510, 0.746
No. of measured, independent and observed [$I > 2\sigma(I)$] reflections	21621, 8442, 7359	22406, 7691, 7169	42064, 16616, 15080
R_{int}	0.020	0.036	0.019
$(\sin\theta/\lambda)_{max}$ (Å^{-1})	0.649	0.617	0.649
Refinement			
$R[F^2 > 2\sigma(F^2)]$, $wR(F^2)$, S	0.029, 0.073, 1.06	0.062, 0.162, 1.08	0.031, 0.112, 1.20
No. of reflections	8442	7691	16616
No. of parameters	517	506	1015
No. of restraints	642	511	0
	$w = 1/[\sigma^2(F_o^2) + (0.0277P)^2 + 10.5019P]$ where $P = (F_o^2 + 2F_c^2)/3$	$w = 1/[\sigma^2(F_o^2) + (0.0734P)^2 + 44.1129P]$ where $P = (F_o^2 + 2F_c^2)/3$	$w = 1/[\sigma^2(F_o^2) + (0.0591P)^2 + 21.696P]$ where $P = (F_o^2 + 2F_c^2)/3$
$\Delta\rho_{max}$, $\Delta\rho_{min}$ (e Å^{-3})	1.34, -1.78	7.89, -3.90	3.07, -1.83

Table 3.7. Summary of crystallographic data for **2c, 2d** and **2e**

	2c	**2d**	**2e**
CCDC	191339	191340	191341
Crystal data			
Chemical formula	$C_{44}H_{30}F_4IrN_7$	$C_{44}H_{27}F_4IrN_8$	$C_{38}H_{26}F_4IrN_7$
M_r	924.95	935.93	848.86
Crystal system, space group	Triclinic, $P\bar{1}$	Monoclinic, $P2_1/c$	Monoclinic, $C2/c$
a, b, c (Å)	11.8119 (12), 11.9432 (12), 14.7901 (15)	17.897 (5), 8.693 (3), 23.444 (7)	26.377 (4), 24.953 (4), 12.001 (2)
α, β, γ (°)	108.9555 (12), 91.9403 (13), 109.1664 (13)	90, 91.553 (4), 90	90, 114.140 (2), 90
V (Å^3)	1840.7 (3)	3646.1 (18)	7208 (2)
Z	2	4	8
μ (mm^{-1})	3.69	3.73	3.76
Crystal size (mm)	0.40 × 0.26 × 0.16	0.21 × 0.10 × 0.05	0.47 × 0.09 × 0.07
Data collection			
T_{min}, T_{max}	0.602, 0.746	0.562, 0.746	0.491, 0.746
No. of measured, independent and observed [$I > 2\sigma(I)$] reflections	10228, 7383, 7003	22114, 8437, 7123	22704, 8354, 6955
R_{int}	0.014	0.039	0.027
$(\sin\theta/\lambda)_{max}$ (Å^{-1})	0.625	0.652	0.653
Refinement			
$R[F^2 > 2\sigma(F^2)]$, $wR(F^2)$, S	0.026, 0.063, 1.05	0.028, 0.058, 1.01	0.053, 0.139, 1.08
No. of reflections	7383	8437	8354
No. of parameters	526	515	452
No. of restraints	100	0	465
	$w = 1/[\sigma^2(F_o^2) + (0.029P)^2 + 3.7672P]$ where $P = (F_o^2 + 2F_c^2)/3$	$w = 1/[\sigma^2(F_o^2) + (0.0189P)^2]$ where $P = (F_o^2 + 2F_c^2)/3$	$w = 1/[\sigma^2(F_o^2) + (0.0546P)^2 + 83.6126P]$ where $P = (F_o^2 + 2F_c^2)/3$
$\Delta\rho_{max}$, $\Delta\rho_{min}$ (e Å^{-3})	2.07, -0.93	0.95, -0.52	4.42, -3.37

Table 3.8. Summary of crystallographic data for **3a** and **4a**

	3a·MeOH	**4a**·CH_2Cl_2
CCDC	191342	191343
Crystal data		
Chemical formula	$C_{49}H_{41}IrN_6O_2S_2$	$C_{53}H_{43}Cl_2IrN_6O$
M_r	1002.20	1043.03
a, *b*, *c* (Å)	11.1354 (5), 11.9908 (5), 16.0273 (7)	12.4439 (8), 13.9851 (9), 14.2806 (10)
α, β, γ (°)	91.100 (1), 99.67, 99.502 (1)	114.817 (1), 96.371 (1), 99.887 (1)
V (Å^3)	2078.23 (16)	2175.2 (3)
μ (mm^{-1})	3.36	3.24
Crystal size (mm)	0.30 × 0.19 × 0.12	0.38 × 0.23 × 0.20
Data collection		
T_{min}, T_{max}	0.583, 0.746	0.541, 0.746
No. of measured, independent and observed [$I > 2\sigma(I)$] reflections	36357, 9379, 8811	13034, 9360, 8486
R_{int}	0.029	0.019
$(\sin\theta/\lambda)_{max}$ (Å^{-1})	0.646	0.641
Refinement		
$R[F^2 > 2\sigma(F^2)]$, $wR(F^2)$, *S*	0.019, 0.044, 1.06	0.034, 0.091, 1.06
No. of reflections	9379	9360
No. of parameters	556	571
No. of restraints	15	0
$\Delta\rho_{max}$, $\Delta\rho_{min}$ (e Å^{-3})	0.93, -0.59	2.14, -1.63

3.5 References

(1) Kaim, W. "Manifestations of Noninnocent Ligand Behavior." *Inorg. Chem.* **2011**, *50*, 9752–9765.

(2) Kaim, W.; Schwederski, B. "Non-Innocent Ligands in Bioinorganic Chemistry—An Overview." *Coord. Chem. Rev.* **2010**, *254*, 1580–1588.

(3) Lyaskovskyy, V.; de Bruin, B. "Redox Non-Innocent Ligands: Versatile New Tools to Control Catalytic Reactions." *ACS Catal.* **2012**, *2*, 270–279.

(4) Luca, O. R.; Crabtree, R. H. “Redox-Active Ligands in Catalysis.” *Chem Soc Rev* **2013**, *42*, 1440–1459.

(5) Pavlova, I. S.; Pervova, I. G.; Belov, G. P.; Khasbiullin, I. I.; Slepukhin, P. A. “Ethylene Oligomerization Mediated by Iron Formazanates and Organoaluminum Compounds.” *Pet. Chem.* **2013**, *53*, 127–133.

(6) Nineham, A. W. “The Chemistry of Formazans and Tetrazolium Salts.” *Chem. Rev.* **1955**, *55*, 355–483.

(7) Szymczyk, M.; El-Shafei, A.; Freeman, H. S. “Design, Synthesis, and Characterization of New Iron-Complexed Azo Dyes.” *Dyes Pigments* **2007**, *72*, 8–15.

(8) Gruden, C. L.; Fevig, S.; Abu-Dalo, M.; Hernandez, M. “5-Cyano-2,3-Ditolyl Tetrazolium Chloride (CTC) Reduction in a Mesophilic Anaerobic Digester: Measuring Redox Behavior, Differentiating Abiotic Reduction, and Comparing FISH Response as an Activity Indicator.” *J. Microbiol. Methods* **2003**, *52*, 59–68.

(9) Frederiks, W. M.; Marle, J. van; Oven, C. van; Comin-Anduix, B.; Cascante, M. “Improved Localization of Glucose-6-Phosphate Dehydrogenase Activity in Cells with 5-Cyano-2, 3-Ditolyl-Tetrazolium Chloride as Fluorescent Redox Dye Reveals Its Cell Cycle-Dependent Regulation.” *J. Histochem. Cytochem.* **2006**, *54*, 47–52.

(10) Hunter, L.; Roberts, C. B. “145. The Associating Effect of the Hydrogen Atom. Part IX. The N–H–N Bond. Virtual Tautomerism of the Formazyl Compounds.” *J. Chem. Soc. Resumed* **1941**, *0*, 820–823.

(11) Irving, H.; Gill, J. B.; Cross, W. R. “423. The Structure of Some Di-(3-Methyl-1,5-Diarylformazyl)-Nickel(II) Complexes.” *J. Chem. Soc. Resumed* **1960**, *0*, 2087–2095.

(12) Budesinsky, B.; Svecova, J. “Hydrogen and Metal Complexes of Some 3-Cyanoformazans.” *Inorg. Chem.* **1971**, *10*, 313–317.

(13) Siedle, A. R.; Pignolet, L. H. “Formazanylpalladium Compounds. Synthesis and Structure of Bis(1,3,5-Tri-p-Tolylformazanyl)Palladium.” *Inorg. Chem.* **1980**, *19*, 2052–2056.

(14) Zarkesh, R. A.; Ichimura, A. S.; Monson, T. C.; Tomson, N. C.; Anstey, M. R. “Voltage Clustering in Redox-Active Ligand Complexes: Mitigating Electronic Communication through Choice of Metal Ion.” *Dalton Trans.* **2016**, *45*, 9962–9969.

(15) Ketterer, N. A.; Fan, H.; Blackmore, K. J.; Yang, X.; Ziller, J. W.; Baik, M.-H.; Heyduk, A. F. “$\pi^{\bullet}-\pi^{\bullet}$ Bonding Interactions Generated by Halogen Oxidation of

Zirconium(IV) Redox-Active Ligand Complexes." *J. Am. Chem. Soc.* **2008**, *130*, 4364–4374.

(16) Mandal, A.; Schwederski, B.; Fiedler, J.; Kaim, W.; Lahiri, G. K. "Evidence for Bidirectional Noninnocent Behavior of a Formazanate Ligand in Ruthenium Complexes." *Inorg. Chem.* **2015**, *54*, 8126–8135.

(17) Chang, M.-C.; Dann, T.; Day, D. P.; Lutz, M.; Wildgoose, G. G.; Otten, E. "The Formazanate Ligand as an Electron Reservoir: Bis(Formazanate) Zinc Complexes Isolated in Three Redox States." *Angew. Chem. Int. Ed.* **2014**, *53*, 4118–4122.

(18) Singha Hazari, A.; Mandal, A.; Beyer, K.; Paretzki, A.; Kaim, W.; Lahiri, G. K. "Metal–Metal Bridging Using the DPPP Dye System: Electronic Configurations within Multiple Redox Series." *Inorg. Chem.* **2017**, *56*, 2992–3004.

(19) Gilroy, J. B.; Patrick, B. O.; McDonald, R.; Hicks, R. G. "Transition Metal Complexes of 3-Cyano- and 3-Nitroformazans." *Inorg. Chem.* **2008**, *47*, 1287–1294.

(20) Hong, S.; Hill, L. M. R.; Gupta, A. K.; Naab, B. D.; Gilroy, J. B.; Hicks, R. G.; Cramer, C. J.; Tolman, W. B. "Effects of Electron-Deficient β-Diketiminate and Formazan Supporting Ligands on Copper(I)-Mediated Dioxygen Activation." *Inorg. Chem.* **2009**, *48*, 4514–4523.

(21) Hong, S.; Gupta, A. K.; Tolman, W. B. "Intermediates in Reactions of Copper(I) Complexes with N-Oxides: From the Formation of Stable Adducts to Oxo Transfer." *Inorg. Chem.* **2009**, *48*, 6323–6325.

(22) Broere, D. L. J.; Mercado, B. Q.; Bill, E.; Lancaster, K. M.; Sproules, S.; Holland, P. L. "Alkali Cation Effects on Redox-Active Formazanate Ligands in Iron Chemistry." *Inorg. Chem.* **2018**, *57*, 9580–9591.

(23) Broere, D. L. J.; Mercado, B. Q.; Lukens, J. T.; Vilbert, A. C.; Banerjee, G.; Lant, H. M. C.; Lee, S. H.; Bill, E.; Sproules, S.; Lancaster, K. M.; et al. "Reversible Ligand-Centered Reduction in Low-Coordinate Iron Formazanate Complexes." *Chem. – Eur. J.* **2018**, *24*, 9417–9425.

(24) Broere, D. L. J.; Mercado, B. Q.; Holland, P. L. "Selective Conversion of CO2 into Isocyanate by Low-Coordinate Iron Complexes." *Angew. Chem. Int. Ed.* **2018**, *57*, 6507–6511.

(25) Milocco, F.; Demeshko, S.; Meyer, F.; Otten, E. "Ferrate(II) Complexes with Redox-Active Formazanate Ligands." *Dalton Trans.* **2018**, *47*, 8817–8823.

(26) Chang, M.-C.; Roewen, P.; Travieso-Puente, R.; Lutz, M.; Otten, E. "Formazanate Ligands as Structurally Versatile, Redox-Active Analogues of β-Diketiminates in Zinc Chemistry." *Inorg. Chem.* **2015**, *54*, 379–388.

(27) Protasenko, N. A.; Poddel'sky, A. I.; Bogomyakov, A. S.; Fukin, G. K.; Cherkasov, V. K. "Heteroligand O-Semiquinonato-Formazanato Cobalt Complexes." *Inorg. Chem.* **2015**, *54*, 6078–6080.

(28) Protasenko, N. A.; Poddel'sky, A. I.; Bogomyakov, A. S.; Starikov, A. G.; Smolyaninov, I. V.; Berberova, N. T.; Fukin, G. K.; Cherkasov, V. K. "The Chemical and Electrochemical Reduction of Heteroligand O-Semiquinonato-Formazanato Cobalt Complexes." *Inorganica Chim. Acta* **2019**, *489*, 1–7.

(29) Maar, R. R.; Catingan, S. D.; Staroverov, V. N.; Gilroy, J. B. "Formazanate Complexes of Hypervalent Group 14 Elements as Precursors to Electronically Stabilized Radicals." *Angew. Chem. Int. Ed.* **2018**, *57*, 9870–9874.

(30) Barbon, S. M.; Reinkeluers, P. A.; Price, J. T.; Staroverov, V. N.; Gilroy, J. B. "Structurally Tunable 3-Cyanoformazanate Boron Difluoride Dyes." *Chem. – Eur. J.* **2014**, *20*, 11340–11344.

(31) Barbon, S. M.; Staroverov, V. N.; Gilroy, J. B. "Effect of Extended π Conjugation on the Spectroscopic and Electrochemical Properties of Boron Difluoride Formazanate Complexes." *J. Org. Chem.* **2015**, *80*, 5226–5235.

(32) Maar, R. R.; Barbon, S. M.; Sharma, N.; Groom, H.; Luyt, L. G.; Gilroy, J. B. "Evaluation of Anisole-Substituted Boron Difluoride Formazanate Complexes for Fluorescence Cell Imaging." *Chem. – Eur. J.* **2015**, *21*, 15589–15599.

(33) Chang, M.-C.; Chantzis, A.; Jacquemin, D.; Otten, E. "Boron Difluorides with Formazanate Ligands: Redox-Switchable Fluorescent Dyes with Large Stokes Shifts." *Dalton Trans.* **2016**, *45*, 9477–9484.

(34) Chang, M.-C.; Otten, E. "Synthesis and Ligand-Based Reduction Chemistry of Boron Difluoride Complexes with Redox-Active Formazanate Ligands." *Chem. Commun.* **2014**, *50*, 7431–7433.

(35) Mondol, R.; Snoeken, D. A.; Chang, M.-C.; Otten, E. "Stable, Crystalline Boron Complexes with Mono-, Di- and Trianionic Formazanate Ligands." *Chem. Commun.* **2017**, *53*, 513–516.

(36) Barbon, S. M.; Novoa, S.; Bender, D.; Groom, H.; Luyt, L. G.; Gilroy, J. B. "Copper-Assisted Azide–Alkyne Cycloaddition Chemistry as a Tool for the Production

of Emissive Boron Difluoride 3-Cyanoformazanates." *Org. Chem. Front.* **2017**, *4*, 178–190.

(37) Hesari, M.; Barbon, S. M.; Staroverov, V. N.; Ding, Z.; Gilroy, J. B. "Efficient Electrochemiluminescence of a Readily Accessible Boron Difluoride Formazanate Dye." *Chem. Commun.* **2015**, *51*, 3766–3769.

(38) Hesari, M.; Barbon, S. M.; Mendes, R. B.; Staroverov, V. N.; Ding, Z.; Gilroy, J. B. "Structural Tuning of Boron Difluoride Formazanate Electrochemiluminescence Mediated by Tri- *n* -Propylamine." *J. Phys. Chem. C* **2018**, *122*, 1258–1266.

(39) Dhindsa, J. S.; Maar, R. R.; Barbon, S. M.; Olivia Avilés, M.; Powell, Z. K.; Lagugné-Labarthet, F.; Gilroy, J. B. "A π-Conjugated Inorganic Polymer Constructed from Boron Difluoride Formazanates and Platinum(II) Diynes." *Chem. Commun.* **2018**, *54*, 6899–6902.

(40) Novoa, S.; Paquette, J. A.; Barbon, S. M.; Maar, R. R.; Gilroy, J. B. "Side-Chain Boron Difluoride Formazanate Polymers via Ring-Opening Metathesis Polymerization." *J. Mater. Chem. C* **2016**, *4*, 3987–3994.

(41) Chang, M.-C.; Otten, E. "Reduction of (Formazanate)Boron Difluoride Provides Evidence for an *N* -Heterocyclic B(I) Carbenoid Intermediate." *Inorg. Chem.* **2015**, *54*, 8656–8664.

(42) Barbon, S. M.; Staroverov, V. N.; Gilroy, J. B. "Structurally Diverse Boron–Nitrogen Heterocycles from an N2O23− Formazanate Ligand." *Angew. Chem. Int. Ed.* **2017**, *56*, 8173–8177.

(43) Meriwether, L. S.; Breitner, E. C.; Sloan, C. L. "The Photochromism of Metal Dithizonates." *J. Am. Chem. Soc.* **1965**, *87*, 4441–4448.

(44) Petersen, R. L.; McFarland, J. T.; Watters, K. L. "Resonance Raman Study of Metal-Formazans: A Model for Complexes of Metalloenzymes with Chelate Inhibitors." *Bioinorg. Chem.* **1978**, *9*, 355–367.

(45) Zhang, H.-Y.; Sun, W.-X.; Wu, Q.-A.; Zhangb, H.-Q.; Chen, Y.-Y. "Study on 1,5-Bis(2-Carboxyphenyl)-3-Phenylformazan and Its Complexes." *Synth. React. Inorg. Met.-Org. Chem.* **2000**, *30*, 571–582.

(46) Bait, S.; Meuldijk, J.; Renkema, W. E. "Square Planar Complexes of Nickel(II), Palladium(II) and Platinum(II) with 1-(2-Hydroxyphenyl)-3,5-Diphenylformazan." *Transit. Met. Chem.* **1980**, *5*, 357–361.

(47) Balt, S.; Meuldijk, J. “Solvent Effects in Square Planar Complexes: Kinetics of Substitution at 1-(2-Hydroxyphenyl)-3,5-(Diphenylformazanato)-Platinum(II) Complexes.” *Inorganica Chim. Acta* **1981**, *47*, 217–223.

(48) Kabir, E.; Wu, C.-H.; Wu, J. I.-C.; Teets, T. S. “Heteroleptic Complexes of Cyclometalated Platinum with Triarylformazanate Ligands.” *Inorg. Chem.* **2016**, *55*, 956–963.

(49) Kabir, E.; Patel, D.; Clark, K.; Teets, T. S. “Spectroscopic and Electrochemical Properties of Electronically Modified Cycloplatinated Formazanate Complexes.” *Inorg. Chem.* **2018**, *57*, 10906–10917.

(50) Mu, G.; Cong, L.; Wen, Z.; Wu, J. I.-C.; Kadish, K. M.; Teets, T. S. “Homoleptic Platinum Azo-Iminate Complexes via Hydrogenative Cleavage of Formazans.” *Inorg. Chem.* **2018**, *57*, 9468–9477.

(51) Tsuboyama, A.; Iwawaki, H.; Furugori, M.; Mukaide, T.; Kamatani, J.; Igawa, S.; Moriyama, T.; Miura, S.; Takiguchi, T.; Okada, S.; et al. “Homoleptic Cyclometalated Iridium Complexes with Highly Efficient Red Phosphorescence and Application to Organic Light-Emitting Diode.” *J. Am. Chem. Soc.* **2003**, *125*, 12971–12979.

(52) Tamayo, A. B.; Garon, S.; Sajoto, T.; Djurovich, P. I.; Tsyba, I. M.; Bau, R.; Thompson, M. E. “Cationic Bis-Cyclometalated Iridium(III) Diimine Complexes and Their Use in Efficient Blue, Green, and Red Electroluminescent Devices.” *Inorg. Chem.* **2005**, *44*, 8723–8732.

(53) Lowry, M. S.; Goldsmith, J. I.; Slinker, J. D.; Rohl, R.; Pascal, R. A.; Malliaras, G. G.; Bernhard, S. “Single-Layer Electroluminescent Devices and Photoinduced Hydrogen Production from an Ionic Iridium(III) Complex.” *Chem. Mater.* **2005**, *17*, 5712–5719.

(54) Lo, K. K.-W.; Ng, D. C.-M.; Chung, C.-K. “First Examples of Luminescent Cyclometalated Iridium(III) Complexes as Labeling Reagents for Biological Substrates.” *Organometallics* **2001**, *20*, 4999–5001.

(55) Lo, K. K.-W.; Chung, C.-K.; Lee, T. K.-M.; Lui, L.-H.; Tsang, K. H.-K.; Zhu, N. “New Luminescent Cyclometalated Iridium(III) Diimine Complexes as Biological Labeling Reagents.” *Inorg. Chem.* **2003**, *42*, 6886–6897.

(56) Cordero, B.; Gómez, V.; Platero-Prats, A. E.; Revés, M.; Echeverría, J.; Cremades, E.; Barragán, F.; Alvarez, S. “Covalent Radii Revisited.” *Dalton Trans.* **2008**, No. 21, 2832.

(57) Radwan, Y. K.; Maity, A.; Teets, T. S. “Manipulating the Excited States of Cyclometalated Iridium Complexes with β-Ketoiminate and β-Diketiminate Ligands.” *Inorg. Chem.* **2015**, *54*, 7122–7131.

(58) Lai, P.-N.; Brysacz, C. H.; Alam, M. K.; Ayoub, N. A.; Gray, T. G.; Bao, J.; Teets, T. S. “Highly Efficient Red-Emitting Bis-Cyclometalated Iridium Complexes.” *J. Am. Chem. Soc.* **2018**, *140*, 10198–10207.

(59) Lamansky, S.; Djurovich, P.; Murphy, D.; Abdel-Razzaq, F.; Lee, H.-E.; Adachi, C.; Burrows, P. E.; Forrest, S. R.; Thompson, M. E. “Highly Phosphorescent Bis-Cyclometalated Iridium Complexes: Synthesis, Photophysical Characterization, and Use in Organic Light Emitting Diodes.” *J. Am. Chem. Soc.* **2001**, *123*, 4304–4312.

(60) Li, J.; Djurovich, P. I.; Alleyne, B. D.; Yousufuddin, M.; Ho, N. N.; Thomas, J. C.; Peters, J. C.; Bau, R.; Thompson, M. E. “Synthetic Control of Excited-State Properties in Cyclometalated Ir(III) Complexes Using Ancillary Ligands.” *Inorg. Chem.* **2005**, *44*, 1713–1727.

(61) Pangborn, A. B.; Giardello, M. A.; Grubbs, R. H.; Rosen, R. K.; Timmers, F. J. “Safe and Convenient Procedure for Solvent Purification.” *Organometallics* **1996**, *15*, 1518–1520.

(62) Gilroy, J. B.; McKinnon, S. D. J.; Koivisto, B. D.; Hicks, R. G. “Electrochemical Studies of Verdazyl Radicals.” *Org. Lett.* **2007**, *9*, 4837–4840.

(63) Nonoyama, M. “Benzo[h]Quinolin-10-Yl-N Iridium(III) Complexes.” *Bull. Chem. Soc. Jpn.* **1974**, *47*, 767–768.

(64) Peng, T.; Yang, Y.; Liu, Y.; Ma, D.; Hou, Z.; Wang, Y. “A Phosphorescent Material with High and Balanced Carrier Mobility for Efficient OLEDs.” *Chem. Commun.* **2011**, *47*, 3150–3152.

(65) Sheldrick, G. M. “A Short History of *SHELX*.” *Acta Crystallogr. A* **2008**, *64*, 112–122.

Chapter 4

Tuning the Photophysical and Electrochemical Properties of Red-emitting Bis-cyclometalated Iridium Complexes by Ancillary Ligand Modification

4.1 Introduction

Luminescent cyclometalated iridium(III) complexes have become one of the most prominent classes of molecule phosphors, contributing to numerous applications in photocatalysis,[1–3] bioimaging,[4–8] and sensing,[9,10] and most notably, organic light-emitting diodes (OLEDs)[11–14] and light-emitting electrochemical cells.[15,16] These compounds luminesce from triplet excited states with ligand-centered (^{3}LC or $^3\pi\pi^*$) and metal-to-ligand charge transfer (^{3}MLCT or $^3d\pi^*$) character, mixing through configuration interaction. Homoleptic complexes of the type *fac*-Ir(C^N)$_3$ have received considerable attention[1,17,18] and heteroleptic complexes of type Ir(C^N)$_2$(L^X) have been studied extensively as well (C^N = cyclometalating ligand, L^X = ancillary ligand). The preparation of heteroleptic complexes is often cheaper and easier than the homoleptic analogues, making them an attractive choice for further development. The ancillary ligands in the heteroleptic complexes could be a useful tool to tune the emission color,[19,20] along with their ability to substantially perturb the redox properties and excited state dynamics.[21,22] In particular, ancillary ligand modification often perturbs the energy of the metal centered HOMO, which in turn will influence the MLCT and LC states that contribute to the emissive excited state.

Facile color tunability, highly photoluminescence quantum yields (Φ_{PL}), and relatively short phosphorescence lifetimes (τ) are some of the key features of cyclometalated iridium(III) complexes, which along with their good thermal and photostability leads to applications in diverse fields. There are many examples of iridium(III) complexes which emit in the blue to yellow regions of the spectrum with near

unity quantum yields,[23–27] but orange and red-emitters in the lower-energy regions of the spectrum typically have lower quantum yields, which is an important performance metric to function in commercial devices. The quantum yield (Φ_{PL}) is the ratio of radiative rate constant (k_r) to the sum of radiative and non-radiative (k_{nr}) rate constants. Increasing (k_r) or reducing the (k_{nr}) will result in higher quantum yield. According to the energy gap law,[28,29] the non-radiative rate (k_{nr}) is inversely related to the energy difference between the ground and excited state, where the vibrational overlap between these two steps lead to an increased (k_{nr}) in the low-energy region or for longer wavelength emission.[30] On the other hand, the radiative rate (k_r) has a cubic dependence on the transition energy and is expected to be smaller when longer emission wavelengths are accessed.[11] The spin-orbit interactions between the triplet state and higher-lying singlets allow the possibility of spin-forbidden relative transition by relaxing spin selection rules, which in turn will increase the radiative rate (k_r). Even though this kind of spin-orbit coupling is mostly notable for ^{1,3}MLCT states, it can also minimally influence the lower-lying ligand-centered (^{3}LC) states via configuration interaction. Highly conjugated cyclometalated ligands used in red emitters often have low-energy ligand-centered states with a large energy separation between the LC and MLCT states, resulting in weaker configuration interaction and diminished spin-orbit coupling, leading to smaller k_r. Therefore, a careful choice of cyclometalating ligands which result in enhanced MLCT character is one option to design red-emitting iridium complexes with better quantum efficiency. However, this strategy is not always fruitful as the steric and electronic constraints of the cyclometalating ligand often make the synthesis and purification of such ligands in high yield quite challenging. To counter this limitation, ancillary ligand modification has been

successfully employed in several studies to improve the performance of red-emitting complexes.[19,20,31–34]

Our group previously reported few of the red-emitting bis-cyclometalated iridium(III) complexes with better quantum efficiency, high color purity and good device performance, by using β-ketoiminate (acNac), β-dikitiminate (NacNac) and N,N-diisopropylbenzamidinate (dipba) as ancillary ligands.[35,36] In those works, the ancillary ligand modification influenced the electronic and photophysical properties if the bis-cyclometalated iridium complexes. A significant red-shift in the emission maxima along with enhanced phosphorescence quantum yield was also observed in some cases relative to the corresponding isoelectronic acetylacetonate (acac) analogue or the homoleptic tris-cyclometalated complexes of same C^N ligand.[22,37] In a continuation of that study, our work here describes a suite of ten new heteroleptic iridium(III) complexes with systematic modification of ancillary ligands with strong π-donating properties and different chelate ring size. Pairing two different cyclometalating ligands with six different ancillary ligands in these new complexes provide some insight about the influence of ancillary ligand modification on the electrochemical and photophysical properties. Even though the emission colors are still dependent on the choice of the cyclometalated ligand, the π-donating ancillary ligand structure has a profound impact on the photophysical properties, namely quantum yield, lifetime, and radiative rate constant. In particular, this work investigates the effects of replacing aryl substituent(s) on nitrogen with alkyl groups and adding electron-donating substituents, two new insights in this work not available from our previous studies. This work also indicates that sterically encumbered versions of

some of these ancillary ligands can increase the radiative rate constant (k_r) or decrease the non-radiative rate constant (k_{nr}) as another means of increasing the photoluminescence quantum yields of these compounds, making them ideal choices for designing top-performing red phosphors.

4.2 Results

4.2.1 Synthesis of heteroleptic iridium complexes

The general synthetic procedure for the ten new complexes of type $Ir(C\hat{}N)_2(LX)$ (C^N = 1-phenylisoquinoline (piq) and 2-(2-pyridyl)benzothiophene (btp)) is described in Scheme 1. Six different ancillary ligands that are paired with these C^N ligands are a sterically encumbered *ortho*-substituted β-diketiminate ($(dmp)_2NacNac^{Me}$), an electron-rich dimethylamino-substituted β-diketiminate ($NacNac^{NMe2}$), alkyl-substituted β-diketiminate ($(Cy)_2NacNac^{Me}$) and β-ketoiminate ($(Cy)acNac^{Me}$), a substituted *N,N'*-diisopropylbenzamidinate with a central mesityl substituent ($dipba^{mes}$), and an isopropyl-substituted guanidinate ($dipg^{NMe2}$). The cyclometalating ligand were chosen to achieve target emission in the red region of the spectrum, and the bis-cyclometalated iridium fragment forms four-, and six-membered metallacyclic iridium complexes with the ancillary ligands. The numbering scheme uses numerical designators for each C^N ligand (piq=**1**, and btp=**2**), with letters (**a**–**f**) denoting each L^X ligand. The chloro-bridged dimers $[Ir(C\hat{}N)_2(\mu\text{-}Cl)]_2$ were treated with $(dmp)_2NacNac^{Me}K$ or $NacNac^{NMe2}K$ at room temperature in THF to afford complexes **1a**–**b** and **2a**–**b** in moderate yields. A slightly different method was used to obtain complex **1c**–**d** and **2c**–**d**, where the chloro-bridged dimers were treated with the in situ-generated lithium salt of $dipba^{Mes}$ and $dipg^{NMe2}$ in

tetrahydrofuran (THF) at 85 °C, whereas for **1e**–**f** the piq-ligated dimer were reacted with $(Cy)_2NacNac^{Me}K$ and $(Cy)acNac^{Me}K$ in toluene at 130 °C. All reagents were measured and purification steps were conducted inside the glovebox, and heating was done in Teflon-sealed vessels to ensure moisture and air-free conditions. The identity and the bulk purity of the complexes were confirmed by ^{1}H and $^{13}C\{^{1}H\}$ NMR.

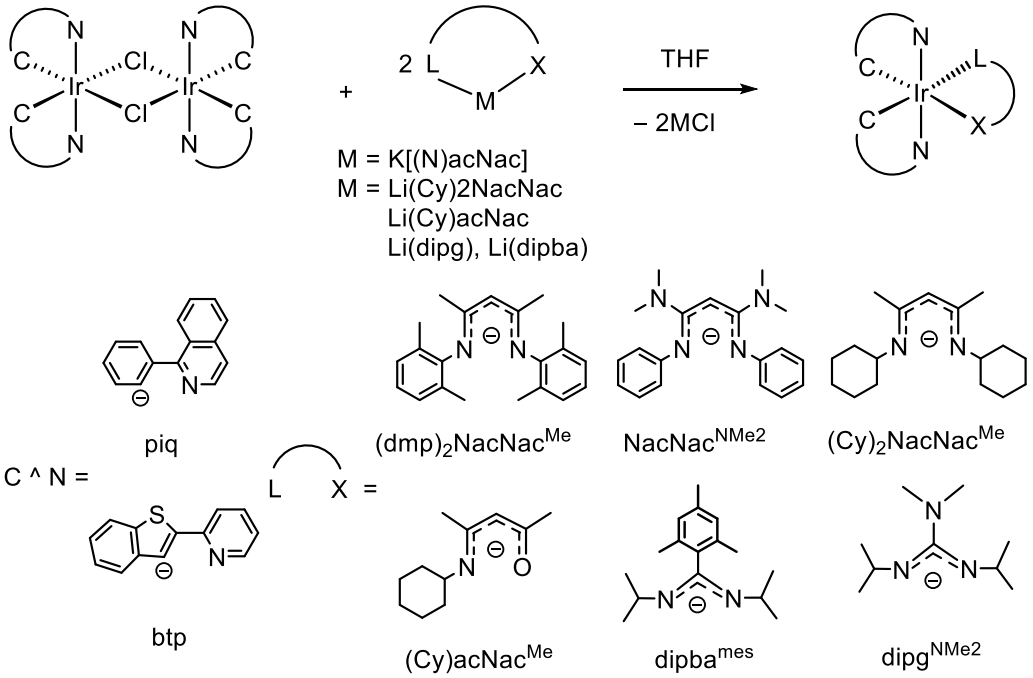

1a: C^N = piq, L^X = $(dmp)_2NacNac^{Me}$
1b: C^N = piq, L^X = $NacNac^{NMe2}$
1c: C^N = piq, L^X = $dipba^{mes}$
1d: C^N = piq, L^X = $dipg^{NMe2}$
1e: C^N = piq, L^X = $(Cy)_2NacNac^{Me}$
1f: C^N = piq, L^X = $(Cy)acNac^{Me}$

2a: C^N = btp, L^X = $(dmp)_2NacNac^{Me}$
2b: C^N = btp, L^X = $NacNac^{NMe2}$
2c: C^N = btp, L^X = $dipba^{mes}$
2d: C^N = btp, L^X = $dipg^{NMe2}$

Scheme 4.1. Synthesis of bis-cyclometalated iridium complexes.

The NMR spectra of all complexes displayed C_2 symmetry except complex **1f**, where the point group is C_1 for the (Cy)acNac complex, giving rise to distinct NMR resonances for

each proton and carbon nucleus of **1f**. All NMR spectra show the presence of single product in each case, confirming the absence of any isomeric products in the reaction mixture.

4.2.2 Structural characterization by X-ray crystallography

Complexes **1c**, **1d**, **2a**, **2b**, and **2d** are characterized by single crystal X-ray diffraction, with the structures depicted in Figure 4.1. Relevant bond lengths and angles for all complexes are provided in Tables 4.3–4.4 Single crystals for complexes were grown via vapor diffusion of pentane into dichloromethane or tetrahydrofuran solution or by layering pentane onto a dichloromethane solution of the appropriate compound at room temperature inside the glovebox. The iridium center is found to be at the center of a distorted octahedral geometry in all of the characterized structures and the expected trans disposition of the two nitrogen atoms of the cyclometalating ligands is observed. Excepting NacNac^{NMe2} complex **2b**, the ancillary ligand core and the chelated iridium atom are planar. The C–O, C–N, and C–C bond distances of the ancillary ligand chelated rings in all five characterized complexes are intermediate between typical single- and double-bond distances, consistent with a π-localized core. The equal C–N and C–C bond distances in all complexes suggest C_2 symmetry which is also evinced from their NMR spectra.

An interesting feature of NacNac complexes **2a** and **2b** is the close approach of one or both N-aryl groups and a nearby Ir-aryl, which are arranged in a nearly eclipsed orientation with apparent π–π stacking between the rings. This type of structural motif was also observed in some other iridium NacNac complexes previously described by our

group.[22,37] Analyzing different ring size of the ancillary ligand, the enhancement of N–C–N bite angle was observed with the expansion of the ancillary ligand ring size, and similar observation was noted in other recently disclosed compounds from our group.[35,36,38] The average N–C–N bite angle for complex **1c**, **1d,** and **2d** is 60.49(10)°, whereas the N–C–N angle for complex **2b** is 85.26(7)°, and for complex **2a** is 90.27(10)° which was the largest in the series of characterized complexes.

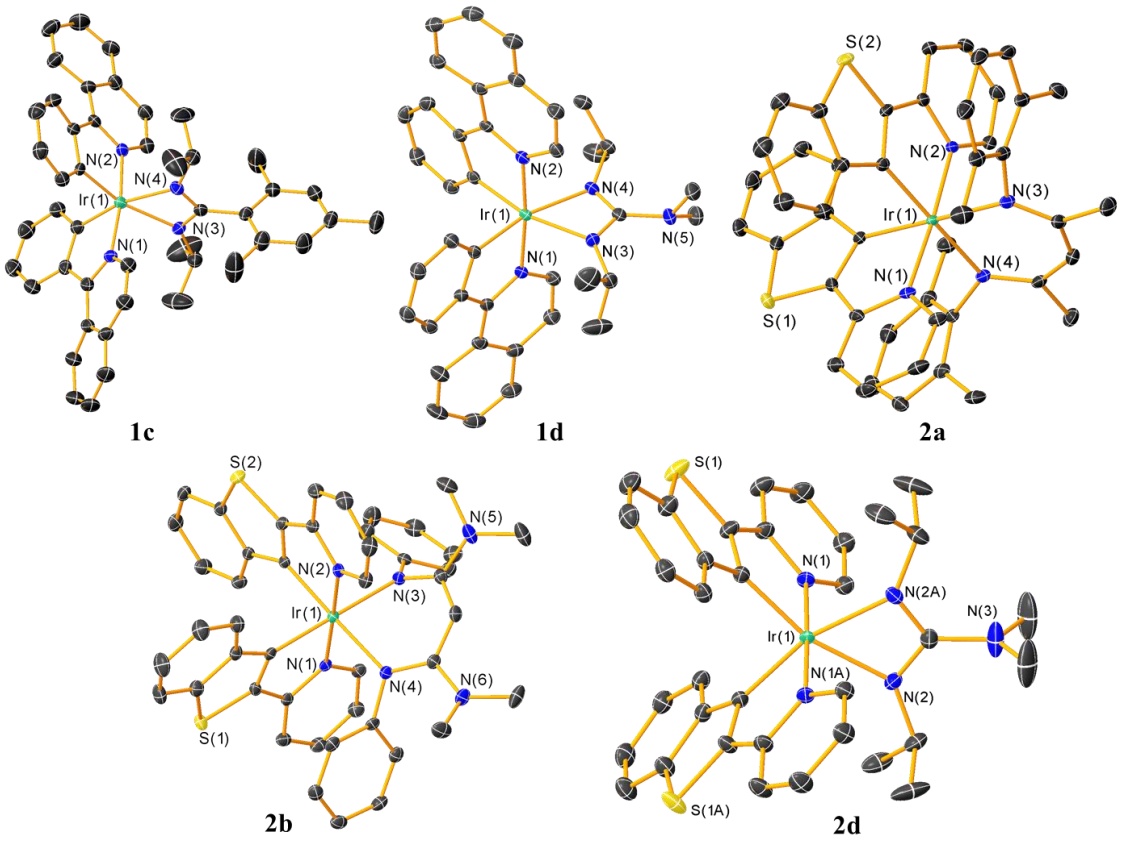

Figure 4.1. X-ray crystal structure of complexes **1c, 1d**, **2a**, **2b**, and **2d**. Hydrogen atoms and solvated molecules are omitted for clarity. Ellipsoids are shown at the 50% probability level.

4.2.3 Electrochemical properties

Figures 4.2 and 4.3 display overlaid cyclic voltammograms of the complexes, arranged by C^N ligands, and their results are summarized in Table 4.1. The electrochemical properties were investigated in acetonitrile (MeCN) solution and all complexes display both oxidation and reduction features in the cyclic voltammetry experiments. All the complexes described in this work display a formally Ir^{IV}/Ir^{III} redox couple (E^{ox}), with half-wave potentials that are strongly dependent on the identity of the ancillary ligand.

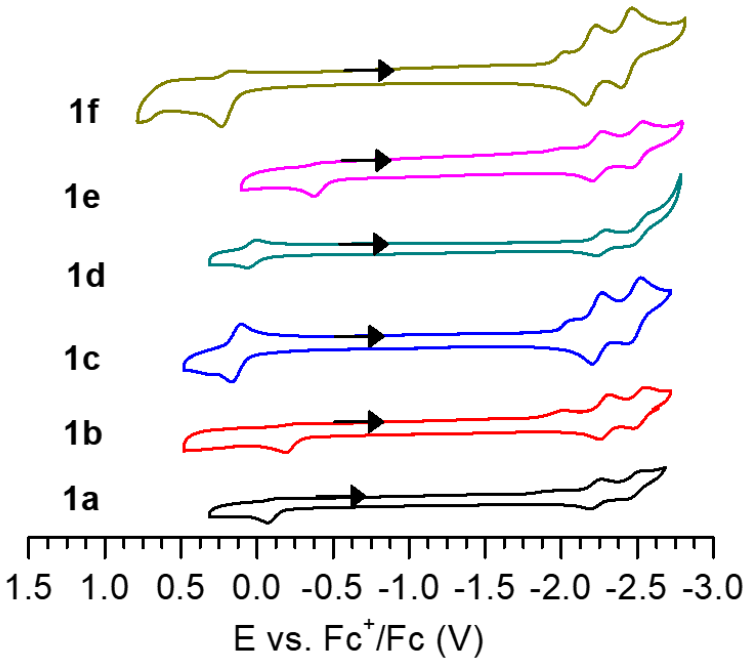

Figure 4.2. Overlaid cyclic voltammograms of complexes **1a**–**f**. CVs were recorded in acetonitrile with 0.1 M NBu_4PF_6 supporting electrolyte, using a glassy carbon working electrode and a scan rate of 0.1 V/s. The arrows indicate the scan direction. Concentrations were not carefully controlled, and currents are low in some of plots because of the limited solubility of some of the compounds in acetonitrile.

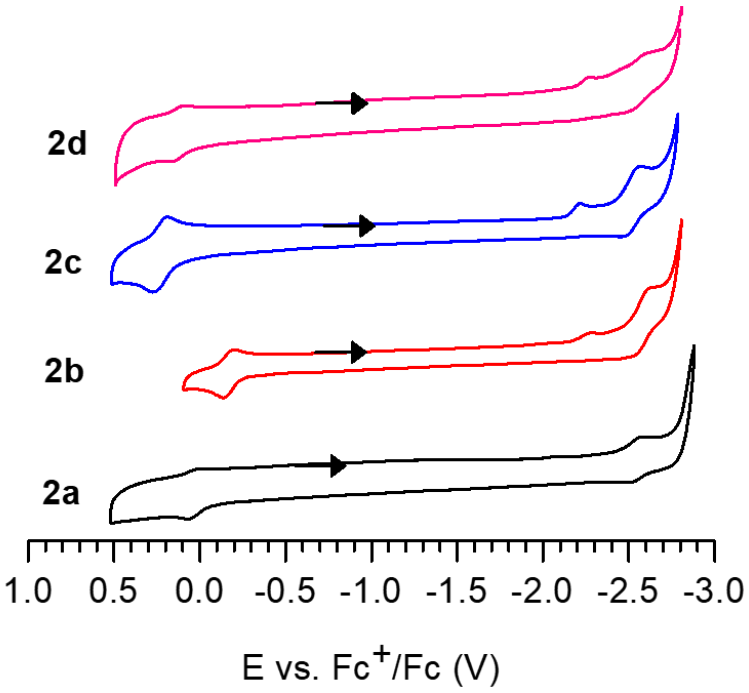

Figure 4.3. Overlaid cyclic voltammograms of complexes **2a**–**d**. CVs were recorded in acetonitrile with 0.1 M NBu_4PF_6 supporting electrolyte, using a glassy carbon working electrode and a scan rate of 0.1 V/s. The arrows indicate the scan direction. Concentrations were not carefully controlled, and currents are low in some of plots because of the limited solubility of some of the compounds in acetonitrile.

Complexes supported by $(dmp)_2NacNac^{Me}$, **1a** (E^{ox} = +0.06 V) and **2a** (E^{ox} = +0.06 V), have potentials close to the ferrocenium/ferrocene couple and thus were quite easy to oxidize. The presence of electron donating *N*,*N*-dimethylamine group in complexes **1b** and **2b** made the molecules electron rich and easier to oxidize, which was evident from the oxidation potentials for these two complexes. Replacing the 2,6-dimetylphenyl group with the cyclohexyl group in NacNac ancillary ligand resulted in a larger cathodic shift of ca. 430 mV for complex **1e** (E^{ox} = −0.37 V), indicating that the alkyl groups made the complex even more electron-rich. Complexes with smaller N–C–N bite angle **1c/d** and **2c/d** were more difficult to oxidize than the NacNac complexes, and

similar trend was observed for a previously described series of four-membered metallacyclic iridium complexes.[35,36] The potential for dipba^{Mes}-ligated complex **1c** (E^{ox} = +0.17 V) was more positive than that of the dipg^{NMe2}-ligated complex **1d** (E^{ox} = +0.06 V), with a similar trend was observed for btp complexes **2c** (E^{ox} = +0.27 V) and its dipg^{NMe2} congener **2d** (E^{ox} = +0.15 V). Complex **1f** (E^{ox} = +0.24 V) with mixed *N,O*-chelate was the most difficult to oxidize of the complexes in the piq series, and the reported potential is quite similar to the previously reported acNac iridium complexes with other cyclometalating ligands.[22,35,36]

Table 4.1. Summary of electrochemical data for piq- and btp-ligated complexes.

	E vs. Fc^+/Fc (V)[a]	
C^N = piq (**1**)	E^{red}	E^{ox}
L^X = $(dmp)_2$NacNac^{Me} **(a)**	−2.25, −2.51[c]	+0.06[b]
L^X = NacNac^{NMe2} **(b)**	−2.31 −2.56	−0.19[b]
L^X = dipba^{Mes} **(c)**	−2.27, −2.52	+0.17
L^X = dipg^{NMe2} **(d)**	−2.29, −2.59[c]	+ 0.06
L^X = $(Cy)_2$NacNac^{Me} **(e)**	−2.27, −2.54	−0.37[b]
L^X = (Cy)acNac^{Me} **(f)**	−2.23, −2.47	+0.24[b]

	E vs. Fc^+/Fc (V)[a]	
C^N = btp (**2**)	E^{red}	E^{ox}
L^X = $(dmp)_2$NacNac^{Me} **(a)**	−2.58[c]	+0.06[c]
L^X = NacNac^{NMe2} **(b)**	−2.23[b], −2.62[c]	−0.14
L^X = dipba^{Mes} **(c)**	−2.21[b], −2.57[c]	+0.27
L^X = dipg^{NMe2} **(d)**	−2.26[b] , −2.60[c]	+0.15[c]

[a]= Experiments were performed in acetonitrile solvent with 0.1 M NBu_4PF_6 electrolyte with scan rate of 0.1 V/s using a glassy carbon working electrode and a silver wire pseudo-reference electrode. Potentials are referenced against the ferrocene/ferrocenium redox couple, [b]= Irreversible wave, [c]=Quasi-reversible.

Oxidation waves for btp-ligated complexes described here were mostly reversible (**2b/c**) or quasi-reversible (**2a/2d**), whereas the Ir^{IV}/Ir^{III} potentials were completely irreversible for all piq-ligated complexes except **1c** (L^X = $dipba^{Mes}$) and **1d** (L^X = $dipg^{NMe2}$). The reduction potentials (E^{red}) of the new complexes described here are quite similar for both piq- and btp-ligated complexes with slight dependence on the identity of the L^X ligands, and the associated population of a π* orbital on each C^N ligand results in reduction waves beyond −2.0 V. The first reduction potentials for all piq-ligated complexes were reversible, ranging from −2.23 V to −2.31 V. Another subsequent reduction wave was observed for complexes **1a**–**f**, assuming the phenomena was most likely caused by the subsequent reduction of each C^N ligand, this second reduction wave was reversible in all cases except **1a** (E^{red} = −2.51 V) and **1d** (E^{red} = −2.59 V) which were observed to be quasi-reversible. Btp-ligated complex **2a** (E^{red} = −2.58 V) displayed only one reduction wave at a far negative potential. For complexes **2b**–**d** two one-electron reduction waves were observed, where the first reduction waves were irreversible and the second reduction waves were quasi-reversible in all cases. The observed potentials of the new complexes indicated minimal perturbation of the C^N-centered LUMO energies with the alteration of the ancillary ligands.

4.2.4 Photophysical properties

The UV-vis absorption spectra and steady-state and time-resolved emission spectra of all the complexes were recorded in THF at room temperature. The overlaid UV-vis absorption spectra of complexes are depicted in Figure 4.3. In all cases intense absorption bands in the UV region with molar extinction coefficients ranging from 5 – 38

× 10^3 M^{-1} cm^{-1} were observed, which can be assigned as the spin-allowed ligand-centered π→π* transition (^{1}LC) involving cyclometalating and ancillary ligands. The *N*-substituent variation in the ancillary ligands exerts little influence on the extinction coefficients. All complexes showed a less intense, overlapping absorption bands tailing beyond 500 nm for btp (**2a**–**d**) and 600 nm for piq (**1a**–**f**) complexes. These weaker low-energy bands absorption can be assigned as both singlet and triplet metal-to-ligand charge transfer (^{1}MLCT/^{3}MLCT) transitions, as has been previously observed for other cyclometalated iridium complexes.[35,36] The position of these MLCT bands were rarely affected by the identity of the ancillary ligands, on the contrary dependence on cyclometalating ligand was obvious from the spectra in Figure 4.3. However, complexes with cyclohexyl groups on the ancillary ligand (**1e** and **1f**) displayed intense absorption bands between 380–405 nm in this lower-energy region (17–23) × 10^3 M^{-1} cm^{-1} compared to other compound in the piq series where the MLCT band is red shifted.

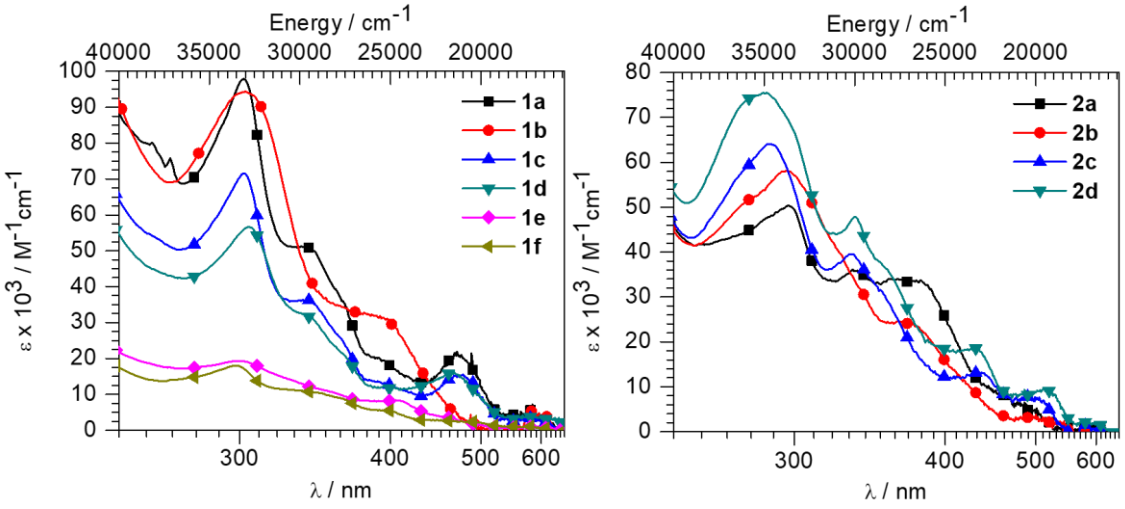

Figure 4.4. Overlaid UV-vis absorption spectra of **1a**–**f** and **2a**–**d**.

Table 4.2. Summary of emission data for all complexes

	λ_{max}(nm)[a]			Φ_{PL}	τ(μs)	(k_r[c] × 10^{-5} s^{-1}) / (k_{nr}[c] × 10^{-5} s^{-1})
	THF at 293 K	Toluene at 293 K	Toluene at 77 K			
1a	660	655	642	0.53	0.81	6.5/5.8
1b	707	701	611, 666	0.071	0.90[b]	0.78/10
1c	661	656	640, 699	0.58	0.74	7.8/5.6
1d	683	683	620, 678	0.37	0.53	6.8/11.8
1e	658	658	643	0.022	0.74[b]	0.30/13
1f	657	655	634, 687	0.49	0.78	6.2/6.6
2a	624	622	605, 664	0.27	4.0	0.68/1.8
2b	633	627	616, 669	0.18	2.8	0.63/2.9
2c	619, 668	619, 665	609, 667	0.31	3.9[b]	0.80/1.8
2d	626	626	611, 671	0.30	3.1	0.98/2.3

[a]= λ_{exc} = 420 nm. [b]= bi-exponential. Reported lifetime is a weighted average of the two time constants. [C]=$k_r = \Phi/\tau$ and $k_{nr} = (1 - \Phi)/\tau$.

All of the complexes described here were luminescent at room temperature in deareated solution of tetrahydrofuran (THF) when excited within their absorption manifold. Table 4.2 summarizes the steady-state and time-resolved emission data, and Figure 4.4 and 4.5 show overlaid room temperature and low temperature (77 K) emission spectra of **1** and **2**. The excitation spectra of the new complexes were also collected and shown in Figures 4.6 and 4.7. In each case, the superimposed absorption and excitation spectra indicates that the emission signal arises solely from the iridium complex and ruling out emission that originates from minor impurity. The observed room-temperature emission maxima for all of the complexes with C^N = piq were beyond 650 nm strongly dependent on the ancillary ligand, with the luminescence λ_{max} of **1a**–**f** spanning a range of 657–707 nm and quantum yields that vary between 0.071 to 0.58.

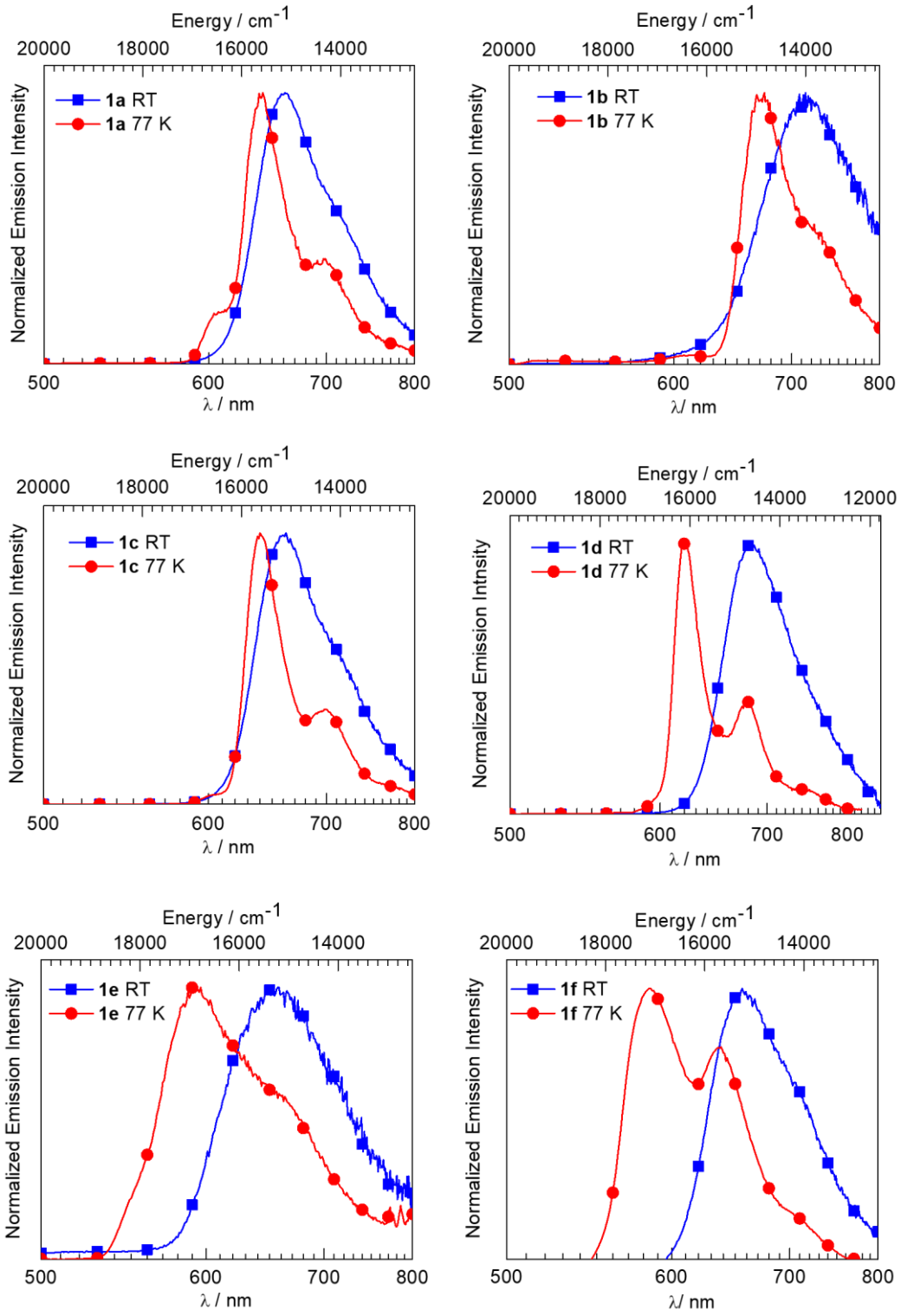

Figure 4.5. Overlaid emission spectra of **1a–f**, recorded in toluene at room temperature (blue, squares) and 77 K (red, circles), with λex = 420 nm.

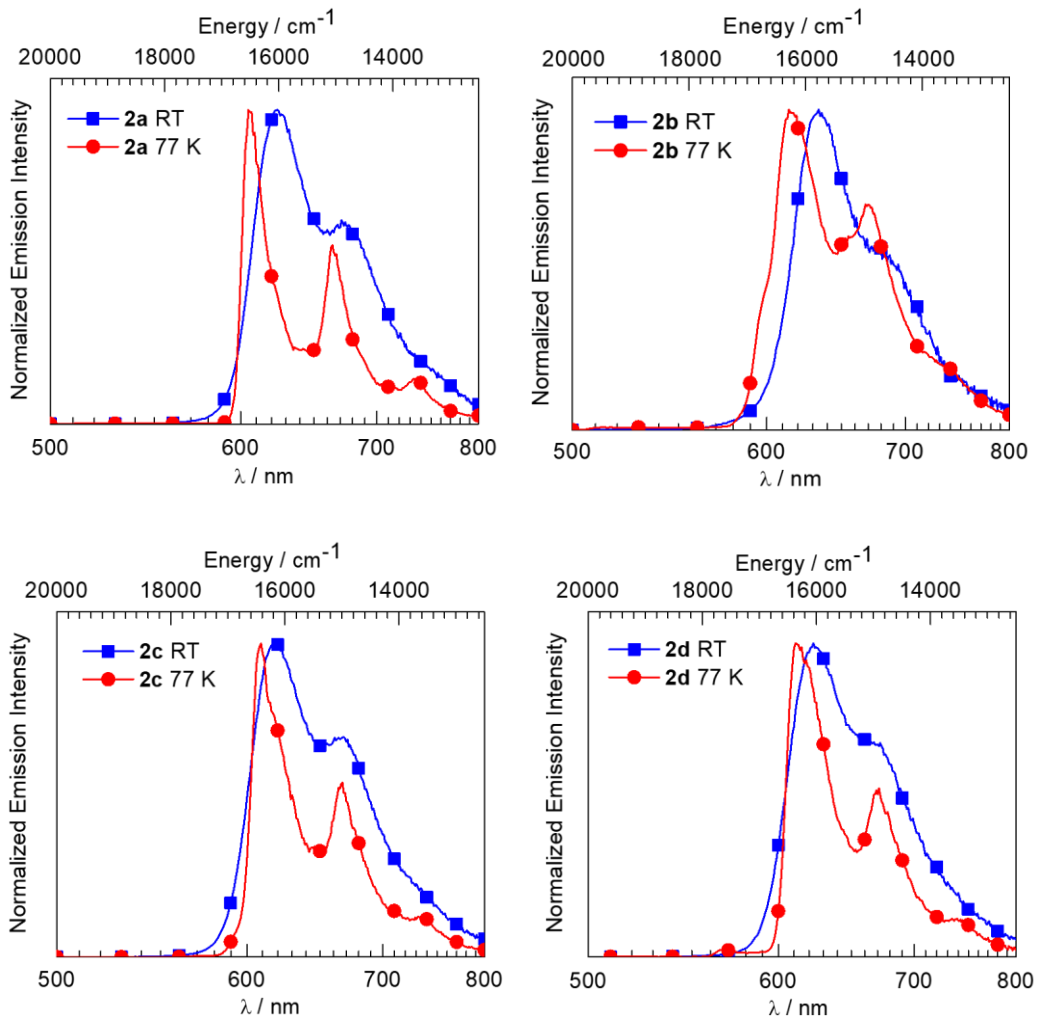

Figure 4.6. Overlaid emission spectra of **2a–d**, recorded in toluene at room temperature (blue, squares) and 77 K (red, circles), with λex = 420 nm.

The electron-rich π-donating guanidinate (dipg^{NMe2}) ligand in complex **1d** red-shifted the λ_{max} (683 nm) with moderate quantum yield (Φ_{PL} = 0.37) when compared with amidinate complex **1c** which has λ_{max} at 656 nm but with a higher quantum yield (Φ_{PL} = 0.58). The backbone modified β-dekitiminate ligand NacNac^{NMe2} also profoundly influences the emission maxima (λ_{max}), which is 707 nm in **1b**. Mixed *N*,*O*-chelated (Cy)acNac complex **1f** displays a ca. 20 nm red shift of the emission maxima (λ_{max} = 658 nm) along with slight attenuation of the quantum efficiency (Φ_{PL} = 0.49) when comparing it with the

phenyl-substituted acNac analogue described previously from our group (λ_{max} = 637 nm, Φ_{PL} = 0.80).[35] For the piq-ligated complexes the emission lifetimes (τ) were in the range of 0.5 to 4 μs with radiative rate constants (k_r) vary between 0.53–0.90 × 10^5 s^{-1}. The increase in k_r in **1a**, **1c**, **1d**, and **1f** were accompanied by a small decrease in k_{nr}, resulting in augmented quantum efficiencies of the complexes.

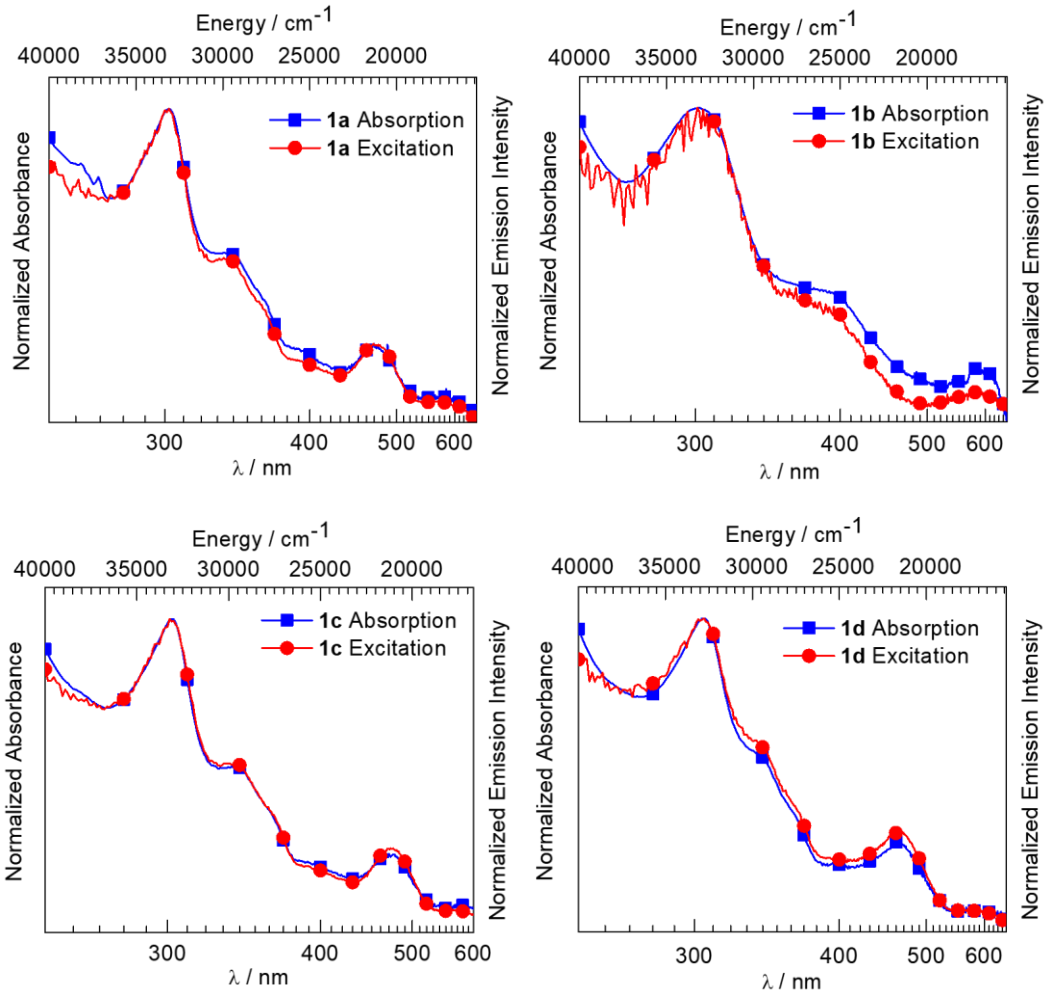

Figure 4.7. Overlaid UV-vis absorption and excitation spectra of **1a–d**. Spectra were recorded in THF at room temperature. λem for the excitation spectra are corresponding to the emission maxima of each compound.

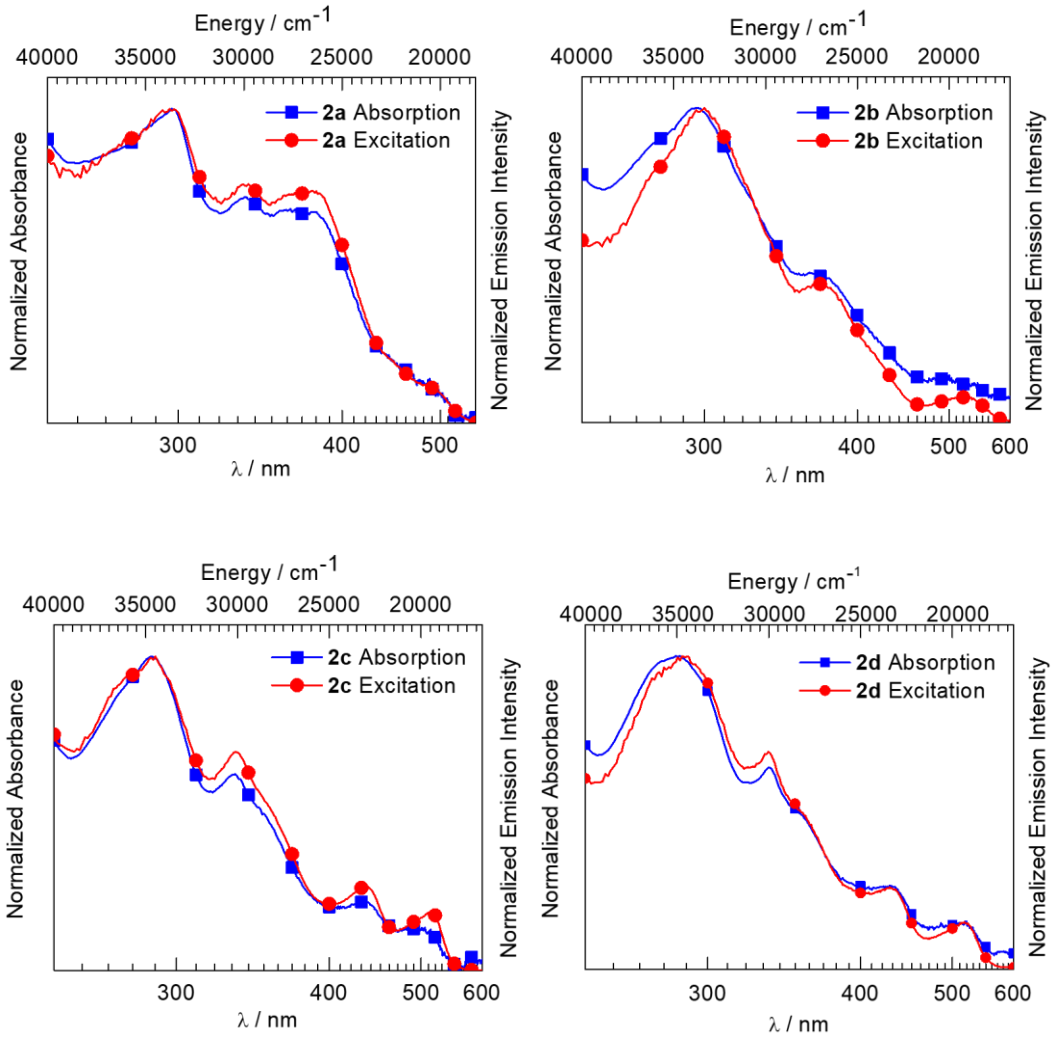

Figure 4.8. Overlaid UV-vis absorption and excitation spectra of **2a–d**. Spectra were recorded in THF at room temperature. λem for the excitation spectra are corresponding to the emission maxima of each compound.

The low-temperature (77 K) emission spectra of complexes **1a**–**f** (Figure 4.4) showed a well-defined vibronic structure with approximately 39 nm (ca. 923 cm^{-1}) on average.For btp complexes **2a**–**d**, the emission wavelengths (λ_{max} = 619–633 nm) are found to be less sensitive to the identity of the ancillary ligands and the vibronic structures are more defined in the emission spectra at room temperature. For complexes **2a**–**d** the quantum yields range from 0.18–0.45 with 0.41–4.0 μs lifetimes. Complex **2c**

displayed an increase of k_r and gave rise to a slightly higher quantum yield (Φ_{PL} = 0.45) compared to the rest of the members in the btp series. Compared to piq complexes, the k_r value of the btp complexes were observed to be smaller in magnitude, such that the k_r value for most of the btp complexes were in the order of 10^4 s^{-1}. Better-resolved emission spectra was observed for btp complexes at 77 K with an average rigidochromic shift of about 15 nm (ca. 400 cm^{-1}). (Table 4.2 and Figure 4.5).

4.3 Discussion

The work presented here was mainly focused on investigating the effects of incorporating nitrogen-containing, strongly π-donating ancillary ligand on the photoluminescence of cyclometalated iridium red phosphors. Designing efficient red-emitting cyclometalated iridium complexes with higher quantum yield and higher radiative rate constant (k_r) has been especially challenging because of the energy-gap law which dictates that the rate of nonradiative decay is inversely related to the energy difference between the ground and excited states,[29] and the radiative rate constant shows cubic dependence with the excited state energy gap. Modifications of the cyclometalating ligand have been commonly employed to design red phosphors via tuning of the HOMO–LUMO gap by incorporating electron-donating sulfur-containing heterocycles or extending the π-conjugations.[12,39] In this way, many red-emitting complexes primarily of the type $Ir(C\hat{}N)_3$ and $Ir(C\hat{}N)_2(acac)$, have been described. Effects of ancillary ligand modifications have been extensively studied in our group recently, and few of the complexes of type $Ir(C\hat{}N)_2(acNac)$ and $Ir(C\hat{}N)_2(dipba)$ were observed to have very high quantum yields of more than 0.80 in solution (C^N = benzothiazole (bt), piq or btp),

which can rival some of the top-performing yellow and red emitters.[40–45] The work described here represents a continued study on the effects of ancillary ligand modification on excited state dynamics, in pursuit of optimized quantum yields and augmented radiative rate constant (k_r). The general synthesis employed in this work is similar to the procedure that was previously published from our group and some other groups. Treatment of the chloro-bridged dimer $[Ir(C\text{^}N)_2(\mu\text{-}Cl)]_2$ with two equivalents of potassium salt of six-membered (N)acNac compounds or in situ-generated lithium salt of four-membered dipba/dipg ligand affords the isolation of the new complexes in moderate yields. Five of the complexes were characterized by X-ray crystallography and the observed structures match well the structures that were assigned by ^{1}H and $^{13}C\{^{1}H\}$ NMR spectroscopy. Excepting the different chelate angles that result from different chelate-ring sizes of the ancillary ligands, the bond lengths and bond angles at the iridium center were found to be similar across the series, and π-electron delocalization was observed in all complexes in the ancillary ligand.

In spite of the minimal structural perturbation brought on by the substitution of the L^X ligands, profound influence was observed on electronic properties for such substitutions. The electrochemical data, depicted in Table 4.1, indicates that the Ir^{IV}/Ir^{III} potential depended strongly on the identity of the ancillary ligand. For the piq series, the mixed *N,O*-chelated complex **1f** was more difficult to oxidize whereas the oxidation potentials of the other *N,N*-chelated complexes shifted cathodically. Among the *N,N*-chelated ligands for both piq- and btp-ligated complexes, the oxidation potential of the six-membered NacNac ligands exhibited more cathodic shift compared to four-membered

dipba or dipg ligands. On the contrary, the reduction potentials changed minimally when the ancillary ligand was altered, due to fact that the reduction process corresponds to adding an electron in the C^N centered π* orbital. Energies of iridium complexes in the excited triplet-state (T_1) generally involve significant HOMO→LUMO character, and consequently were affected by the energies of the highest occupied molecular orbital (HOMO) and the lowest occupied molecular orbital (LUMO). The LUMO in most of the cyclometalated iridium complexes were generally located on the C^N ligands whereas the HOMO consisted of a mixture of the C^N aryl and the iridium dπ orbitals. All of the above-mentioned electrochemical results were coherent with the notion that the ancillary ligands strongly perturb the energy of the metal centered HOMO while the LUMO energies were not affected significantly. Substituting electron-rich ancillary ligands increased the π donating ability of the L^X ligand, resulting in higher destabilized HOMO energies and lower oxidation potentials.

The luminescent properties of the complexes **1**–**2** highlights the effects of ancillary ligand structure, but the differences caused by the cyclometalating ligands are also taken into consideration. The substitution patterns of the ancillary ligands of different chelate ring size and their electron-donating nature influence the photophysical properties, and give rise to an opportunity of comparison among the complexes. Replacing the ancillary ligand from the *O,N* donor acNac to the isoelectronic *N,N* donor caused a substantial red shift in the emission wavelength. The strong π-electron donor $dipg^{NMe2}$ ligand red shifted the emission maximum (λ_{max} = 683 nm) close to the near-IR region, a larger shift than the isoelectronic $dipba^{mes}$ ligand (λ_{max} = 661 nm) in the piq

series. Augmented k_r values were observed in both cases compared to the dipba^{Ph} analogue previously reported from our group.[35] The btp-ligated complexes **2a**–**d** seemed to be less influenced by electron-rich ancillary ligands. In general btp-ligated iridium complexes exhibited emission maxima that are blue shifted compared to the piq-ligated complexes and the incorporation of the L^X ligands with different electronic properties did not alter the trend.[35,36]

The different ring size of the ancillary ligand also influenced the emissive properties of the new complexes. Four-membered electron-rich dipba/dipg ligands have a smaller bite angle compared to the six-membered (N)acNac ligands. The complexes with smaller bite angle influence the k_r value as **1c**, **1d,** and **2c** displayed the larger k_r (6.8–11 $\times 10^{-5}$ s^{-1}) values in the series resulting in higher quantum yields (Φ_{PL} = 0.37–0.58). The emission spectra of piq complexes were minimally perturbed by the six-membered (N)acNac ligands except **1b** where a much lower quantum yield (Φ_{PL} = 0.07) was observed along with a very low k_r value (0.78 $\times 10^{-5}$ s^{-1}), and almost similar patterns were noted for six-membered btp complexes. The substituent pattern on the ancillary ligand was another factor to consider studying the effect of L^X ligands. In btp series the *N*-*i*Pr substituted guanidinate complex **1d/2d** also had moderate quantum yields. *N*,*N*'-cyclohexyl substitution in complex **1e** seemed to have a detrimental effect on the quantum yield (Φ_{PL} = 0.022) while the *N*-cyclohexyl substitution in acNac complex **1f** still resulted in a rather high photoluminescence quantum yield (Φ_{PL} = 0.49).

The emissive excited state in cyclometalated iridium complexes is generally a mixture of ligand centered (LC) and metal-to-ligand charge transfer (^{1}MLCT/^{3}MLCT)

states. The complexes described in this work indicate an increased MLCT character which can be evinced from few of the emission properties like lifetime value, rigidochromic shift in the low-temperature emission spectra, and augmented k_r value. Incorporating π-donating ligands generally influenced the MLCT character by increasing the spin-orbit coupling, which in turn increased the k_r value as well as the quantum yield. All the complexes displayed a very pronounced rigidochromic shift of in the emission spectra when cooled down to 77 K from room temperature. This shift was substantially larger in the piq complexes than btp complexes, and such trend is associated with the enhancement of charge-transfer character in the emissive excited state. At room temperature the emission spectra of the piq complexes had less pronounced vibronic structure which is consistent with the notion of enhanced MLCT character. The emission spectra of complexes with the thiophene-containing btp ligand was mostly ligand-localized, as proved by the well-defined vibronic structure at room temperature which became even better-resolved at 77 K. The shorter lifetime values and increased k_r values in piq complexes also supports the enhanced MLCT character of the iridium complexes.

As discussed above, the incorporation of electron-rich π-donating ancillary ligands was able to tune the electrochemical and photophysical properties of the cyclometalated iridium complexes which was confirmed from some of the experimental evidence presented in this work. Building of previous works in our group,[22,35–37] this suite of complexes allows us to answer important lingering questions about how the structure of the ancillary ligand influences photoluminescence, although it was not possible to point out a specific trend from the limited set of 10 complexes discussed here.

4.4 Conclusion

We have presented here a thorough study of the effect of ancillary ligand modification on the electrochemical and optical properties of cyclometalated iridium complexes by incorporating six different strongly π-donating ancillary ligands with two different ring sizes. Most of the ancillary ligands are paired with two different cyclometalated ligand, piq and btp, as they tend to emit in the red region of the spectrum. Electron-rich, strongly π-donating ancillary ligands were used based on the fact that they can lead to larger radiative rates and higher phosphorescence quantum yields in the red and near-IR regions, which has proven to be effective for some of the complexes. In general, the piq complexes are more sensitive to the ancillary ligand modification compared to the btp complexes, as most members of the btp series have very similar emission properties. Electron-donating substituents, like those present in amidinate (dipba), guanidinate ($dipg^N$), β-ketoiminates (acNac), or β-diketiminates (NacNac), can augment the radiative rate constant (k_r) and/or shift the luminescence to the near-IR region. Also, the sterically encumbered versions of these ancillary ligands can decrease the non-radiative rate constant (k_{nr}) as another means of increasing the photoluminescence quantum yields of these compounds. The work described here motivate further pursuit of the more ancillary ligand modification along with computational studies to control and optimize the structural properties to design better red phosphors.

4.5 Experimental section

4.5.1 Materials

Starting materials and reagents were of commercial origin and used without further purification. All reactions were executed in a nitrogen-filled glovebox operating at <1 ppm of O_2 and H_2O. Anhydrous solvents for reactions and optical measurements were dried by the method of Grubbs,[46] passing through dual alumina columns on a commercial solvent purification system (SPS), and stored over 3 Å molecular sieves. All NMR solvents were dried and stored over 3 Å molecular sieves in the glovebox; $CDCl_3$ was also stored over potassium carbonate in addition to sieves. Cyclometalated iridium dimers $[Ir(C\hat{}N)_2(\mu\text{-}Cl)]_2$ (C^N = 1-phenylisoquinoline (piq) and 2-(2-pyridyl)benzothiophene (btp)) were prepared by the method of Nonoyama,[47] refluxing $IrCl_3 \cdot nH_2O$ with 2−2.3 equiv of the cyclometalating ligand in a 3:1 mixture of 2-ethoxyethanol and water. Potassium or lithium salts of the acNac and NacNac ligands were prepared by the general procedure as described previously by our lab.[22] Tetrabutylammonium hexafluorophosphate ($TBAPF_6$) was recrystallized from hot ethanol and ferrocene was sublimed before use in electrochemical experiments.

4.5.2 Physical methods

^1H and $^{13}C\{^1H\}$ NMR spectra were recorded at room temperature using a JEOL ECA-400, ECA-500, or ECA-600 NMR spectrometer. UV−vis absorption spectra were recorded in THF solution in screw-capped quartz cuvettes using an Agilent Carey 60 UV−vis spectrophotometer. Luminescence lifetimes were measured with a Horiba

DeltaFlex Lifetime System, using 390 nm pulsed diode excitation. Steady-state emission spectra were recorded using a Horiba FluoroMax-4 spectrofluorometer with appropriate long-pass filters to exclude stray excitation light from detection. In order to exclude air, samples for emission spectra were prepared in a nitrogen-filled glovebox using anhydrous solvents. Samples for room-temperature emission were housed in 1 cm quartz cuvettes with septum-sealed screw caps, and samples for low-temperature emission were contained in a custom quartz EPR tube with high-vacuum valve and immersed in liquid nitrogen using a finger dewar. Solution quantum yields were determined relative to a standard of tetraphenylporphyrin in toluene, which has a reported fluorescence quantum yield (Φ_{PL}) of 0.11.[48] Cyclic voltammetry (CV) measurements were performed with a CH Instruments 602E potentiostat interfaced with a nitrogen glovebox via wire feedthroughs. Samples were dissolved in acetonitrile with 0.1 M $TBAPF_6$ as a supporting electrolyte. A 3 mm diameter glassy-carbon working electrode, a platinum wire counter electrode, and a silver wire pseudo-reference electrode were used. Potentials were referenced to an internal standard of ferrocene.

4.5.3 Synthesis

[(Cy)$_2$NacNacMe]H. Acetylacetone (6.0 g, 60 mmol) and *p*-toluenesulfonic acid monohydrate (10.3 g, 60 mmol) were dissolved into 250 mL of toluene. The mixture was cooled to 0 °C and the first equivalent of cyclohexylamine (5.9 g, 60 mmol) was added dropwise. The slightly yellow solution was then heated to a reflux and reaction water was removed using a Dean-Stark trap. After boiling overnight the solution was cooled to room temperature and the second equivalent of cyclohexylamine was added.

Subsequently the mixture was refluxed for three days, again using the Dean-Stark trap. The solution was then cooled to room temperature and the resulting precipitate was filtered off. The obtained solid was dissolved by stirring it rapidly with 100 mL of Ether and a solution of 13.86 g KOH in 150 mL of water. The organic layer was seperated and the aqueous phase was extracted two more times with 100 mL of Et_2O. The combined organic phases were dried over Na_2SO_4, filtered and freed from solvent by rotary evaporation. The crude product was obtained as a yellowish solid. Recrystallization from hot ethanol gave colorless crystals. Yield: 9.97 g (63.3%). ^{1}H NMR (400 MHz, $CDCl_3$) δ: 11.42 (bs, 1H, N*H*), 4.39 (s, 1H, C*H*(C=N)$_2$), 3.36-3.29 (m, 2H, Cy*H*), 1.89 (s, 6H, CH_3), 1.80-1.24 (m, 20H, Cy).

[(Cy)acNac^{Me}]H. Acetylacetone (5.00 g, 50 mmol, 1.0 equiv) and cyclohexylamine (4.46 g, 45 mmol, 0.9 equiv) were dissolved into 20 mL of DCM and the solution was stirred at room-temperature for two days. To the opaque, yellow mixture 20 mL of water were added and the organic layer was separated and dried over Na_2SO_4. The solvent was removed under reduced pressure and gave a yellow liquid. Analysis by NMR-spectroscopy indicated sufficient purity for further use. Yield 5.59 g (68.8%). ^{1}H-NMR (400 MHz, $CDCl_3$) δ: 10.97 (bs, 1H, N*H*), 4.89 (s, 1H, (C=O)C*H*(C=N)), 3.32-3.37 (m, 1H, Cy*H*), 1.97 (s, 3H, CH_3), 1.92 (s, 3H, CH_3), 1.75-1.87 (m, 4H, Cy), 1.50-1.58 (m, 1H, Cy), 1.23-1.37 (m, 5H, Cy).

Ir(piq)$_2$[(dmp)$_2$NacNac^{Me}] (1a). In the glovebox, [Ir(piq)$_2$(μ-Cl)]$_2$ (50 mg, 0.039 mmol) was suspended in 3 mL THF, and a solution of [(dmp)$_2$NacNac^{Me}K] (29 mg, 0.089 mmol, 2.3 equiv) in 5 mL THF was added to the dimer suspension slowly by pipet.

The resulting reddish-brown mixture was stirred overnight at room temperature, during which time the color of the solution changed to dark red. The solvent was removed under reduced pressure, and the resulting residue was extracted with 5 mL of toluene and filtered through Celite to remove KCl and other insoluble impurities. The toluene was removed in vacuo, and the residue was washed with 2 × 3 mL of room-temperature Et_2O. The final product was obtained by adding pentane to a concentrated DCM solution which was dried under vacuum. Yield: 37 mg (53%). ^{1}H NMR (600 MHz, $CDCl_3$) δ: 9.23 (d, *J* = 6.2 Hz, 2H, ArH), 8.57 (d, *J* = 8.9 Hz, 2H, ArH), 7.89 (d, *J* = 8.2 Hz, 2H, ArH), 7.64–7.72 (m, 4H, ArH), 7.60 (t, *J* = 7.6 Hz, 2H, ArH), 7.42 (d, *J* = 6.2 Hz, 2H, ArH), 6.56–6.67 (m, 6H, ArH), 6.17–6.29 (m, 4H, ArH), 5.99 (d, *J* = 7.6 Hz, 2H, ArH), 4.79 (s, 1H, $(Me)_2$PhNC(Me)C*H*C(Me)NPh$(Me)_2$), 2.04 (s, 6H, CH_3), 1.51 (s, 6H, CH_3), 0.875 (s, 6H, CH_3). ^{13}C{^{1}H} NMR (151 MHz, $CDCl_3$) δ: 171.3, 159.8, 155.2, 149.7, 146.5, 146.3, 136.8, 133.0, 132.7, 131.7, 130.5, 129.2, 128.1, 127.8, 127.5, 127.4, 127.3, 126.5, 126.4, 125.7, 122.7, 119.6, 117.5, 96.74, 25.26, 21.53, 17.02. UV-vis (THF): λ/nm (ε/M^{-1} cm^{-1}) 302(98000), 343(sh)(50000), 390(sh)(20000), 468(21000).

Ir(piq)$_2$NacNac^{NMe2} (1b). In the glovebox, $[Ir(piq)_2(\mu\text{-}Cl)]_2$ (60 mg, 0.047 mmol) was suspended in 3 mL of THF, and a solution of NacNac^{NMe2}K (35 mg, 0.010 mmol, 2.2 equiv) in 5 mL of THF was added to the dimer suspension slowly by pipet. The resulting reddish orange mixture was stirred overnight at room temperature, during which time the color of the solution changed to dark green. The solvent was removed under reduced pressure, and the resulting residue was extracted with 5 mL of toluene and filtered through Celite to remove KCl and other insoluble impurities. The toluene was removed in

vacuo, and the residue was washed with 2 × 3 mL of room-temperature Et_2O. Final product was obtained by adding pentane to a concentrated DCM solution which was dried under vacuum. Yield: 62 mg (73%). ^{1}H NMR (400 MHz, $CDCl_3$) δ: 8.73 (d, *J* = 8.9 Hz, 2H, ArH), 8.51 (d, *J* = 6.9 Hz, 2H, ArH), 8.03 (d, *J* = 8.2 Hz, 2H, ArH), 7.71 (d, *J* = 8.2 Hz, 2H, ArH), 7.47–7.58 (m, 4H, ArH), 6.96 (d, *J* = 6.2 Hz, 2H, ArH), 6.85 (t, *J* = 7.6 Hz, 2H, ArH), 6.47–6.65 (m, 8H, ArH), 6.32 (t, *J* = 7.6 Hz, 2H, ArH), 6.04 (d, *J* = 8.2 Hz, 2H, ArH), 3.83 (s, 1H, PhNC(NMe_2)C*H*C(NMe_2)NPh), 2.29 (s, 12H, CH_3). ^{13}C{^{1}H} NMR (151 MHz, $CDCl_3$) δ: 170.1, 167.8, 162.3, 153.8, 146.2, 144.6, 136.5, 133.2, 130.2, 129.9, 128.2, 127.1, 127.0, 126.5, 126.2, 125.7, 125.6, 119.4, 119.3, 117.0, 86.17, 40.99. UV-vis (THF): λ/nm (ε/M^{-1} cm^{-1}) 302(94000), 370(sh)(24000), 500(4000).

Ir(piq)$_2$dipba^{mes} (1c). In the glovebox, 2-bromomesitylene (~36 mg, 0.18 mmol) was dissolved in 5 mL THF and the solution was kept at −35° C for 1 h. After that a hexane solution of *n*-BuLi (~0.11 mL, 1.6 M) was added, and the reaction mixture was stirred at −35 °C for 10 min. Then N,N′-diisopropylcarbodiimide (~23 mg, 0.18 mmol) was added to the solution and the reaction mixture was stirred at room temperature for another 10 min. The colorless solution was then added dropwise to a Teflon-capped glass tube containing [Ir(piq)$_2$(μ-Cl)]$_2$ (100 mg, 0.0786 mmol) in 5 mL THF. The resulting reddish orange mixture was stirred overnight outside of glovebox at 80–85 °C, during which time the color of the solution changed to dark brown. The mixture was cooled to room temperature and the sealed tube was taken inside the glovebox for further workup procedure. The solvent was removed under reduced pressure and the residue was extracted in 2 mL toluene and evaporated under reduced pressure to remove THF

completely. The product was redissolved in 10mL toluene and filtered through Celite to remove LiCl and other insoluble impurities. The crude product was washed with 3 × 3 mL of Et_2O and 2 × 3 of mL hexane. The solid was redissolved in minimum amount of DCM and pentane was added to slowly induce precipitation and the resulted reddish-brown solid was concentrated to dryness. Yield: 55 mg (48%). ^{1}H NMR (600 MHz, $CDCl_3$) δ: 9.55 (d, *J* = 6.4 Hz, 2H, ArH), 8.96 (d, *J* = 8.2 Hz, 2H, ArH), 8.17 (d, *J* = 7.8 Hz, 2H, ArH), 7.96 (d, *J* = 7.3 Hz, 2H, ArH), 7.63–7.75 (m, 4H, ArH), 7.53 (d, *J* = 6.4 Hz, 2H, ArH), 6.77–6.93 (m, 4H, ArH), 6.61–6.67 (m, 2H, ArH), 6.36 (d, *J* = 7.8 Hz, 2H, ArH), 3.04 (sept, *J* = 6.2 Hz, 2H, $(CH_3)_2CHN$), 2.43 (s, 6H, CH_3), 2.25 (s, 6H, CH_3), 0.72 (d, *J* = 5.6 Hz, 6H, CH_3), −0.06 (d, *J* = 6.4 Hz, 6H, CH_3). ^{13}C{^{1}H} NMR (151 MHz, $CDCl_3$) δ: 173.0, 170.1, 159.5, 146.3, 145.8, 137.2, 136.5, 136.2, 133.7, 132.6, 130.2, 129.7, 128.8, 128.3, 127.3, 127.2, 127.1, 126.2, 119.2, 119.0, 48.73, 25.17, 24.88, 21.33, 21.14. UV-vis (THF): λ/nm (ε/M^{-1} cm^{-1}) 302(87000), 337(44000), 393(sh)(16000), 476(19000), 582(sh)(4000).

$Ir(piq)_2dipg^{NMe2}$ (1d). In the glovebox, lithium dimethylamide (~4 mg, 0.08 mmol) was dissolved in 5 mL THF and the solution was kept at −35 °C for 1 h. After that N,N′-diisopropylcarbodiimide (11 mg, 0.083 mmol) was added to the solution and the mixture was stirred at room temp for 30 min. The colorless guanidinate solution was then added dropwise to the Teflon-capped glass tube containing $[Ir(piq)_2(\mu\text{-}Cl)]_2$ (50 mg, 0.039 mmol) in 5 mL THF. The resulting red mixture was stirred overnight outside of the glovebox at 80–85 °C, during which time the color of the solution changed to light brown. The mixture was cooled to room temperature and the sealed tube was taken inside

the glovebox for further workup procedure. The solvent was removed under reduced pressure and the residue was extracted in 3 mL of toluene and evaporated under reduced pressure to remove THF completely. The product was redissolved in 5 mL of toluene and filtered through Celite to remove LiCl and other insoluble impurities. The crude product was washed with 3 × 3 mL of Et_2O and 2 × 3 mL of pentane. The crude product was redissolved in minimum amount of THF and pentane was added to the solution to slowly induced precipitation. The light brown solid was washed again with 2 × 2 mL of Et_2O and the resulting solution was concentrated to dryness. Yield: 33 mg (54%). ^{1}H NMR (600 MHz, $CDCl_3$) δ: 9.32 (d, *J* = 6.3 Hz, 2H, ArH), 8.92 (d, *J* = 8.0 Hz, 2H, ArH), 8.13 (d, *J* = 8.0 Hz, 2H, ArH), 7.93 (d, *J* = 7.4 Hz, 2H, ArH), 7.59–7.76 (m, 4H, ArH), 7.48 (d, *J* = 6.3 Hz, 2H, ArH), 6.80 (t, *J* = 7.4 Hz, 2H, ArH), 6.56 (d, *J* = 6.9 Hz, 2H, ArH), 6.22 (d, *J* = 7.4 Hz, 2H, ArH), 3.71 (sept, *J*= 6.3 Hz, 2H, $(CH_3)_2CHN$), 2.86 (s, 6H, CH_3), 0.57 (d, *J* = 6.3 Hz, 2H, CH_3), −0.05 (d, *J* = 6.3 Hz, 2H, CH_3). ^{13}C{^{1}H} NMR (151 MHz, $CDCl_3$) δ: 170.2, 169.9, 161.2, 146.2, 143.3, 136.2, 132.6, 130.0, 129.8, 128.7, 127.2, 127.1, 126.4, 119.1, 118.9, 47.66, 40.77, 24.79, 24.33. UV-vis (THF): λ/nm (ε/M^{-1} cm^{-1}) 305(57000), 341(sh)(31000), 464(16000), 583(sh)(4000).

Ir(piq)$_2$[(Cy)$_2$NacNac^{Me}] (1e). In the glovebox, $[Ir(piq)_2(\mu\text{-}Cl)]_2$ (100 mg, 0.079 mmol) was suspended in 5 mL of toluene in a Teflon-capped glass tube. A suspension of $[(Cy)_2NacNac]K$ (45 mg, 0.15 mmol) in 5 mL of toluene was added into the tube slowly via pipette. The reaction mixture was heated outside of glovebox at 130 °C for five days. The mixture was cooled to room temperature and the sealed tube was taken inside the glovebox for further workup procedure. The resulting dark mixture

was filtered through Celite and concentrated in vacuo. The residue was crystallized using 2 mL of Et_2O at −30 °C. The supernatant liquid was removed via pipette and the solid residue was washed again with 2 × 3 mL of Et_2O at −30 °C and 3 × 3 mL of pentane. The resulting solid was dried in vacuo and obtained as dark brown solid. Yield: 47 mg (37%). ^{1}H-NMR (500 MHz, CD_2Cl_2) δ: 9.07 (d, J = 6.3 Hz, 2H, Ar*H*), 8.91 (d, J = 8.0 Hz, 2H, Ar*H*), 8.14 (d, J = 8.0 Hz, 2H, Ar*H*), 7.93 (d, J = 7.4 Hz, 2H, Ar*H*), 7.65−7.71 (m, 4H, Ar*H*), 7.42 (d, J = 6.3 Hz, 2H, Ar*H*), 6.85 (t, J = 7.4 Hz, 2H, Ar*H*), 6.56 (t, J = 7.2 Hz, 2H, Ar*H*), 4.00 (s, 1H, CyNC(Me)C*H*C(Me)NCy), 2.97 (t, J = 11.5 Hz, 2H, Cy*H*), 1.89 (s, 6H, CH_3), 0.01–1.63 (m, 20H, Cy). ^{13}C{^{1}H} NMR (126 MHz, CD_2Cl_2) δ: 169.67, 162.76, 158.34, 146.51, 144.38, 136.82, 132.25, 130.37, 129.74, 128.65, 127.22, 126.99, 126.91, 126.35, 119.38, 118.51, 99.84, 66.35, 34.41, 33.75, 26.94, 26.30, 26.09, 24.88. UV-vis (THF): λ/nm (ε/M^{-1} cm^{-1}) 299 (38000), 405(17000), 533(sh)(12000).

Ir(piq)$_2$[(Cy)acNac^{Me}] (1f). In the glovebox, [Ir(piq)$_2$(μ-Cl)]$_2$ (100 mg, 0.079 mmol) was suspended in 5 mL of toluene in a Teflon-capped glass tube. A suspension of [(Cy)acNac]K (33 mg, 0.15 mmol) in 5 mL of toluene was added into the tube slowly via pipette. The reaction mixture was heated outside of glovebox at 130 °C for five days. The mixture was cooled to room temperature and the sealed tube was taken inside the glovebox for further workup procedure. The resulting dark red mixture was filtered through Celite and concentrated in vacuo. The residue was crystallized using 2 mL of Et_2O at −35 °C. The supernatant liquid was removed via pipette and the solid residue was washed again with 2 × 3 mL of cold Et_2O and 3 × 3 mL of pentane. The resulting solid was dried in vacuo and obtained as dark red solid. Yield: 41 mg (35%).

^{1}H-NMR (400 MHz, CD_2Cl_2) δ: 8.98–9.04 (m, 1H, Ar*H*), 8.92 (d, *J* = 7.8 Hz, 1H, Ar*H*), 8.75 (q, *J* = 6.6 Hz, 2H, Ar*H*), 8.30 (d, *J* = 8.2 Hz, 1H, Ar*H*), 8.15 (d, *J* = 7.8 Hz, 1H, Ar*H*), 7.92–7.99 (m, 2H, Ar*H*), 7.66–7.75 (m, 4H, Ar*H*), 6.91 (q, *J* = 7.2 Hz, 2H, Ar*H*), 6.58–6.70 (m, 2H, Ar*H*), 6.45 (d, *J* = 7.8 Hz, 1H, Ar*H*), 6.19 (d, *J* = 6.9 Hz, 1H, Ar*H*), 4.56 (s, 1H, CyNC(Me)C*H*C(O)Me), 3.06 (s, 1H, Cy*H*), 1.99 (s, 3H, CH_3), 1.59 (s, 3H, CH_3), 0.11–1.38 (m, 9H, Cy). ^{13}C{^{1}H} NMR (126 MHz, CD_2Cl_2) δ: 173.73, 169.38, 168.70, 163.12, 158.47, 157.57, 147.01, 146.22, 142.97, 141.42, 137.03, 136.89, 133.16, 132.33, 130.59, 130.56, 130.34, 129.63, 129.07, 128.30, 127.75, 127.52, 127.04, 126.94, 126.46, 126.41, 126.32, 120.55, 119.83, 119.37, 99.77, 66.07, 32.40, 31.97, 26.51, 26.21, 25.73. UV-vis (THF): λ/nm (ε/M^{-1} cm^{-1}) 298(36000), 322(sh)(23000), 384(sh)(11000), 486(5300).

Ir(btp)$_2$[(dmp)$_2$NacNac^{Me}] (2a). Prepared by the method described above for complex **1a**, using [Ir(btp)$_2$(μ-Cl)$_2$] (50 mg, 0.038 mmol) and [(dmp)$_2$NacNac^{Me}]K (30 mg, 0.089 mmol). The purified product was a dark orange colored solid. Yield: 43 mg (63%). ^{1}H NMR (600 MHz, $CDCl_3$) δ: 9.24 (d, *J* = 6.2 Hz, 2H, ArH), 7.70 (t, *J* = 7.6 Hz, 2H, ArH), 7.33 (d, *J* = 7.6 Hz, 2H, ArH), 7.27 (d, *J* = 7.6 Hz, 2H, ArH), 7.03 (t, *J* = 6.2 Hz, 2H, ArH), 6.86 (t, *J* = 6.9 Hz, 2H, ArH), 6.57 (t, *J* = 7.6 Hz, 2H, ArH), 6.38–6.47 (m, 4H, ArH), 5.95 (d, *J* = 6.9 Hz, 2H, ArH), 5.90 (d, *J* = 8.3 Hz, 2H, ArH), 4.79 (s, 1H, (Me)$_2$PhNC(Me)C*H*C(Me)NPh(Me)$_2$), 1.82 (s, 6H, CH_3), 1.68 (s, 6H, CH_3), 1.32 (s, 6H, CH_3). ^{13}C{^{1}H} NMR (151 MHz, $CDCl_3$): 167.5, 159.2, 155.0, 152.5, 148.5, 146.1, 142.4, 137.6, 136.0, 133.0, 132.6, 127.4, 126.9, 126.0, 124.0, 123.4, 122.2, 122.0, 117.5, 117.4,

98.08, 25.61, 23.88, 17.53. UV-vis (THF): λ/nm (ε/M^{-1} cm^{-1}) 297(51000), 332(36000), 359(33000), 383(sh)(32000), 498(sh)(5000).

Ir(btp)$_2$NacNac^{NMe2} (2b). Prepared by the method described above for complex **1b**, using [Ir(btp)$_2$(μ-Cl)$_2$] (50 mg, 0.038 mmol) and [(dmp)$_2$NacNac^{Me}]K (27 mg, 0.078 mmol, 2.1 equiv). The purified product was a light orange colored solid. Yield: 35 mg (50%). ^{1}H NMR (400 MHz, $CDCl_3$) δ: 8.75 (d, *J* = 5.5 Hz, 2H, ArH), 7.60 (d, *J* = 8.2 Hz, 2H, ArH), 7.43 (t, *J* = 6.9 Hz, 2H, ArH), 7.13–7.17 (m, 2H, ArH), 6.99 (t, *J* = 8.2 Hz, 2H, ArH), 6.66–6.76 (m, 4H, ArH), 6.44–6.58 (m, 6H, ArH), 6.09 (d, *J* = 8.2 Hz, 2H, ArH), 5.96 (d, *J* = 7.6 Hz, 4H, ArH), 4.06 (s, 1H, PhNC(NMe_2)C*H*C(NMe_2)NPh), 2.38 (s, 12H, CH_3). ^{13}C{^{1}H} NMR (151 MHz, $CDCl_3$) δ: 167.1, 166.7, 155.4, 152.4, 151.1, 147.4, 142.5, 136.7, 135.0, 129.1, 128.3, 127.1, 126.3, 126.1, 124.4, 123.2, 122.5, 119.6, 117.2, 116.9, 84.61, 41.21. UV-vis (THF): λ/nm (ε/M^{-1} cm^{-1}) 296(58000), 370(sh)(24000), 500(4000).

Ir(btp)$_2$dipba^{mes} (2c). In the glovebox, 2 -bromomesitylene (~33 mg, 0.17 mmol) was dissolved in 5 mL THF and the solution was kept at −35° C for 1 h. After that a hexane solution of *n*-BuLi (~0.11 mL, 1.6 M) was added, and the reaction mixture was stirred at −35° C for 10 min. Then N,N′-diisopropylcarbodiimide (~21 mg, 0.17 mmol) was added to the solution and the reaction mixture was stirred at room temp for 10 min. The colorless solution was then added dropwise to the Teflon-capped glass tube containing [Ir(btp)$_2$(μ-Cl)]$_2$ (100 mg, 0.0769 mmol) in 5 mL of THF. The resulting yellow mixture was stirred overnight outside of glovebox at 80–85 °C, during which time the color of the solution changed to light orange. The mixture was cooled to room

temperature and the sealed tube was taken inside the glovebox for further workup procedure. The solvent was removed under reduced pressure and the residue was extracted into 3 mL of toluene and evaporated under reduced pressure to remove THF completely. The product was redissolved in 15 mL of toluene and filtered through Celite to remove LiCl and other insoluble impurities. The crude product was washed with 3 × 3 mL of Et_2O and 2 × 3 of mL hexane. The solid was redissolved in minimum amount of DCM and pentane was added to slowly induce precipitation and the resulted orange solid was concentrated to dryness. Yield: 42 mg (32%). ^{1}H NMR (600 MHz, $CDCl_3$) δ: 9.52 (d, *J* = 5.5 Hz, 2H, ArH), 7.77 (t, *J* = 7.9 Hz, 2H, ArH), 7.63 (dd, *J* = 7.6, 35 Hz, 4H, ArH), 7.01–7.11 (m, 4H, ArH), 6.76–6.88 (m, 4H, ArH), 6.21 (d, *J* = 8.2 Hz, 2H, ArH), 2.96 (sept, *J* = 6.2 Hz, 2H, $(CH_3)_2CHN$), 2.37 (s, 6H, CH_3), 2.25 (s, 6H, CH_3), 0.59 (d, *J* = 6.2 Hz, 6H, CH_3), 0.07 (d, *J* = 6.2 Hz, 6H, CH_3). $^{13}C\{^1H\}$ NMR (151 MHz, $CDCl_3$) δ: 174.3, 167.1, 154.4, 153.5, 147.6, 142.7, 137.7, 136.9, 136.0, 134.5, 132.7, 128.6, 126.0, 124.7, 123.4, 122.7, 117.4, 117.6, 48.08, 24.75, 24.55, 21.54, 21.15. UV-vis (THF): λ/nm ($\varepsilon/M^{-1}\,cm^{-1}$) 288(64000), 331(40000), 432(13000), 486(sh)(8000), 583(sh)(1000).

$Ir(btp)_2dipg^{NMe2}$ (2d). Prepared by the method described above for complex **1d**, using $[Ir(btp)_2(\mu\text{-}Cl)_2]$ (100 mg, 0.0768 mmol), lithium dimethylamide (~8 mg, 0.16 mmol, 2.1 equiv), and N,N′-diisopropylcarbodiimide (~20 mg, 0.16 mmol). The purified product was a light orange colored solid. Yield: 61 mg (51%). ^{1}H NMR (600 MHz, $CDCl_3$) δ: 9.26 (d, *J* = 5.5 Hz, 2H, ArH), 7.58 (dd, *J* = 8.3, 33 Hz, 4H, ArH), 6.97–7.07 (m, 4H, ArH), 6.76 (t, *J* = 7.6 Hz, 2H, ArH), 6.16 (d, *J* = 7.6 Hz, 2H, ArH), 3.60 (septa, *J* = 6.2 Hz, 2H, $(CH_3)_2CHN$), 2.80 (s, 6H, CH_3), 0.47 (d, *J* = 6.2 Hz, 6H, CH_3), 0.01 (d, *J* =

6.2Hz, 6H, CH_3). $^{13}C\{^1H\}$ NMR (151 MHz, $CDCl_3$) δ: 170.6, 167.2, 151.6, 147.6, 145.5, 142.7, 136.2, 133.6, 125.9, 124.6, 123.2, 122.5, 118.0, 117.7, 47.0, 40.6, 24.2, 24.0. UV-vis (THF): λ/nm (ε/M^{-1} cm^{-1}) 334(48000), 427(19000), 517(10000), 595(sh)(2000).

4.5.4 X-ray crystallography details

Single crystals were grown by vapor diffusion of pentane vapor into concentrated THF or dichloromethane solutions. Crystals were mounted on a Bruker Apex II three-circle diffractometer using MoKa radiation (λ=0.71073 Å). The data was collected at 123(2) K and was processed and refined within the APEXII software. Structures were solved by direct methods in SHELXS and refined by standard difference Fourier techniques in the program SHELXL.[49] Hydrogen atoms were placed in calculated positions using the standard riding model and refined isotropically; all non-hydrogen atoms were refined anisotropically. All of the crystal structures were solved by Dr. Thomas S. Teets, Department of Chemistry at University of Houston.

Table 4.3. Summary of crystallographic data for complex **1c**, **1d**, and **2a**

	1c	**1d**	**2a**
Crystal data			
Chemical formula	$C_{46.50}H_{46}ClIrN_4$	$C_{39}H_{40}IrN_5$	$C_{48}H_{43}Cl_2IrN_4S_2$
M_r	888.52	770.96	1003.08
Crystal system, space group	Monoclinic, $P2_1/c$	Monoclinic, $P2_1/c$	Monoclinic, $P2_1/n$
Temperature (K)	173	123	123
a, *b*, *c* (Å)	18.501 (3), 9.1561 (16), 26.146 (5)	15.929 (3), 10.934 (2), 19.318 (4)	12.461 (4), 19.090 (6), 17.319 (6)
b (°)	107.620 (4)	107.740 (2)	91.902 (4)
V (Å^3)	4221.3 (13)	3204.6 (12)	4118 (2)
m (mm^{-1})	3.26	4.20	3.51
Crystal size (mm)	0.19 × 0.17 × 0.04	0.41 × 0.25 × 0.19	0.33 × 0.28 × 0.19
Data collection			
T_{min}, T_{max}	0.570, 0.746	0.542, 0.746	0.627, 0.746
No. of measured, independent and observed [$I > 2s(I)$] reflections	36622, 9330, 7747	19757, 7396, 6784	25770, 9507, 8749
R_{int}	0.040	0.027	0.026
(sin q/l)$_{max}$ (Å^{-1})	0.641	0.651	0.651
Refinement			
$R[F^2 > 2s(F^2)]$, $wR(F^2)$, S	0.039, 0.100, 1.09	0.020, 0.048, 1.04	0.027, 0.075, 1.05
No. of reflections	9330	7396	9507
No. of parameters	494	412	520
No. of restraints	16	0	0
	$w = 1/[s^2(F_o^2) + (0.0474P)^2 + 7.2873P]$ where $P = (F_o^2 + 2F_c^2)/3$	$w = 1/[s^2(F_o^2) + (0.017P)^2 + 2.1759P]$ where $P = (F_o^2 + 2F_c^2)/3$	$w = 1/[s^2(F_o^2) + (0.0328P)^2 + 12.1077P]$ where $P = (F_o^2 + 2F_c^2)/3$
$\Delta\rho_{max}$, $\Delta\rho_{min}$ (e Å^{-3})	1.59, -0.99	0.94, -0.81	0.99, -1.84

Table 4.4. Summary of crystallographic data for complexes **2b** and **2d**

	2b	**2d**
Crystal data		
Chemical formula	$C_{50}H_{51}IrN_6S_2$	$C_{35}H_{36}IrN_5S_2$
M_r	992.28	783.01
Crystal system, space group	Triclinic, $P\bar{1}$	Monoclinic, $C2/c$
a, b, c (Å)	11.551 (3), 13.444 (4), 15.248 (4)	20.457 (4), 9.7209 (18), 17.889 (3)
a, b, g (°)	111.457 (2), 101.216 (2), 94.278 (2)	90, 117.435 (2), 90
V (Å^3)	2134.0 (10)	3157.5 (10)
Z	2	4
m (mm^{-1})	3.27	4.39
Crystal size (mm)	0.23 × 0.20 × 0.17	0.44 × 0.28 × 0.10
Data collection		
T_{min}, T_{max}	0.586, 0.746	0.512, 0.746
No. of measured, independent and observed [$I > 2s(I)$] reflections	37861, 9724, 9188	9112, 3490, 3402
R_{int}	0.027	0.019
$(\sin q/l)_{max}$ (Å^{-1})	0.649	0.641
Refinement		
$R[F^2 > 2s(F^2)]$, $wR(F^2)$, S	0.019, 0.055, 1.22	0.016, 0.040, 1.05
No. of reflections	9724	3490
No. of parameters	538	199
$\Delta\rho_{max}$, $\Delta\rho_{min}$ (e Å^{-3})	1.67, -0.85	0.95, -1.01

4.6 References

(1) Prier, C. K.; Rankic, D. A.; MacMillan, D. W. C. "Visible Light Photoredox Catalysis with Transition Metal Complexes: Applications in Organic Synthesis." *Chem. Rev.* **2013**, *113*, 5322–5363.

(2) Zuo, Z.; Ahneman, D. T.; Chu, L.; Terrett, J. A.; Doyle, A. G.; MacMillan, D. W. C. "Merging Photoredox with Nickel Catalysis: Coupling of α-Carboxyl Sp3-Carbons with Aryl Halides." 5.

(3) Yoon, T. P.; Ischay, M. A.; Du, J. "Visible Light Photocatalysis as a Greener Approach to Photochemical Synthesis." *Nat. Chem. Lond.* **2010**, *2*, 527–532.

(4) Zhao, Q.; Huang, C.; Li, F. "Phosphorescent Heavy-Metal Complexes for Bioimaging." *Chem. Soc. Rev.* **2011**, *40*, 2508.

(5) Baggaley, E.; Gill, M. R.; Green, N. H.; Turton, D.; Sazanovich, I. V.; Botchway, S. W.; Smythe, C.; Haycock, J. W.; Weinstein, J. A.; Thomas, J. A. "Dinuclear Ruthenium(II) Complexes as Two-Photon, Time-Resolved Emission Microscopy Probes for Cellular DNA." *Angew. Chem. Int. Ed.* **2014**, *53*, 3367–3371.

(6) Yang, Y.; Zhao, Q.; Feng, W.; Li, F. "Luminescent Chemodosimeters for Bioimaging." *Chem. Rev.* **2013**, *113*, 192–270.

(7) You, Y. "Recent Progress on the Exploration of the Biological Utility of Cyclometalated Iridium(III) Complexes." *J. Chin. Chem. Soc.* **2018**, *65*, 352–367.

(8) Maity, A.; Choi, J.-S.; Teets, T. S.; Deligonul, N.; Berdis, A. J.; Gray, T. G. "Cyclometalated Iridium(III) Complexes with Deoxyribose Substituents." *Chem. – Eur. J.* **2013**, *19*, 15924–15932.

(9) Zhao, Q.; Li, F.; Liu, S.; Yu, M.; Liu, Z.; Yi, T.; Huang, C. "Highly Selective Phosphorescent Chemosensor for Fluoride Based on an Iridium(III) Complex Containing Arylborane Units." *Inorg. Chem.* **2008**, *47*, 9256–9264.

(10) Zhao, Q.; Li, F.; Huang, C. "Phosphorescent Chemosensors Based on Heavy-Metal Complexes." *Chem. Soc. Rev.* **2010**, *39*, 3007–3030.

(11) Yersin, H. (Hartmut). *Highly Efficient OLEDs with Phosphorescent Materials*; Weinheim : Wiley-VCH, 2008.

(12) Lamansky, S.; Djurovich, P.; Murphy, D.; Abdel-Razzaq, F.; Lee, H.-E.; Adachi, C.; Burrows, P. E.; Forrest, S. R.; Thompson, M. E. "Highly Phosphorescent Bis-

Cyclometalated Iridium Complexes: Synthesis, Photophysical Characterization, and Use in Organic Light Emitting Diodes." *J. Am. Chem. Soc.* **2001**, *123*, 4304–4312.

(13) Lowry, M. S.; Bernhard, S. "Synthetically Tailored Excited States: Phosphorescent, Cyclometalated Iridium(III) Complexes and Their Applications." *Chem. – Eur. J.* **2006**, *12*, 7970–7977.

(14) Sarma, M.; Tsai, W.-L.; Lee, W.-K.; Chi, Y.; Wu, C.-C.; Liu, S.-H.; Chou, P.-T.; Wong, K.-T. "Anomalously Long-Lasting Blue PhOLED Featuring Phenyl-Pyrimidine Cyclometalated Iridium Emitter." *Chem* **2017**, *3*, 461–476.

(15) Costa, R. D.; Ortí, E.; Bolink, H. J.; Monti, F.; Accorsi, G.; Armaroli, N. "Luminescent Ionic Transition-Metal Complexes for Light-Emitting Electrochemical Cells." *Angew. Chem. Int. Ed.* **2012**, *51*, 8178–8211.

(16) Gao, T.-B.; Zhang, J.-J.; Yan, R.-Q.; Cao, D.-K.; Jiang, D.; Ye, D. "Aggregation-Induced Electrochemiluminescence from a Cyclometalated Iridium(III) Complex." *Inorg. Chem.* **2018**, *57*, 4310–4316.

(17) Dedeian, K.; Djurovich, P. I.; Garces, F. O.; Carlson, G.; Watts, R. J. "A New Synthetic Route to the Preparation of a Series of Strong Photoreducing Agents: Fac-Tris-Ortho-Metalated Complexes of Iridium(III) with Substituted 2-Phenylpyridines." *Inorg. Chem.* **1991**, *30*, 1685–1687.

(18) Tamayo, A. B.; Alleyne, B. D.; Djurovich, P. I.; Lamansky, S.; Tsyba, I.; Ho, N. N.; Bau, R.; Thompson, M. E. "Synthesis and Characterization of Facial and Meridional Tris-Cyclometalated Iridium(III) Complexes." *J. Am. Chem. Soc.* **2003**, *125*, 7377–7387.

(19) You, Y.; Park, S. Y. "Inter-Ligand Energy Transfer and Related Emission Change in the Cyclometalated Heteroleptic Iridium Complex: Facile and Efficient Color Tuning over the Whole Visible Range by the Ancillary Ligand Structure." *J. Am. Chem. Soc.* **2005**, *127*, 12438–12439.

(20) Chang, C.-J.; Yang, C.-H.; Chen, K.; Chi, Y.; Shu, C.-F.; Ho, M.-L.; Yeh, Y.-S.; Chou, P.-T. "Color Tuning Associated with Heteroleptic Cyclometalated Ir(III) Complexes: Influence of the Ancillary Ligand." *Dalton Trans.* **2007**, No. 19, 1881–1890.

(21) Li, J.; Djurovich, P. I.; Alleyne, B. D.; Yousufuddin, M.; Ho, N. N.; Thomas, J. C.; Peters, J. C.; Bau, R.; Thompson, M. E. "Synthetic Control of Excited-State Properties in Cyclometalated Ir(III) Complexes Using Ancillary Ligands." *Inorg. Chem.* **2005**, *44*, 1713–1727.

(22) Radwan, Y. K.; Maity, A.; Teets, T. S. “Manipulating the Excited States of Cyclometalated Iridium Complexes with β-Ketoiminate and β-Diketiminate Ligands.” *Inorg. Chem.* **2015**, *54*, 7122–7131.

(23) Nazeeruddin, Md. K.; Humphry-Baker, R.; Berner, D.; Rivier, S.; Zuppiroli, L.; Graetzel, M. “Highly Phosphorescence Iridium Complexes and Their Application in Organic Light-Emitting Devices.” *J. Am. Chem. Soc.* **2003**, *125*, 8790–8797.

(24) Sajoto, T.; Djurovich, P. I.; Tamayo, A. B.; Oxgaard, J.; Goddard, W. A.; Thompson, M. E. “Temperature Dependence of Blue Phosphorescent Cyclometalated Ir(III) Complexes.” *J. Am. Chem. Soc.* **2009**, *131*, 9813–9822.

(25) Yang, C.-H.; Mauro, M.; Polo, F.; Watanabe, S.; Muenster, I.; Fröhlich, R.; De Cola, L. “Deep-Blue-Emitting Heteroleptic Iridium(III) Complexes Suited for Highly Efficient Phosphorescent OLEDs.” *Chem. Mater.* **2012**, *24*, 3684–3695.

(26) Shavaleev, N. M.; Monti, F.; Costa, R. D.; Scopelliti, R.; Bolink, H. J.; Ortí, E.; Accorsi, G.; Armaroli, N.; Baranoff, E.; Grätzel, M.; et al. “Bright Blue Phosphorescence from Cationic Bis-Cyclometalated Iridium(III) Isocyanide Complexes.” *Inorg. Chem.* **2012**, *51*, 2263–2271.

(27) Haneder, S.; Como, E. D.; Feldmann, J.; Lupton, J. M.; Lennartz, C.; Erk, P.; Fuchs, E.; Molt, O.; Münster, I.; Schildknecht, C.; et al. “Controlling the Radiative Rate of Deep-Blue Electrophosphorescent Organometallic Complexes by Singlet-Triplet Gap Engineering.” *Adv. Mater.* **2008**, *20*, 3325–3330.

(28) Bixon, M.; Jortner, J. “Intramolecular Radiationless Transitions.” *J. Chem. Phys.* **1968**, *48*, 715–726.

(29) Englman, R.; Jortner, J. “The Energy Gap Law for Radiationless Transitions in Large Molecules.” *Mol. Phys.* **1970**, *18*, 145–164.

(30) Cummings, S. D.; Eisenberg, R. “Tuning the Excited-State Properties of Platinum(II) Diimine Dithiolate Complexes.” *J. Am. Chem. Soc.* **1996**, *118*, 1949–1960.

(31) Zhao, K.-Y.; Shan, G.-G.; Fu, Q.; Su, Z.-M. “Tuning Emission of AIE-Active Organometallic Ir(III) Complexes by Simple Modulation of Strength of Donor/Acceptor on Ancillary Ligands.” *Organometallics* **2016**, *35*, 3996–4001.

(32) Martínez-Alonso, M.; Busto, N.; Aguirre, L. D.; Berlanga, L.; Carrión, M. C.; Cuevas, J. V.; Rodríguez, A. M.; Carbayo, A.; Manzano, B. R.; Ortí, E.; et al. “Strong Influence of the Ancillary Ligand over the Photodynamic Anticancer Properties of

Neutral Biscyclometalated IrIII Complexes Bearing 2-Benzoazole-Phenolates." *Chem. – Eur. J.* **2018**, *24*, 17523–17537.

(33) Torres, J.; Carrión, M. C.; Leal, J.; Jalón, F. A.; Cuevas, J. V.; Rodríguez, A. M.; Castañeda, G.; Manzano, B. R. "Cationic Bis(Cyclometalated) Ir(III) Complexes with Pyridine–Carbene Ligands. Photophysical Properties and Photocatalytic Hydrogen Production from Water." *Inorg. Chem.* **2018**, *57*, 970–984.

(34) Axtell, J. C.; Kirlikovali, K. O.; Djurovich, P. I.; Jung, D.; Nguyen, V. T.; Munekiyo, B.; Royappa, A. T.; Rheingold, A. L.; Spokoyny, A. M. "Blue Phosphorescent Zwitterionic Iridium(III) Complexes Featuring Weakly Coordinating *Nido* -Carborane-Based Ligands." *J. Am. Chem. Soc.* **2016**, *138*, 15758–15765.

(35) Lai, P.-N.; Brysacz, C. H.; Alam, M. K.; Ayoub, N. A.; Gray, T. G.; Bao, J.; Teets, T. S. "Highly Efficient Red-Emitting Bis-Cyclometalated Iridium Complexes." *J. Am. Chem. Soc.* **2018**, *140*, 10198–10207.

(36) Lai, P.-N.; Teets, T. S. "Ancillary Ligand Effects on Red-Emitting Cyclometalated Iridium Complexes." *Chem. – Eur. J.* **2019**, *25*, 6026–6037.

(37) Maya, R. A.; Maity, A.; Teets, T. S. "Fluorination of Cyclometalated Iridium β-Ketoiminate and β-Diketiminate Complexes: Extreme Redox Tuning and Ligand-Centered Excited States." *Organometallics* **2016**, *35*, 2890–2899.

(38) Shon, J.-H.; Teets, T. S. "Potent Bis-Cyclometalated Iridium Photoreductants with β-Diketiminate Ancillary Ligands." *Inorg. Chem.* **2017**, *56*, 15295–15303.

(39) Okada, S.; Okinaka, K.; Iwawaki, H.; Furugori, M.; Hashimoto, M.; Mukaide, T.; Kamatani, J.; Igawa, S.; Tsuboyama, A.; Takiguchi, T.; et al. "Substituent Effects of Iridium Complexes for Highly Efficient Red OLEDs." *Dalton Trans.* **2005**, No. 9, 1583.

(40) Deaton, J. C.; Young, R. H.; Lenhard, J. R.; Rajeswaran, M.; Huo, S. "Photophysical Properties of the Series *Fac*- and *Mer*- (1-Phenylisoquinolinato-N ^ C $^{2'}$) $_{x}$ (2-Phenylpyridinato-N ^ C $^{2'}$) $_{3-x}$ Iridium(III) ($x = 1-3$) ^{61†}." *Inorg. Chem.* **2010**, *49*, 9151–9161.

(41) Fan, C.-H.; Sun, P.; Su, T.-H.; Cheng, C.-H. "Host and Dopant Materials for Idealized Deep-Red Organic Electrophosphorescence Devices." *Adv. Mater.* **2011**, *23*, 2981–2985.

(42) Duan, J. P.; Sun, P. P.; Cheng, C. H. "New Iridium Complexes as Highly Efficient Orange–Red Emitters in Organic Light-Emitting Diodes." *Adv. Mater.* **2003**, *15*, 224–228.

(43) Tsujimoto, H.; Yagi, S.; Asuka, H.; Inui, Y.; Ikawa, S.; Maeda, T.; Nakazumi, H.; Sakurai, Y. “Pure Red Electrophosphorescence from Polymer Light-Emitting Diodes Doped with Highly Emissive Bis-Cyclometalated Iridium(III) Complexes.” *J. Organomet. Chem.* **2010**, *695*, 1972–1978.

(44) Kim, D. H.; Cho, N. S.; Oh, H.-Y.; Yang, J. H.; Jeon, W. S.; Park, J. S.; Suh, M. C.; Kwon, J. H. “Highly Efficient Red Phosphorescent Dopants in Organic Light-Emitting Devices.” *Adv. Mater.* **2011**, *23*, 2721–2726.

(45) Fang, Y.; Tong, B.; Hu, S.; Wang, S.; Meng, Y.; Peng, J.; Wang, B. “A Highly Efficient Tris-Cyclometalated Iridium Complex Based on Phenylphthalazine Derivative for Organic Light-Emitting Diodes.” *Org. Electron.* **2009**, *10*, 618–622.

(46) Pangborn, A. B.; Giardello, M. A.; Grubbs, R. H.; Rosen, R. K.; Timmers, F. J. “Safe and Convenient Procedure for Solvent Purification.” *Organometallics* **1996**, *15*, 1518–1520.

(47) Nonoyama, M. “Benzo[h]Quinolin-10-Yl-N Iridium(III) Complexes.” *Bull. Chem. Soc. Jpn.* **1974**, *47*, 767–768.

(48) Seybold, P. G.; Gouterman, M. “Porphyrins: XIII: Fluorescence Spectra and Quantum Yields.” *J. Mol. Spectrosc.* **1969**, *31*, 1–13.

(49) Sheldrick, G. M. “A Short History of *SHELX*.” *Acta Crystallogr. A* **2008**, *64*, 112–122.